Summer 7-30-2021

DEVELOPMENT OF VACCINES AND ANTIVIRALS AGAINST ZIKA VIRUS

Aryamav Pattnaik
University of Nebraska-Lincoln, ary@huskers.unl.edu

DEVELOPMENT OF VACCINES AND ANTIVIRALS AGAINST ZIKA VIRUS

by

Aryamav Pattnaik

A DISSERTATION

Presented to the Faculty of

The Graduate College at the University of Nebraska

In Partial Fulfillments of Requirements

For the Degree of Doctor of Philosophy

Major: Integrative Biomedical Sciences

Under the Supervision of Professor Fernando A. Osorio

Lincoln, Nebraska

August 2021

DEVELOPMENT OF VACCINES AND ANTIVIRALS AGAINST ZIKA VIRUS

Aryamav Pattnaik, Ph.D.

University of Nebraska, 2021

Advisor: Fernando A. Osorio

The re-emergence of Zika virus (ZIKV), an arbovirus, poses a major global human health concern because of its ability to cause congenital abnormalities and neurological diseases. While many candidate vaccines and antiviral drugs are in the developmental pipeline, none have been approved for use against ZIKV infection. This dissertation describes the characterization of one vaccine and two antiviral drug candidates against ZIKV infection. A bacterial ferritin-based nanoparticle vaccine, termed zDIII-F, is designed to display multiple copies of ZIKV E protein domain III on its surface. These stable nanoparticles are shown to induce robust antibody-mediated protection against lethal ZIKV infection in mice. Additionally, passive transfer of sera from zDIII-F immunized mice also conferred protection in animals following ZIKV challenge. By employing a homology-based modelling approach, we predicted the structure of ZIKV RNA-dependent RNA polymerase (RdRp) and used it to screen for small molecule compounds that bind the viral RdRp. Among the top 10 compounds with high docking scores, we observed that the molecule with the highest score, TPB, strongly suppressed ZIKV replication *in vitro* and *in vivo*. With the ability to target the conserved regions of flavivirus RdRp, a high selective index of 206 combined with a low molecular weight of ~500 daltons, TPB promises to be an excellent candidate for

development as an anti-ZIKV as well as an anti-flavivirus drug. Analysis of ZIKV genome sequences suggested the presence of conserved guanine (G)-rich motifs that can fold under physiological conditions to form secondary structures called G-quadruplexes. Such structures, when stabilized, can inhibit transcription, translation, and replication. We have demonstrated that stabilization of ZIKV genome G-quadruplexes by G-quadruplex-binding ligands, BRACO-19 and TMPyP4, significantly suppressed ZIKV protein synthesis and replication. Therefore, we propose further development and potential use of G-quadruplex-binding ligands as a strategy for treatment of ZIKV infection. Overall, the studies described in this dissertation significantly contribute to development of anti-ZIKV therapeutics.

ACKNOWLEDGMENTS

I take this oppurtunity to express my heartfelt gratitude to my advisor, Dr. Fernando A. Osorio. Working under his guidance, I have learnt a great deal about scientific research. I sincerely thank him for believing in me, allowing me to work as an individual and as part of a team, encouraging me to think critically and for naming me 'Ary'.

I would like to thank Dr. Asit K. Pattnaik for allowing me to conduct my studies in his laboratory. His approach in scientific research has been a constant source of inspiration to me. I consider myself lucky to have worked under his guidance and am confident that this will help me in building my career as a scientifc researcher. I also thank him for critically reading and helping me refine my dissertation.

I also thank the members of my graduate committee. Dr. Hiep Vu, for his help in my research work in the initial days of my graduate program. Dr. Gustavo Delhon, for his helpful advices and critically correcting this dissertaiton. Dr. Daniel Ciobanu, for insightful discussions during my committee meetings. I extend my gratitude to Dr. Thomas Petro for his help in the nanoparticle based vaccine studies, Dr. Gloria Borgstahl and Dr. Lucas Struble for their assistance in purifying the chimeric nanoparticles, Dr. Shi-Hua Xiang, for his help in the *in silico* drug screening studies, Dr. Sathish Kumar Natarajan for providing me with several cell lines for my studies, Dr. You (Joe) Zhou for acquiring the TEM images of the nanoparticles and Dr. Santosh Behera, for modelling the structure of the chimaric nanoparticles.

Throughout my PhD program, I was fortunate to have amazing colleages. Arun

Saravanakumar Annamalai, who taught me the basics of molecular cloning. My special thanks for Bikash Ranjan Sahoo and Prakash Kumar Sahoo for being very supportive and helpful. Both of them have been at my side at times of need and I shall always cherish their friendship and the time we spent together. This dissertation would not have been possible without them. Kay Kimspton-Burkgren, Ignacio Correas, Haiyan Sun, Jayeshbhai Chaudhary, Ninaad Lasrado, Rajkumar Arumugam for reminding to have fun. I am fortunate to have known Dr. Bhopal Mohapatra and Dr. Prasanta Dash and their families in Omaha for countless memories of fun, frolic and joy.

I thank Rebecca Richardson-Carlson for her help in the lab. I am grateful to the faculty and staff at School of Veterinary Medicine and Biomedical Sciences and Nebraska Center for Virology for their constant support. I am grateful to Jan Edwards, Mark Garett, Donna Bode and Jennifer Lottman for making my life at the Unviersity of Nebraska-Lincoln easy.

I am very grateful to my Badababa, Dr. Asit K. Pattnaik and Mummy, Suchitra Pattnaik for being a constant source of support and strength and never making me miss home. Last but not least, I am thankful to my parents, family and friends for their support throughout the period of my PhD.

Aryamav Pattnaik, Ph.D.

University of Nebraska-Lincoln

August, 2021

Dedication

To my grandparents

TABLE OF CONTENTS

LIST OF FIGURES

LIST OF TABLES

LIST OF ABBREVIATIONS

Ad	Adenovirus
AHFV	Alkhurma hemorrhagic fever virus
aa	Amino acids
TBE	Tick-borne Encephalitis
ADE	antibody-dependent enhancement
BCRs	B-cell receptor
BCA	Bicinchoninic acid
CZS	Congenital Zika syndrome
CPE	Cytopathic effect
CC_{50}	Cytotoxic concentration 50
DENV	Dengue virus
DMEM	Dulbecco's modified Eagle's medium
ER	Endoplasmic reticulum
E	Envelope
FBS	Fetal bovine serum
GQs	G-quadruplex structures
GC	Germinal center
GBS	Guillain-Barré syndrome
Hpi	Hour post-infection
HEPES	Hydroxyethyl piperazine ethane sulfonic acid
IC_{50}	Inhibitory concentration 50
IVM	Ivermectin

JEV	Japanese Encephalitis Virus
kb	Kilo bases
kDa	Kilo dalton
KFD	Kyasanur Forest Disease
LNP	Lipid nanoparticles
MV	Measles virus
M	Membrane
MTase	Methyltransferase
MVD	Molegro Virtual Docker
MOI	Multiplicity of infection
MPA	Mycophenolic acid
NHPs	Non-human primates
NS	Non-structural
NFW	Nuclease-free water
OHFV	Omsk hemorrhagic fever virus
ORF	Open reading frame
PS	Penicillin/Streptomycin
PK	Pharmacokinetic
PBS	Phosphate buffered saline
PRNT	Plaque reduction neutralization test
prM	Precursor membrane
PDS	Pyridostatin
qRT-PCR	Quantitative RT-PCR
RIPA	Radio-immunoprecipitation assay
RdRp	RNA-dependent RNA polymerase
STAT2	Signal transducer and activator of transcription 2
SEC	Size exclusion chromatography
SC	Subcutaneous
Tfh	T follicular helper cells
TM	Transmembrane
TEM	Transmission electron microscopy

TBS	Tris-buffered saline
UTR	Untranslated region
VSV	Vesicular stomatitis virus
VGM	Virus growth medium
VLP	Virus-like particles
WNV	West Nile virus
WHO	World Health Organization
YFV	Yellow fever virus
ZIKV	Zika virus

CHAPTER I: INTRODUCTION

1.1. Classification of Zika virus

Zika virus (ZIKV) is a member of the family *Flaviviridae*. Viruses of this family are enveloped and carry a positive sense, non-segmented single stranded RNA genome of about 9-13 kilo bases (kb) in length. The family *Flaviviridae* is classified into four genera: Flavivirus, Pestivirus, Hepacivirus and Pegivirus (Simmonds et al., 2017). The genus Flavivirus encompasses more than 70 arthropod-borne viruses. These are further categorized based on vector transmission: (i) Tick vectored viruses include Alkhurma hemorrhagic fever virus (AHFV), Kyasanur Forest Disease (KFD), Omsk hemorrhagic fever virus (OHFV) and Tick-borne Encephalitis (TBE), and (ii) Mosquito vectored viruses include, dengue virus (DENV), Japanese Encephalitis Virus (JEV), yellow fever virus (YFV), West Nile virus (WNV), and ZIKV (Kuno et al., 1998). Most of them are responsible for fatal hemorrhagic fever or neurological disease such as encephalitis in humans.

Serologic and genome analyses of ZIKV suggest the existence of only one single serotype with three distinct genetic lineages: East African (that includes the first isolate from Uganda, MR766 in 1947), West African, and Asian, including the first isolate from Malaysia,Asia (P6-740) in 1966 and all contemporary strains from Asia, Oceania, and the Americas (Dowd et al., 2016; Lanciotti et al., 2008; Lanciotti et al., 2016; Musso et al., 2016a).

1.2. ZIKV and diseases associated with ZIKV infections

The primary mode of ZIKV transmission is through mosquito bite; however, the virus has also been shown to be transmitted sexually (Atkinson et al., 2016; Foy et al., 2011; Turmel et al., 2016), from mother to fetus (Fiorentino and Montero, 2016; Pomar et al., 2018; Zanluca et al., 2018), through blood transfusion (Liu et al., 2019; Musso et al., 2016b) and also by contact with contaminated body fluids such as saliva and urine (Brasil et al., 2016; D'Ortenzio et al., 2016; Mlakar et al., 2016; Russell et al., 2017). The incubation period of disease is estimated to range from 3 to 14 days. The majority (≥80%) of individuals infected with ZIKV do not show any symptoms while some develop mild self-resolving symptoms including fever, rash, conjunctivitis, headache, malaise, muscle, and joint pain lasting for 2 to 7 days. However, in a very small number of cases, infections can lead to severe diseases, such as Guillain-Barré syndrome (GBS), an autoimmune disease of the peripheral nervous system in adults and congenital Zika syndrome (CZS) in developing fetuses that includes a variety of pathological abnormalities such as craniofacial, musculoskeletal, ocular, and pulmonary malformations (de Paula Freitas et al., 2016; de Paula Guimaraes et al., 2019; Miranda et al., 2016; Russell et al., 1984; Zacharias et al., 2017). In addition, infant case in the recent Brazil outbreak were associated with a severe reduction in the size of the skull and developmental deficits in the brain, a condition known as microcephaly (Alvarado and Schwartz, 2017; Panchaud et al., 2016). Furthermore, studies have suggested that ZIKV infection may be responsible for reduced fertility in men (Avelino-Silva et al., 2018). ZIKV infection also causes conjunctivitis persistent chorioretinal lesions, and uveitis in humans (Manangeeswaran et al., 2018; Miner et al., 2016). Unlike previous ZIKV outbreaks, genomic changes responsible forthe high pathogenicity of the virus in recent

outbreaks are unknown.

1.3. History and emergence of ZIKV

ZIKV was first isolated in 1947 from the blood sample of a sentinel rhesus monkey in the Zika forest of Uganda (Dick et al., 1952). Although the first case of human infection by ZIKV was described in Nigeria in the early 1950s, only sporadic outbreaks were reported in Africa and Asia over the next few decades. The virus re-emerged in 2007 causing an outbreak in the Yap Island of Federated States of Micronesia, with the majority of symptomatic patients exhibiting fever, rash, and arthritis/arthralgia (Duffy et al., 2009). A larger ZIKV outbreak occurred in French Polynesia and other Pacific Islands in late 2013, where, in addition to the above-described symptoms, conjunctivitis was also noted (Cao-Lormeau et al., 2014; Musso et al., 2014). The virus was subsequently detected for the first time in Brazil in 2015, causing infections of epidemic proportions (Zanluca et al., 2015), although epidemiological studies through viral genome sequence analysis suggest that the virus may have been circulating in the northeastern part of the country as early as late 2013 (Grubaugh et al., 2018). The virus rapidly spread to many countries in the Americas and other parts of the world (Faria et al., 2017; Weaver et al., 2016). The incidences of ZIKV infections in the Americas peaked in early 2016 with the cumulative number of documented and suspected cases exceeding 1 million. However, the the incidence of ZIKV infectionin the Americas and the rest of the world has waned significantly after 2017.

The ZIKV epidemic in Brazil, as well as other countries, was linked to devastating CZS including microcephaly, congenital malformation, and fetal demise,

particularly when women are infected with the virus during the first trimester of pregnancy (Brasil et al., 2016; Coyne and Lazear, 2016; Heymann et al., 2016; Hoen et al., 2018; Mlakar et al., 2016; Panchaud et al., 2016). ZIKV infections were also found to be associated with GBS in adults, an auto-immune disease of the peripheral nerves that can result in muscle weakness and paralysis (Barbi et al., 2018; Besnard et al., 2014; Mendez et al., 2017; Styczynski et al., 2017). While ZIKV infections prior to 2013 were mostly associated with mild disease symptoms, the new severe disease forms associated with the virus infections such as GBS and CZS led the World Health Organization (WHO) to declare ZIKV a Public Health Emergency of International Concern (2016). This prompted the global health and research community to not only study the biology and pathogenesis of the virus but also devise strategies for prevention and control measures, including the development of safe and efficacious vaccines and antivirals against ZIKV.

1.4. ZIKV virion structure

In the recent years, two independent groups have solved the cryo-EM structure of the mature ZIKV virion particle at atomic resolution of 3.8 Å. Similar to other closely related flaviviruses, the ZIKV particle is spherical (Shi and Gao, 2017), with a size of 50nm for the mature particle and 60nm for the immature particle.. (Barreto-Vieira et al., 2016; Heinz and Stiasny, 2017; Prasad et al., 2017). The mature ZIKV particle consists of a of ~11 kb long, non-segmented, positive-sense RNA genome, which is enclosed by the capsid protein (Boyer et al., 2018) and further surrounded by a host derived lipid bilayer into which 180 copies of each of the membrane (M) and envelope (E) glycoproteins are

anchored through their respective transmembrane regions (Dai et al., 2016; Kuhn et al., 2002). The E protein forms the outermost layer of the virus particle (Fig 1.1), which protects the viral genome from the external environment and is known to interact with host cell surface during infection (Shi and Gao, 2017). The monomeric form of ZIKV E protein is embodied with four subdomains: three ectodomains (domains I, II and III) and a stem –transmembrane domain. Structural analysis of a mature virion shows that the two E protein monomers dimerize and three such dimers lie parallel to each other adopting a raft configuration. A mature virion exhibits icosahedral structure and contains a total of 30 such rafts. One half of a raft constitutes an asymmetric unit of the virion resulting in the presence of 90 such asymmetric units in a mature ZIKV particle. The virion consists of 180 units of the E and M proteins forming the raft configuration (Fig. 1.1). The M protein, unlike the E protein, is short and resides under the E protein, displaying a similar icosahedral organization (Dai et al., 2016; Shi and Gao, 2017; Sirohi et al., 2016).

1.5. Genome organization of ZIKV

Similar to flaviviruses, ZIKV also contains a single-stranded positive-sense RNA genome ~11 kb in length. The viral genome (Fig. 1.2 A) has a single open reading frame (ORF) of ~10,200 bases and is flanked by 5′ untranslated region (UTR) and 3′ UTR (van Hemert and Berkhout, 2016). The 5’ UTR and 3’ UTRs are about 106 and 430 nucleotides long, respectively. In addition, the genome has a type I cap structure and 3’ UTR contains multiple pseudoknot structures and lacks poly (A) tails. The ORF encodes a single polyprotein of ~3,400 amino acids (aa) in length, which is translated in the cytoplasm and in association with the rough endoplasmic reticulum of the infected cells

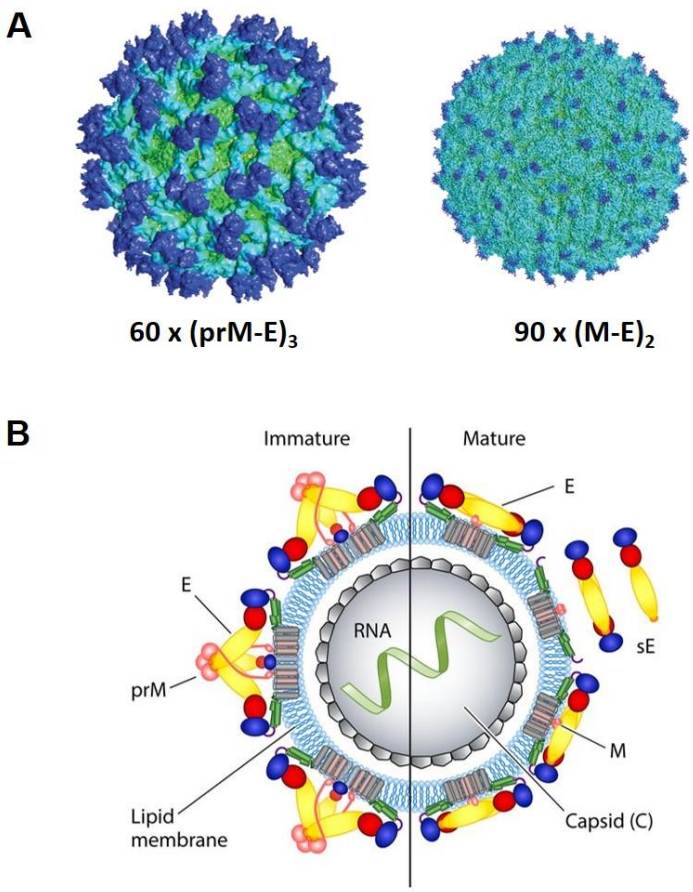

Fig. 1.1. Structure of ZIKV particles. (A) Left and right images represent surface-shaded, radially colored immature and mature ZIKV particles. The immature particle contains 60 trimers of prM-E heterodimers, while the mature particles contain 90 dimers of conformationally rearranged heterodimers of M-E along with loss of pr peptide by furin cleavege. The images were adapted from Sirohi, D. and Kuhn, R.J. (2017). **(B)** Schematic representation of a prototypical flavivirus (including ZIKV) immature and mature particle showing a cross-sectional organization of viral proteins and RNA. sE, soluble E protein. The image is from Heinz, F.X. and Stiansy, K. (2017).

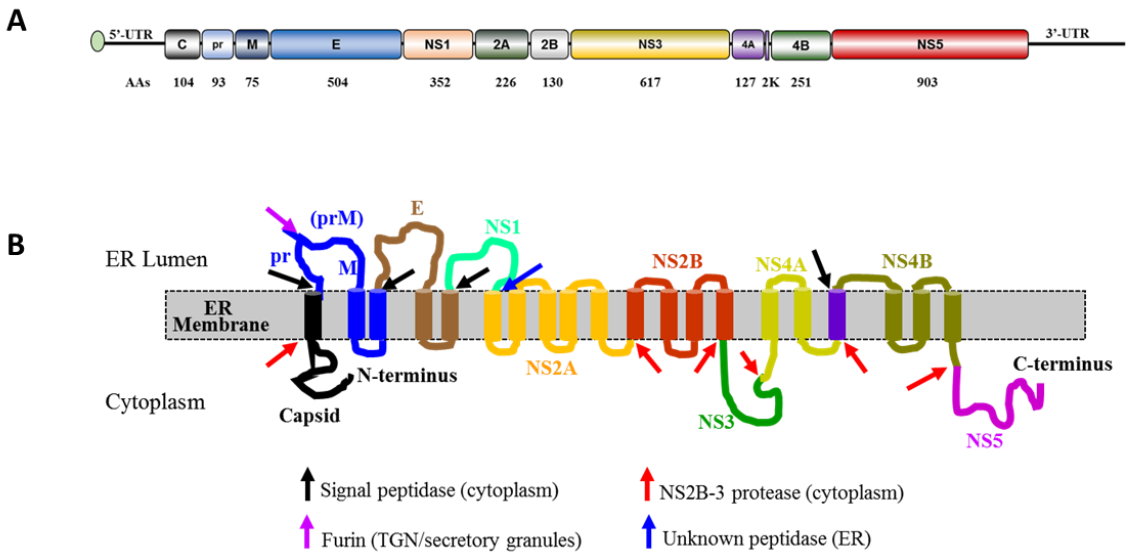

Fig. 1.2. ZIKV genome organization, encoded proteins, and their topology. (A) The viral genome is shown as a black line with a cap structure at the 5' end, followed by an untranslated region (5'UTR), various proteins (with amino acid residue length) generated from a single open reading frame that is translated from the genome, and the 3' UTR. **(B)** Topology of the viral proteins is shown. Colored arrows show various protease cleavage sites for generation of the mature proteins. A small protein (2K) present between NS4A and NS4B is entirely membrane-associated. The cylindrical structures represent membrane-associated domains of the proteins. Image redrawn from Tan *et.al*, 2020.

(Hamel et al., 2015). The single polyprotein is cleaved and processed by viral and host proteases (Fig. 1.2 B) to generate three structural (capsid, C; precursor-membrane, prM; and envelope, E) proteins present at the amino-terminus and seven non-structural (NS1, NS2A, NS2B, NS3, NS4A, NS4B, and NS5) proteins present at the carboxy-terminus (Medeiros et al., 2007). The proteins of ZIKV have structurally and functionally equivalent counterparts in other members of *Flaviviridae* such as DENV, WNV, YFV and JEV. The structural proteins are involved in virion formation, protection of the viral genome, attachment to , and entry into the host cells (Lindenbach and Rice, 2013). The NS proteins are associated with the endoplasmic reticulum (ER) and participate in genome replication, polyprotein processing, virion assembly, and evasion of host antiviral responses (Grant et al., 2016; Kumar et al., 2016; Pierson and Diamond, 2015)

1.6. Protein products

1.6.1. Capsid (C) protein

The three proteins that are part of the mature Zika virion are: the capsid protein (C), the membrane protein (M), and the envelope protein (E). Following infection, the viral genome is first translated in the cytoplasm as a single large polypeptide containing the viral C protein at its amino-terminus. The C proteins plays a central role in the ZIKV assembly process (Samsa et al., 2009; Shang et al., 2018). It is a small cytosolic protein of 122 amino acids (aa) long with a molecular weight of approximately 14 kDa. The mature C protein that is incorporated into virions is smaller. The C protein contains a highly positively charged loop followed by five alpha helices (α1- α5) at the N-terminal end (Tan et al., 2020). The α5 helix is present just upstream of the prM protein. In order

to make a mature C protein, a sequential cleavage occurs which is executed by both cellular and viral proteases. The first cleavage, mediated by a cellular protease, occurs at the signal peptide present in the α5-prM junction, and separates C from prM. The second cleavage, mediated by the viral proteases NS2B/Ns3, occurs at the capsid helix α4–α5 junction, and results in release of the 98 aa mature capsid protein (Tan et al., 2020). The mature C protein forms a homodimer. During virus assembly, the mature C protein binds to the viral RNA and to the trans-membrane domains of E and M proteins (Freire et al., 2015; Ni and Cheng Kao, 2013).

1.6.2. Precursor membrane (prM) and membrane (M) proteins

The prM protein consists of ~166 amino acids and is cleaved into pr and M proteins as the assembled virions mature during virus egress. The M protein consists of ~75 amino acids and is essential to virus assembly (Khou and Pardigon, 2017; Kuno et al., 1998). Its chaperone-like activity promotes proper folding and maturation of E protein (Konishi and Mason, 1993; Lorenz et al., 2002; Yoshii et al., 2012). During virus assembly, the prM protein protects the E protein from premature fusion due to the low pH environment in the transport vesicle while the immature virion traverses the ER and trans-Golgi network (Guirakhoo et al., 1991; Heinz et al., 1994; Nambala and Su, 2018). Host cellular furin protease cleaves the pr portion from the M resulting in formation of mature virus particle. The mature virions subsequently become fusogenic and infectious (Nambala and Su, 2018; Zhang et al., 2018). It has been reported that the S139Nin prM is involved in neurovirulence in neonatal mice and may explain the association of ZIKV with congenital birth defects (Krauer et al., 2017; Yuan et al., 2017).

1.6.3. Envelope (E) protein

The envelope protein is 504 aa long with a molecular weight of ~53kDa (Dai et al., 2016). The E protein is key to virus infection and is known to interact with multiple cell surface receptors like DC-SIGN, AXL, Tyro3 and TIM-1. This interaction facilitates virus entry into host cells. The viral E protein is an important target for neutralizing antibodies (Agrelli et al., 2019; Gallichotte et al., 2019; Hamel et al., 2015; Richard et al., 2017) and the entire protein or various domains of the protein have been used to develop subunit vaccine candidates.

The E monomer protein has one transmembrane (TM) domain and three structurally distinct ectodomains, I, II, and III. The domain I (DI) is located in the middle to link DII which contains the hydrophobic fusion loop with DIII fold at its C-terminus. A total of ninety E protein dimers are arranged in an icosahedral symmetry and exhibit a "herringbone"- like pattern (Modis et al., 2004). The virion surface is covered with 30 rafts and each raft structure is formed by three parallel array of E dimers. The hydrophobic fusion loop located within DII is covered by the DIII of the neighboring protomer in pre-fusion state. After synthesis, E protein heterodimerizes with prM rapidly resulting in proper folding (Li et al., 2008). The heterodimers in the ER membrane form trimeric spikes and bud off with nucleocapsid containing immature virions. Subsequently, the fusion loop is exposed and inserts into the cell membrane leading to endosome acidification and formation of mature virus particles (Li et al., 2008; Sirohi et al., 2016; Zhang et al., 2017). Like other Flavivirus members, ZIKV E protein is the major target for the neutralizing antibody responses (Beltramello et al., 2010; Oliphant et al., 2005)

and contains multiple neutralizing epitopes. ZIKV E specific antibodies have been used for the detection of ZIKV infection. (Sapparapu et al., 2016; Zhao et al., 2016). The structural changes in the E protein can affect the virus ligand interactions like cell receptors, antibodies, and drugs (Zhang et al., 2017). Therefore, E protein targeted drugs and monoclonal antibodies have been used to block the entry of ZIKV (Li et al., 2019).

1.6.4. Nonstructural (NS) proteins

1.6.4.1. NS1

ZIKV NS1 is a 352 aa multifunctional, highly immunogenic glycoprotein. Depending on its glycosylation status, the molecular weight of the protein ranges from ~46 to ~54 kDa (Muller et al., 2012; Rastogi et al., 2016). Flavivirus NS1 is known to homodimerize and translocate to the ER lumen where it aides in virus replication. The NS1 monomer contains three domains: (i) a β- hairpin domain present at the amino (N)-terminal, (ii) a wing domain, and (iii) β- ladder domain at the carboxy (C)-terminal (Hilgenfeld, 2016). Structural studies suggest interaction between the flexible loop present at the N- terminal of NS1 with E and prM and these interactions are essential for the production of mature virus particles (Scaturro et al., 2015). The subcellular localization of NS1 can either be in the cytosol or associated with the cell membrane or can also be secreted as hexamers (Somnuke et al., 2011; Viranaicken et al., 2017). In addition to its role in virus replication, the NS1 protein is also known to play an important role in the evasion of host immune response (Rastogi et al., 2016). The presence of NS1 can also be useful in the diagnosis of ZIKV infection (Kam et al., 2019).

1.6.4.2. NS2

Flavivirus NS2 is encoded as a single immature polypeptide which is further processed into the mature proteins, NS2A and NS2B. The aa length of NS2A and NS2B are 226 and 130, respectively (Sirohi and Kuhn, 2017). The flavivirus NS2 protein is a transmembrane polypeptide that associates with the ER membranes and orchestrates the formation of viral replication complexes (Xie et al., 2013). NS2A functions as an antagonistic factor to the host immune responses and is required for the proteolytic processing and proper functioning of NS1 (Leung et al., 2008). NS2B is known to associate with NS3 and serves as an essential cofactor for NS2B-NS3 protease activity (Arias et al., 1993; Xie et al., 2013). It has been demonstrated that an alanine to valine substitution at residue 175 of NS2A (A175V) affects viral RNA synthesis and leads to viral attenuation in immunodeficient mice (Marquez-Jurado et al., 2018).

1.6.4.3. NS3

NS3 is 617 aa long with a molecular weight of ~82 kDa and is the second largest protein encoded by the ZIKV genome after NS5 protein (Rodriguez et al., 2019). The NS3 protein contains two separate domains, namely, (i) a serine and a chymotrypsin protease domain (NS3Pro) at the N-terminal region, and (ii) RNA helicase (NS3Hel) and RNA triphosphatase (NTPase) domain at the C-terminal region (Hill et al., 2018; Li et al., 2018b; Phoo et al., 2018). The C-terminal helicase domain comprises NTPase pocket and a RNA binding tunnel (Tian et al., 2016a; Tian et al., 2016b). The NTPase pocket contains a highly flexible P-loop while the RNA binding tunnel contains a RNA binding loop that are important for the helicase function of NS3 (Giri et al., 2016; Tian et al., 2016a; Tian et al., 2016b). Additionally, NS3 associates with NS2B and forms an active

protease complex (Falgout et al., 1991). NS3 is known to interact with NS5 protein to stimulate its helicase activity (Xu et al., 2019). ZIKV NS3 has also been implicated in abnormnal brain development and has been shown to induce brain calcification in human fetuses, contributing to the ZIKV induced pathology in the fetal brain (Chen et al., 2021). These findings demonstrate the critical involvement of NS3 protein in flavivirus replication, virion assembly, and pathogenesis (Chambers et al., 1993) and therefore, can serve as an important target to curb flavivirus replication. Indeed, several inhibitors targeting the ZIKV NS3 have been developed in recent years and they have been shown to inhibit virus replication (Choudhry et al., 2019; Coluccia et al., 2020; Kumar et al., 2018; Pathak et al., 2020).

1.6.4.4. NS4

ZIKV NS4 consists of two mature proteins, NS4A and NS4B which are cleaved from the immature NS4 peptide by NS3 and other cellular proteases (Sun chen, 2017). NS4A is 127 aa and NS4B is 251 aa in length and are separated by a small linker, 2K, peptide of 23 amino acids (Sirohi and Kuhn, 2017). NS4 serves as a critical component of the viral replication complex, responsible for the replication of the viral genomic RNA. It also plays a crucial role in evasion of host immune mechanisms by antagonizing the JAK-STAT and RLR signaling pathways (Gerold et al., 2017; Ma et al., 2018). Additionally, ZIKV NS4A and NS4B have been implicated in ZIKV induced disease and are shown to induce autophagy and subsequent cell death in human neural stem cells by inhibiting the Akt-mTOR signaling cascade. This is a probable mechanism by which ZIKV depletes neural stem cells in a developing brain and likely causes microcephaly

(Liang et al., 2016).

1.6.4.5. NS5

NS5 is 903 aa in length and thus the largest protein encoded by ZIKV. It is the viral RNA-dependent RNA polymerase (RdRp) that is responsible for replication of the viral genome. NS5 is the most conserved flavivirus protein (Chen et al., 2018). NS5 consists of two domains; (i) the amino-terminal methyltransferase (MTase) domain and (ii) the carboxy-terminal RNA-dependent RNA polymerase (RdRp) domain (Davidson, 2009). Both domains work together to catalyze RNA polymerization (Elshahawi et al., 2019). During virus genome replication, the RdRp domain uses the genomic positive-sense RNA as a template to synthesize the negative-sense RNA which in turn serves as the template for generating more positive-sense strands for progeny production (Bollati et al., 2010). The MTase domain interacts with NS3 to facilitate the capping of the newly synthesized viral RNA at guanine N-7 and ribose 2'-O positions (Zhou et al., 2007). Additionally, NS5 plays a major role in antagonizing the host immune response and inducing the immune evasion mechanisms. It has been demonstrated that ectopic expression of ZIKV NS5 results in the proteasomal degradation of human signal transducer and activator of transcription 2 (STAT2), a crucial component of type 1 interferon induced antiviral immunity, thereby leading to suppression of host antiviral response (Grant et al., 2016; Kumar et al., 2016; Wang et al., 2017). Additionally, recent studies also demonstrate an additional mechanism by which the NS5 protein of ZIKV may inhibit host antiviral response. The interaction between TBK1 and NS5 results in the deactivation of TBK1, thus preventing TBK1 mediated IRF3 phosphorylation and type 1

IFNs production (Best, 2017; Lin et al., 2019). These studies demonstrate the pivotal role of NS5 in viral replication and host immune evasion and form the basis of antiviral drug design targeting the viral NS5 protein (Pattnaik et al., 2018; Sariyer et al., 2019; Yuan et al., 2020).

1.7. Life cycle of ZIKV

The dramatic increase of ZIKV infection and its association with neuronal diseases in 2015-16 can be attributed to rapid urbanization with increased population growth, lack of sanitation, and ineffective mosquito control. The virus maintains a sylvatic cycle in non-human primates and mosquitoes in the forest (Valentine et al., 2019). In the urban cycle, the virus is transmitted to humans by *Aedes* group of mosquitoes and then to other humans by either mosquito vectors or through body fluids from infected individuals. Typically, virus inoculation in humans occurs by mosquito bites in the epidermal cells and is transported to the nearest draining lymph node by specialized skin-resident dendritic cells, known as Langerhans cells (Hamel et al., 2015). This leads to the infection of other cell types that include mononuclear phagocytic cells like monocytes and macrophages which results in viremia. ZIKV has a broad tissue tropism and is known to infect cells in many different organs such as the brain, eyes, spleen, and organs of the reproductive system. The virus is known to infect the placentas of developing fetuses and can also infect the fetus *in utero* resulting in a variety of developmental complications and fetal demise (Miner and Diamond, 2017).

The life cycle of ZIKV (Fig. 1.3) is a multistep process, which begins with the virion E protein attaching to the cell surface receptors such as DC-SIGN, AXL, Tyro3 and TIM-1

(Hamel et al., 2015; Richard et al., 2017; Sirohi and Kuhn, 2017). This facilitates virus entry into host cells through clathrin-mediated endocytosis (Li et al., 2020). Furthermore, the endocytosed virion travels to early endosome compartment where the acidic pH of the early endosome triggers conformational modifications in the virion leading to the release of the genomic viral RNA into the cytoplasm subsequently leading to initiation RNA translation (Gratton et al., 2019; Mohd Ropidi et al., 2020). The viral RNA is translated into a single polypeptide containing an ER localization signal which leads to translocation of the polyprotein onto the ER surface where it is cleaved by host and viral proteases to form the structural and non-structural proteins (Tomar et al., 2017). Viral genome replication is initiated by the newly synthesized NS proteins to generate a full complement of the negative-sense RNA that can form a dsRNA intermediate with the incoming viral genome. The negative-sense RNA then serves as the template for new viral genome copies (Lindenbach and Rice, 2003). The newly synthesized copies of the viral genome are further translated and replicated leading to accumulation of viral proteins and genome copies in the infected cell. The viral proteins interact with different ER resident chaperones to undergo post-translational modifications resulting in the assembly of immature progeny virions. During transport through the secretory pathway, prM molecules are cleaved by the host furin-like proteases in the trans-Golgi region into pr and M polypeptides, which results in mature virus particles that exit the host cell by budding (Caldas et al., 2020; Cortese et al., 2017; Hamel et al., 2015; Mohd Ropidi et al., 2020).

1.8. Animal models

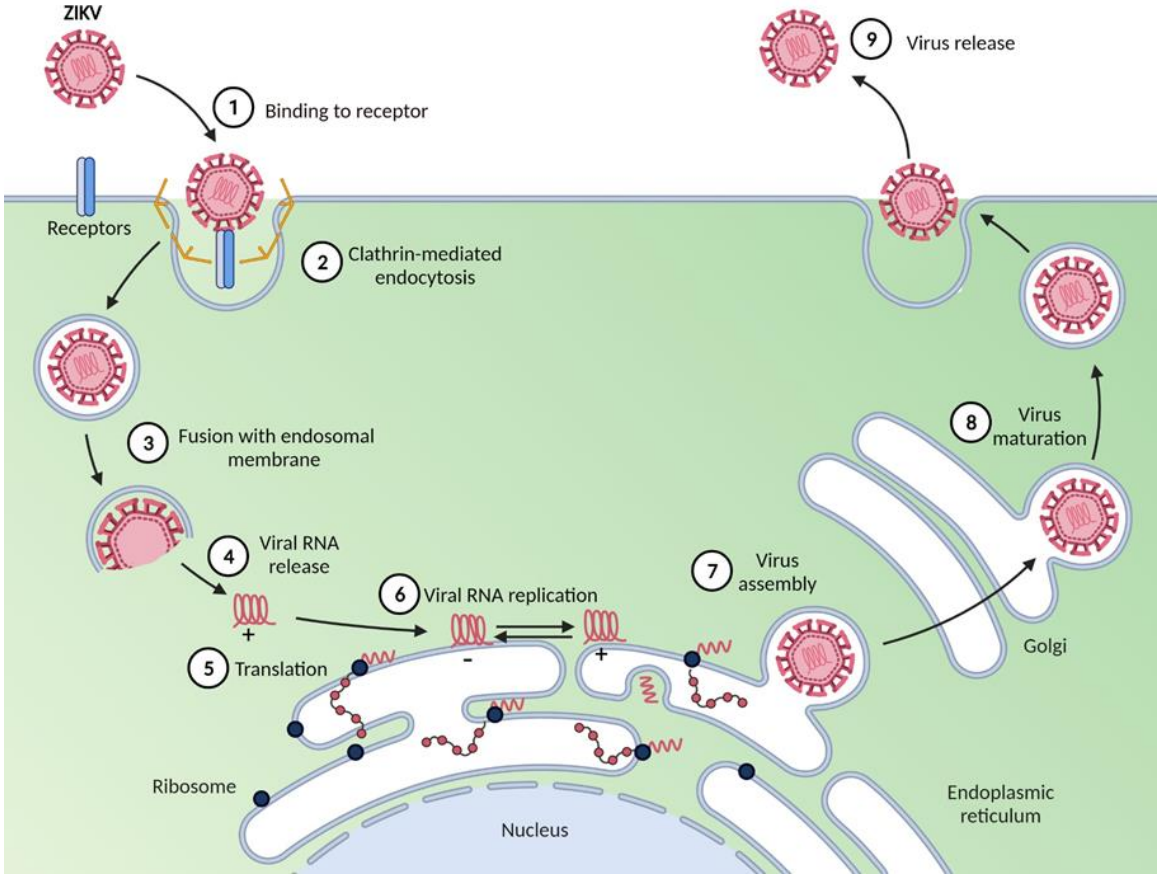

Fig. 1.3. Schematic of ZIKV life cycle. Virus binds to cell surface receptor(s) through the viral E protein (1) and is internalized by receptor-mediated endocytosis (2). Low pH-mediated conformational change in the E protein leads to the fusion of the endosomal membrane with the viral envelope (3). The genomic RNA is released (4) for translation (5) to produce viral proteins by the ER-associated ribosomes (5). The viral genome is replicated by the viral replication proteins to produce more copies of the genomic RNA (6), which are then assembled in the ER along with the structural proteins (7) to produce immature particles. Transport through the trans-Golgi network allows virus maturation (8) to occur and the virus is finally released from the cell (9) by exocytosis.

The recent ZIKV outbreak in 2015-16 was a public health emergency due to increase in the rate of ZIKV induced microcephaly in infants and GBS in adults. In response to this thread, different animal models to investigate ZIKV biology and pathogenesis and to evaluate vaccines and therapeutics were developed. In the past few years, various strains of ZIKV inoculated at different infectious dosages were studied in multiple mouse strain like C57BL/6, BALB/c and CD-1 mice models (Bradley and Nagamine, 2017; Morrison and Diamond, 2017). The inoculation studies in wild-type mice exhibited no disease signs or transient viremia with low levels or no detection of viral RNA/infectious virus titer in different tissue reservoirs such as the brain, spleen, liver, blood, and the reproductive system. (Larocca et al., 2016; Lazear et al., 2016; Rossi et al., 2016b). A possible mechanism for ZIKV infection resistance in immunocompetent mice is that, unlike in humans, ZIKV NS5 does not efficiently degrade murine STAT2, resulting in the inhibition of ZIKV replication (Grant et al., 2016; Kumar et al., 2016).

Studies have suggested that immunocompromised mice, especially mice deficient in the IFN signaling pathway, are highly susceptible to ZIKV infection, thus serving as models for studies on ZIKV pathogenesis (Bradley and Nagamine, 2017; Morrison and Diamond, 2017). ZIKV infections in immunocompromised mice models such as interferon α β receptor knock out (A129) mice , interferon α β and γ receptor knock out (AG129), and *Irf3, Irf5, Irf7* as well as STAT1 gene knockout animals present with symptoms including ruffled fur, ataxia, tremor, weakness, and limb paralysis, and succumb to infection in an age dependent manner. Such models can be used to recapitulate ZIKV infections in humans (Aliota et al., 2016a; Kamiyama et al., 2017; Lazear et al., 2016; Li et al., 2016a; Rossi et al., 2016b; Weger-Lucarelli et al., 2017).

Due to the high cost and tardy availability of such knockout mouse strains, alternative approaches such as pre-treatment with IFNAR1 blocking antibodies in wild type C57BL/6 mice and other models such as guinea pigs and hamsters are being developed to counter such issues (Siddharthan et al., 2017; Smith et al., 2017). Several groups have also used non-human primates (NHPs) such as pigtail macaques, rhesus and cynomolgus macaques to study ZIKV biology and pathogenesis owing to increased clinical relevance (Adams Waldorf et al., 2011; Aliota et al., 2016b; Dudley et al., 2016; Osuna et al., 2016).

1.9. Current status of ZIKV vaccines

The unprecedented magnitude of the ZIKV epidemic and the severity of disease prompted the global research community to understand the immunopathogenic mechanisms of the virus and to rapidly develop safe and efficacious vaccines. Multiple ZIKV vaccine candidates under various platforms have been developed over the last four years (Barouch et al., 2017; Diamond et al., 2019; Poland et al., 2019; Shan et al., 2018). Since ZIKV shares considerable genetic and structural similarities with other flaviviruses, cross-reactive and/or poorly neutralizing antibodies could be generated as a result of flavivirus/ZIKV infection or vaccination. Such antibodies can potentially lead to antibody-dependent enhancement (ADE) of virus infection and disease (Bardina et al., 2017; Castanha et al., 2017; Dejnirattisai et al., 2010; Dejnirattisai et al., 2016; Halstead, 2003; Kawiecki and Christofferson, 2016; Priyamvada et al., 2016). Thus while considering developing vaccine candidates for ZIKV, attention must be placed on preventing ADE. In this regard, recent studies have demonstrated that the DIII domain of

the ZIKV E protein induces a neutralizing antibody response without exhibiting ADE (Cabral-Miranda et al., 2019; Tai et al., 2019).

Several different ZIKV vaccine candidates under different platforms have now been developed and tested in preclinical and clinical trials (Pattnaik et al., 2020). These include nucleic acid vaccines (DNA and RNA vaccines), inactivated whole virus vaccines, live attenuated vaccines, virus-vectored vaccines, purified protein antigen vaccines, and virus-like particles (Fig. 1.4).

1.9.1. Nucleic acid vaccines

Both DNA- and mRNA-based vaccines have been developed and tested in preclinical studies. The proof-of-concept for use of a DNA vaccine against ZIKV was first developed using plasmids containing coding sequences of the viral prM-E regions, and later using the coding sequence of viral NS1, and examining immune responses in mice (Larocca et al., 2016) and NHPs (Abbink et al., 2016). In these studies, the plasmid constructs generated prM-E, M-E (with deletion of pr region) or NS1 proteins and induced high levels of neutralizing antibodies when the plasmid DNA was injected into mice or NHPs (Abbink et al., 2016; Dowd et al., 2016; Larocca et al., 2016). The NS1-specific antibodies were found to be long-lasting and were responsible for Fc-mediated effector functions for protection (Bailey et al., 2018). Additionally, other DNA vaccines made by replacing the signal sequence of ZIKV prM-E at the N-terminus and 98 C-terminal aa of E with corresponding sequences of JEV prM-E or the signal sequence of immunoglobulin (Muthumani et al., 2016) were also shown to protect immunocompromised mice during pregnancy from disease, against vertical transmission and fetal demise (Jagger et al., 2019).

Due to the inherent instability of mRNA and its ability to activate innate immune signaling pathways, use of modified nucleosides during *in vitro* transcription was shown to render mRNAs less immunogenic (Kariko et al., 2005) and also enhanced its translational capacity (Andries et al., 2015; Kariko et al., 2008). Thus, prM-E mRNAs synthesized *in vitro* in the presence of the modified nucleoside, 1-methylpseudouridine and encapsulated with lipid nanoparticles (LNP) induced a robust neutralizing antibody response and ZIKV-specific cellular responses that conferred complete protection from virus challenge when injected into immunocompetent mice and rhesus macaques (Pardi et al., 2017; Richner et al., 2017a). Using a prime-boost approach, these mRNA vaccines were shown to mediate protection against ZIKV virus-induced congenital disease (Richner et al., 2017b) and protect immunocompetent and immunocompromised mice during pregnancy (Jagger et al., 2019). With the development of infectious molecular clones of many wild-type and vaccine strains of flaviviruses, it has been possible to generate live attenuated vaccine candidates through genetic manipulation by two major strategies: (i) introducing specific attenuating mutations into ZIKV genome, and (ii) generating chimeric flaviviruses expressing the prM-E genes of ZIKV in the genetic background of DENV, JEV, or YFV. Engineering 10 or 20 nt deletions within the 3′-UTR of ZIKV genome resulted in virus attenuation. The virus conferred sterilizing immunity in immunocompromised mice and in NHPs. Responses in mice exhibited high titers of neutralizing antibodies and a robust T cell response, and prevented testis damage by wild type ZIKV (Shan et al., 2017a; Shan et al., 2017b). Additionally, studies from our laboratory have shown that by eliminating glycosylation sites in E and/or NS1

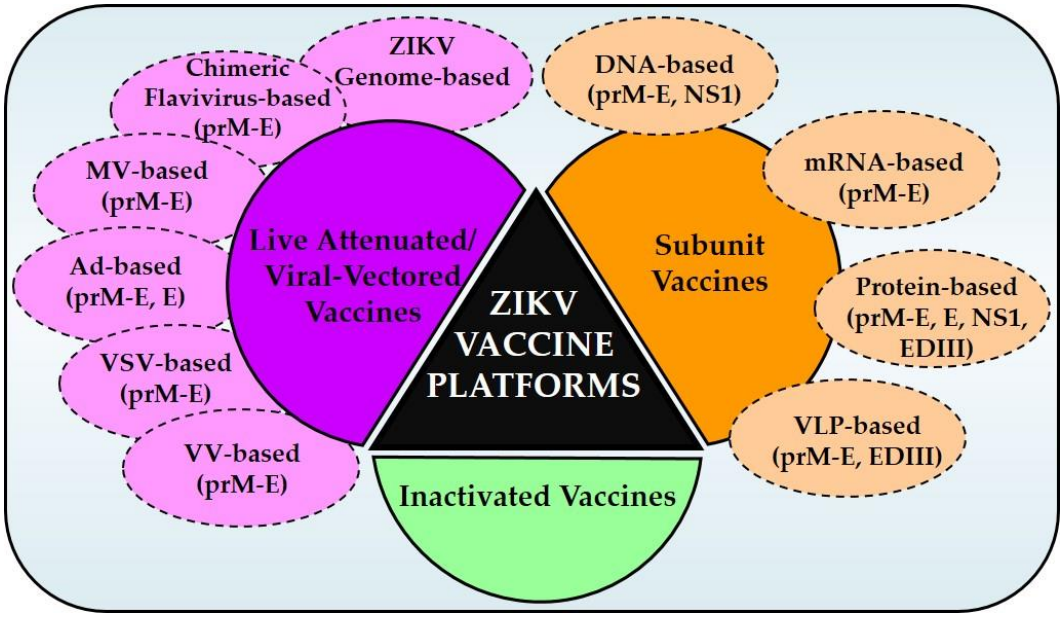

Fig. 1.4. Schematic of various ZIKV vaccine platforms. Three major platforms: inactivated, subunit, and live attenuated/viral-vectored vaccines have been used to generate a number of vaccine candidates for preclinical and clinical testing. A variety of approaches and immunogens as shown were used. MV, measles virus; Ad, adenovirus; VSV, vesicular stomatitis virus; VV, vaccinia virus. The figure is reproduced from Pattnaik, A. et al., (2020).

proteins, the mutant viruses were attenuated, induced robust neutralizing antibody responses as well as T cell responses and conferred protection in immunocompromised mice (Annamalai et al., 2019; Annamalai et al., 2017).

Chimeric DENV serotype 2 and JEV-encoding ZIKV prM-E proteins in place of their corresponding proteins, have also been shown to protect mice and NHPs from ZIKV challenge as well as from placental and fetal damage (Li et al., 2018a; Xie et al., 2017). Perhaps the most interesting live attenuated chimeric ZIKV vaccine candidate that has entered phase I clinical trials (NCT03611946) is the chimeric vaccine generated using the backbone of DENV serotype 4 that expresses the prM-E proteins of ZIKV. This live chimeric vaccine candidate, rZIKV/D4Δ30-713, contains a 30-nucleotide deletion in the 3'-UTR of DENV genome that results in reduced replication and significant attenuation in NHPs and humans. One of the major challenges for an efficacious ZIKV chimeric vaccine based on DENV or JEV as genomic backbones is the presence of pre-existing immunity against these flaviviruses. Since there are cross-reactive antibodies in flavivirus endemic areas, it is possible that these antibodies could inhibit or alter the immune responses elicited by a flavivirus-based chimeric ZIKV vaccine. Additionally, as discussed above, such pre-existing antibodies could also enhance vaccine-mediated pathogenicity, possibly via ADE.

1.9.2. Vaccines employing other recombinant viral vectors

Replication-competent or -defective viral vectors expressing the prM-E genes of ZIKV have also been developed as vaccine candidates. These include vesicular stomatitis virus (VSV), measles virus (MV), vaccinia virus, and adenovirus (Ad). Attenuated

versions of a recombinant VSV and measles virus expressing the prM-E of ZIKV protected ZIKV challenged mice and NHPs (Betancourt et al., 2017; Nurnberger et al., 2019). A vaccinia virus-based single vector construct expressing prM-E of ZIKV and the structural proteins of chikungunya virus (C-E3-E2-6K-E1) induced neutralizing antibody responses to both viruses in immunocompetent and immunocompromised mice and blocked viremia and ZIKV vertical transmission (Prow et al., 2018). Several adenovirus vectors expressing prM-E and/or E alone have also been developed and shown promise as potential vaccines for ZIKV (Abbink et al., 2016; Abbink et al., 2017; Bullard et al., 2018; Guo et al., 2018; Hassan et al., 2019; Larocca et al., 2016; Xu et al., 2018).

1.9.3. Virus-like particle (VLP) vaccines and subunit protein vaccines

VLP containing ZIKV prM-E have been generated in various expression systems and examined for their ability to induce neutralizing antibody response as well as cellular immune responses. The DNA- and RNA-based vaccines and recombinant viral vectors described above generated VLPs directly in the animals for the induction of a protective immune response. However, the use of various expression systems to generate and purify the VLPs for administration into animals has advantages in that the animals respond to only the viral antigens without any other components. Several such vaccine candidates have been tested in preclinical studies and shown to induce neutralizing antibody and cellular immune responses (Boigard et al., 2017; Dai et al., 2018; Espinosa et al., 2018; Garg et al., 2020) and protect immunocompromised mice against lethal virus challenge (Espinosa et al., 2018). In an attempt to avoid antibody dependent enhancement (ADE), several groups have developed subunit vaccines by expressing only the domain III

(EDIII) of the E protein. Such vaccine candidates have been shown to elicit neutralizing antibody response in immunocompetent mice and sera obtained from such animals were able to neutralize ZIKV *in vitro* (Yang et al., 2017a). In another study, the modification of EDIII protein to shield a non-neutralizing epitope induced significantly higher neutralizing antibodies in mice and fully protected pregnant mice and their fetus against lethal challenge (Tai et al., 2019).

1.10. Recent developments in antiviral drugs

With the explosion of ZIKV cases in the Americas in 2016 and its association with neurological and congenital diseases, intense efforts were made towards the development of a number of drug candidates that could be tested in preclinical and clinical trials. So far, a wide range of drugs targeting different steps of ZIKV lifecycle have been shown to effectively inhibit the virus *in vitro* and *in vivo*. Upon infection of cells, ZIKV goes through a series of steps to produce infectious progeny virions. This multistep process starts with the virus attachment to the cell surface receptor and ends with release of mature infectious virus particles. Thus, several inhibitors targeting different steps of the virus lifecycle have been explored as potential antivirals.

1.10.1. Inhibitors and drugs targeting the viral proteins

The interaction of ZIKV E protein with cell surface receptors like Axl, TIM1, and others is the first step in the infection process, and several drugs have been studied that target this interaction (Jemielity et al., 2013; Meertens et al., 2017; Wells et al., 2016). Several natural compounds such as EGCG (a polyphenol present in green tea), Curcumin

(the active ingredient of turmeric) and Nanchangmycin (an antibiotic obtained from *Streptomyces nanchangensis*) have been shown to inhibit the interaction of ZIKV E protein with cellular receptors thereby inhibiting its internalization into host cells (Carneiro et al., 2016; Mounce et al., 2017; Rausch et al., 2017). Additionally, the chemical compound ZINC33683341, Chloroquine (a FDA-approved antimalarial drug), Suramin (an anti-parasitic drug) have been reported to prevent virus infection in host cells by a similar mechanism (Albulescu et al., 2017; Fernando et al., 2016; Li et al., 2017).

ZIKV NS2B-NS3 are critical components of a 'two protease system' that is essential for viral replication and maturation (Kang et al., 2017). Various synthetic compounds such as CN-716 (a boronic acid containing dipeptide), AMPB (5-amino-1-((4-methoxyphenyl)sulfonyl)-1H-pyrazol-3-yl ben-zoate) as well as the broad spectrum serine protease inhibitor, Aprotinin, have been shown to strongly inhibit the protease activity of ZIKV NS2B-NS3 that leads to inhibition of virus replication (Chen et al., 2016; Lei et al., 2016; Li et al., 2018b; Shiryaev et al., 2017). Furthermore, several polyphenol-based compounds (such as myricetin, picatechin gallate, astragalin, etc.), metallopeptides, and novobiocin (am anti-bacterial drug) have also been reported to target ZIKV NS2B-NS3 and suppress virus replication (Bernatchez et al., 2020).

ZIKV NS5 also serves as an ideal target for the development of antiviral drugs. NS5 has both RdRp and methyltransferase activities and several drugs have been demonstrated to inhibit virus replication by directly targeting it. Adenosine analogues NITD008 and 7DMA (7-deaza-2′-C-methyladenosine) have been shown to potently suppress ZIKV replication in cultured cells and reduce viremia and mortality in

immunocompromised mice (Deng et al., 2016; Zmurko et al., 2016). Interestingly, the clinically approved HCV inhibitor, Sofosbuvir and the broad spectrum inhibitor, Galidesivir, have been tested in pregnant women and are shown to reduce disease severity and prevent vertical and sexual transmission of ZIKV (Bernatchez et al., 2020; Ferreira et al., 2017; Julander et al., 2017; Mesci et al., 2018; Mumtaz et al., 2017). Additionally, non-nucleoside RdRp inhibitors have also been reported that allosterically bind to the polymerase active site and interfere with nucleotide incorporation and reduce viral load in mice (Pattnaik et al., 2018).

In addition to the above mentioned classes of inhibitors, several other compounds have been described that suppress ZIKV replication by interfering with viral fusion with autophagosomal membranes, viral assembly, and nucleoside biosynthesis (Bernatchez et al., 2020; Boldescu et al., 2017; Delvecchio et al., 2016; Li et al., 2017).

1.10.2. Inhibitors and drugs targeting the viral genomes that form G-quadruplex structures

The guanine (G)-rich regions in DNA and RNA sequences can fold into four-stranded, right-handed helical structures resulting in the formation of non-canonical secondary structures in which the strands are stabilized by Hoogsteen hydrogen-bonded four guanine bases to form a planar G-quartet or G-tetrad (Gellert et al., 1962; Sasisekharan et al., 1975; Zimmerman et al., 1975). The Hoogsteen hydrogen bonds are formed between N7 groups of one guanine with the exocyclic amino group of the neighboring guanine, leading to planar association of four guanines that are held together by eight such hydrogen bonds to form the G-quartet (Fig. 1.5 A). Stacking of two or more

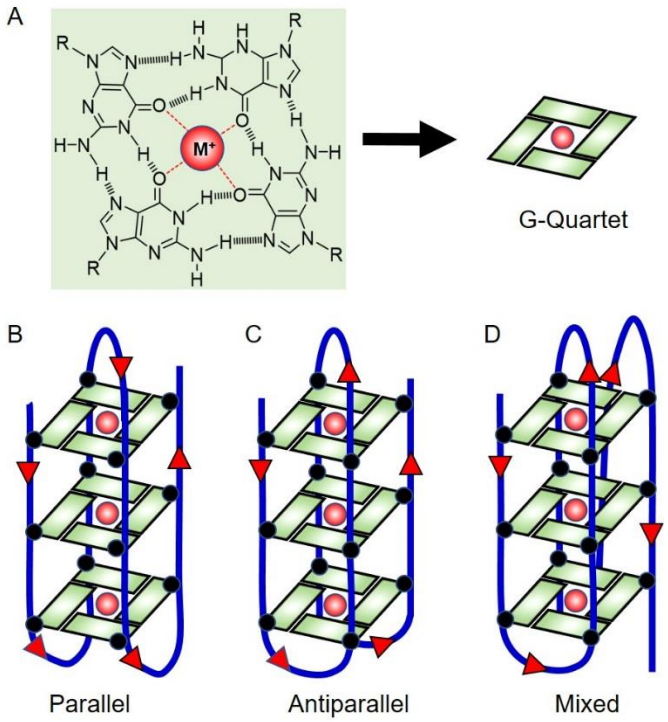

Fig. 1.5. G-Quadruplex structure. (**A**) Four Hoogsteen hydrogen-bonded guanosine residues form a planar structure called G-quartet with a metal ion (M^+). Stacking of two or more such G-quartets results in G-quadruplex structures of parallel (**B**), antiparallel (**C**), and mixed (**D**) topologies.

of such G-quartets upon each other can be stabilized by monovalent cations such as K^+ and Na^+ that are centrally coordinated to O6 atoms of the guanines resulting in the formation of G-quadruplex structures (GQs) (Sen and Gilbert, 1990). Depending upon the sequence of the G-rich regions in the nucleic acids, the structure of the GQs can be highly polymorphic and diverse. The GQs can be formed with one strand of DNA or RNA (intramolecular) or can be formed from two or four separate strands of nucleic acids (intermolecular). Additionally, the topology (parallel, antiparallel, or mixed; Fig. 1.5 B-D), stability, and the dynamics of the GQs appear to be determined by a number of factors including the conformational state of the glycosidic linkage (*anti* or *syn*) between the guanine base and the sugar moiety, number of G tetrads, loop length and sequence composition, directionality of the strands, molecular crowding, etc. (Arora et al., 2009; Burge et al., 2006; Cheng et al., 2018; Guedin et al., 2008; Qin and Hurley, 2008; Sahakyan et al., 2017; Sattin et al., 2013; Shrestha et al., 2017).

A large body of literature over the past two decades suggest that the GQs play crucial regulatory roles in a number of biological processes such as DNA replication, repair, transcription, translation, telomere maintenance, meiosis, etc. (Biffi et al., 2013; Eddy and Maizels, 2006; Eddy et al., 2011; Rhodes and Lipps, 2015; Sen and Gilbert, 1988). Genome-wide analyses have revealed the prevalent existence of GQ-forming sequences as conserved *cis*-acting regulatory elements in human and other eukaryotic genomes (Bedrat et al., 2016; Huppert and Balasubramanian, 2005; Verma et al., 2008) and that such sequences play important roles in biological processes involving DNA and RNA (Du et al., 2008; Maizels and Gray, 2013; Rhodes and Lipps, 2015; Verma et al., 2008). Over the years, considerable attention has been directed at developing search

engines, analysis tools, and algorithms to predict the presence of GQs in the genomes of living organisms. With the development of sophisticated algorithms and analysis tools, the GQs have been predicted to exist in prokaryotes, eukaryotes, as well as in viruses, parasites, and fungi. In general, to search for GQ structures predictive models use the consensus sequence motif of four runs of at least three guanines separated by one to seven short stretches (loops) of any of the four nucleotides (5' G3+N1-7G3+N1-7G3+N1-7G3+ 3' where N is any nucleotide) (Huppert and Balasubramanian, 2005; Todd et al., 2005), although prediction for less stable GQ structures with variations in loop length, discontinuities in G-stretches or GQs with only two tetrads have been incorporated in some algorithms. Furthermore, methods have been developed to experimentally detect and map GQ structures in the genomes of model organisms including human, mouse, and several pathogens (Chambers et al., 2015; Marsico et al., 2019). Overall, the data from these studies reveal that the locations of the observed GQs are not random, particularly in human and mouse; rather, they are enriched in gene regulatory regions such as in the promoter regions and transcription start sites of many cellular genes and oncogenes as well as in repetitive regions such as telomeres. These studies support the prediction from computational and cellular analysis of human genome for potential regulatory roles of GQs (De and Michor, 2011; Hansel-Hertsch et al., 2016).

The GQ-forming sequences have also been predicted to be present in the genomes of all known human viruses (Lavezzo et al., 2018) including recently emerged ZIKV (Fleming et al., 2016), SARS-CoV-2 (Cui and Zhang, 2020). As a result, studies in recent years have focused on the possibility of using these GQ structures as antiviral targets. In support of this possibility, ligands such as Braco-19, TMPyP4, pyridostatin (PDS), etc.

that specifically bind and stabilize GQ structures have been shown to inhibit replication of a number of viruses such as human immunodeficiency virus 1 (Butovskaya et al., 2019), hepatitis C virus (Wang et al., 2016a), Ebola virus (Wang et al., 2016b), etc. Therefore, it is likely that GQ-binding and -stabilizing ligands could be used to inhibit ZIKV replication.

1.11. Hypotheses and objectives in this doctoral thesis

The recent reemergence and large-scale spread of ZIKV and its association with serious neurological disorders, necessitates the development of antiviral countermeasures for the prevention and treatment of ZIKV infections. With no vaccines or antiviral drugs approved for use against ZIKV infections, there is an urgent need to explore strategies to develop viral countermeasures such as established vaccine platforms and drug re-purposing efforts. Alternative strategies such as use of innovative vaccine platforms, screening for small molecule chemical libraries based on their ability to specifically bind viral macromolecules and inhibit viral replication should also be investigated. In recent years, ferritin-based nanoparticles have been used to develop vaccine candidates for a number of viruses. Presentation of multiple copies of an antigen in a repetitive array exemplified by formation of multivalent nanoparticles or nanocages can theoretically induce more potent and long-lived humoral immune responses than the soluble antigen (Lopez-Sagaseta et al., 2016). Based on this premise, we ***hypothesize that ferritin nanoparticles (or nanocages) displaying multiple copies of the DIII domain of ZIKV will produce robust neutralizing antibody responses that will protect the animals from lethal challenge with ZIKV.*** Ferritin nanoparticles self-assemble from 24 subunits

(molecules) into a soccer ball-like structure. Therefore, in one of the objectives of this thesis, we propose experiments to test this hypothesis. A second objective of my thesis is to identify and characterize small molecule inhibitor(s) that target the ZIKV RdRp. Using DENV RdRp as a template, we predicted the structure of ZIKV RdRp which was used for *in silico* screening of a library of compounds. *We* identified a number of small molecule non-nucleoside compounds, including 3-chloro-N-[((4-[4-(2-**t**hienylcarbonyl)-1 **p**iperazinyl]phenyl)amino) carbonothioyl]-1-**b**enzothiophene-2-carboxamide (TPB) that specifically target the catalytic cavity of the RdRp. We ***hypothesize that TPB will inhibit ZIKV replication both in vitro and in vivo and protect animals from ZIKV-induced diseases.*** A third objective of my thesis is to test if drugs and compounds that specifically bind to ZIKV genome would inhibit viral replication and infectious progeny production. This objective is developed based on the recent *in silico* analysis of several ZIKV strains that predicted the presence of non-canonical secondary structures called G-quadruplexes (GQs) in the viral genome. We ***hypothesize that ligands that bind and stabilize GQ structures in ZIKV genome will inhibit virus replication and progeny production. We*** have proposed and conducted studies to test this hypothesis and achieve the objective.

Overall, my thesis presents a set of hypotheses, and the following objectives are developed to test these hypotheses.

1.11.1. Construction and characterization of a nanoparticle based vaccine candidate against ZIKV infection.

The studies and results of this objective are described in chapter III.

1.11.2. Identification and characterization of a non-nucleoside inhibitor of ZIKV RNA polymerase.

The studies and results of this objective are described in chapter IV.

1.11.3. Investigation of ZIKV replication in the presence of G-quadruplex binding ligands.

The studies and results of this objective are reported in chapter V.

CHAPTER II: MATERIALS AND METHODS

2.1. Cell culture

Vero (Cercopithecus aethiops, CCL-81), HEK293T (CRL-3216), HTR-8/SVneo human trophoblast (CRL-3271), SH-SY5Y human neuroblastoma (CRL-2266) and NTERA-2 human embryonal carcinoma (CRL-1973) cells were obtained from ATCC. The cells were grown and maintained in Dulbecco's modified Eagle's medium (DMEM) containing 10% heat-inactivated fetal bovine serum (FBS) and 1X penicillin/streptomycin (PS) solution (complete growth medium) in a humidified incubator with 5% CO_2 at 37 °C. 293-F cells (Cat# R79007) were obtained from ThermoFisher Scientifc and were grown in FreeStyle™ 293 Expression Medium (Cat# 12338018). The cells were grown in sterile conical flasks on a shaker (at 140 rpm) in a humidified incubator with 8% CO_2 at 37 °C.

2.2. ZIKV stock preparation

ZIKV strain PRVABC59 and MR766 were obtained from Barbara Johnson and Brandy Russell at the Centers for Disease Control and Prevention, Fort Collins, Colorado, USA. The viruses were passaged once in Vero cells to prepare stocks. Briefly, 24 hours prior to the infection, Vero cells were set up in a T-75 cell culture flask and allowed to grow to about 90% confluency. Cells were washed with phosphate buffered saline (PBS) followed by infection with either PRVABC59 or MR766 virus at a multiplicity of infection (MOI) of 0.1. For virus adsorption, cells were incubated at 37° C for 1 hour with intermittent shaking every 15 mins to prevent the cell monolayer from drying. The monolayer was then washed with PBS and virus growth medium (VGM)

[DMEM containing 2%FBS, 1X PS, 20 mM hydroxyethyl piperazine ethane sulfonic acid (HEPES), 1 mM sodium pyruvate, and 1X non-essential amino acids] was added. The infected cells were monitored for the development of cytopathic effect (CPE) and on day four post infection, the culture supernatant was harvested and clarified by centrifugation (20000xg) for 10 minutes at 4°C. Small aliquots were made and stored at -80° C until use.

2.3. Plasmids

The plasmid vector pIRES-2-eGFP was obtained from Addgene (Watertown, MA). The expression cassette encoding the soluble ZIKV (MR766) E protein (solE) and *H. pylori* ferritin, termed solE-F was cloned into a pUC57 cloning vector backbone (pUC57-solE-F), commercially synthesized, and obtained from Genscript (Piscataway, NJ). The expression cassette for solE-F was designed keeping restriction sites, coding sequences for ZIKV E, ferritin, and other elements in the following order: NheI, Kozak sequence, Secrecon signal sequence (includes the initiation codon), SmaI/XmaI, solE, linker sequence (aa Ser-Gly-Gly: creating a BspEI restriction site), ferritin, stop codon and NotI. The expression cassette was codon optimized prior to gene synthesis for efficient mammalian cell expression.

2.4. Recombinant DNA construction

2.4.1. DNA cloning

Using restriction sites, NheI and NotI, the expression cassette for solE-F (insert) was digested from the pUC57 cloning vector and cloned into pIRES-2-eGFP expression

vector. Digestion of pIRES-2-eGFP plasmid by NheI and NotI releases a fragment that includes the coding sequence for eGFP (vector) (Fig 3.2A). For the replacement of the consensus secrecon signal sequence with tPA or µ-phosphatase signal sequence, primer combinations A_F and C_R or B_F and C_R (Table 2.1) along with pUC57-solE-F as the template was used to generate DNA fragments encoding tPA or µ-phosphatase signal sequence. For the generation of zDIII-F expression cassette, the solE fragment was replaced with PCR amplified DNA fragment encoding zDIII using primers D_F and C_R (Table 2.1). Q5® High-Fidelity PCR Kit was used for PCR amplification of the DNA fragments. Briefly, a 30 µl reaction mixture contained 15 µl of the Q5 High-Fidelity 2X Master Mix , 1.5 µl (10 µM) each of forward and reverse primers , 1 µl (100 ng/ µl) plasmid DNA template, and 11 µl nuclease-free water (NFW). The PCR cycling conditions were: 1 cycle of 98°C for 30 sec, 35 cycles of 98°C for 10 sec, 58°C for 30 sec and 72°C for 80 sec (depending on fragment size, 40 sec/kb), 1 cycle of final extension at 72°C for 5 min. The PCR amplified fragments were digested with NheI/XmaI and NotI and separated in a 0.8% agarose gel. The DNA fragments were extracted from the gel using a gel purification kit from Thermo Scientific (Cat# K0961) and were subsequently used for ligation in the into pIRES-2-eGFP vector.

2.4.2. DNA ligation

For DNA ligation, a mixture of restriction digested vector and insert fragments in a total volume of 8µl was taken in a microfuge tube followed by the addition of 1 µl T4 ligase buffer (10X) and 1 µl T4 DNA ligase (NEB Cat# M0202S). The mixture was

incubated at room temperature for 4 hr. The ligation mixture was heat inactivated at 65°C for 10 min and chilled on ice before bacterial transformation.

2.4.3. Bacterial transformation

Three µl of the heat inactivated ligation mix was added to 50 µl of competent *E. coli* DH5α bacterial cells followed by incubation for 30 min on ice. The bacterial cells were heat-shocked at 42°C for 90 sec followed by incubation for 5 min on ice. The transformed bacterial cells were re-suspended in 1ml of LB broth incubated at 37°C for 1 hr in a shaker (230 rpm). This was followed by finally, plating on LB agar plates containing Kanamycin (50 ug/ml) for selection of kanamycin resistant clones.

2.4.4. Clone screening and large scale plasmid preparation

Kanamycin resistant bacterial colonies were picked and cultured overnight at 37°C in LB medium containing Kanamycin. Miniprep plasmid extraction was done followed by restriction digestion with appropriate enzymes to confirm bacterial clones containing the expression cassette. Briefly, cultured bacterial cells were pelleted and lysed in 300µl of TENS buffer (10 mM Tris-HCl pH 8.0, 1 mM EDTA, 0.1 M NaOH, 0.5% SDS). The above mixture was neutralized by adding 150 µl of sodium acetate (pH 5.2), was centrifuged and the supernatant was transferred to a new centrifuge tube. For precipitation of plasmid DNA, 2.5 volumes of cold 100% ethanol was added, and the mixture was centrifuged at 13,200 rpm for 5 min. The DNA pellet was washed with cold (-20ºC) 70% ethanol and air-dried. The dried plasmid DNA was resuspended in 30 µl of Tris-EDTA buffer containing 100 µg/ml of RNaseA. The plasmid DNA was checked for

sequence correctness using commercial DNA sequencing services. For large scale plasmid preparation, Qiagen Plasmid Plus Maxi Kit (Cat# 12963) was used. Briefly, bacteria containing the correct plasmid DNA were grown in 500 ml LB medium containing kanamycin. The bacterial cells were pelleted at 6000xg for 15 mins at 4ºC. this was followed by plasmid DNA extraction following the protocol outlined in the kit manual.

2.5. Plasmid transfection and protein expression

HEK293T cells were seeded in a 6-well plate and allowed to grow till ~70% confluency. Plasmid DNA encoding for solE-F or zDIII-F (1 and 2.5 μg) were transfected using Lipofectamine 2000 (Thermo Fisher Cat# 11668027) following manufacturer recommended protocol. Briefly, DNA Lipofectamine mixture was made using the ratio 1:4 in OptiMEM (Thermo Fisher Cat# 31985062) and incubated at RT for 20 mins to facilitate the formation of DNA lipid complexes. Cells were washed with 1X PBS and 250 μl of OptiMEM was added to the monolayer followed by the dropwise addition of an equal volume of the DNA Lipofectamine mixture. The cells were incubated at 37 °C, 5% CO_2 for 6 hr following which the cells were washed with 1X PBS and replenished with complete growth medium and incubated for 2-5 days. For large scale production (500ml) of zDIII-F, 293F cells were seeded at a density of 5-7 x 10^5 cells per ml the day prior to transfection. The following day, the cells were checked for viability using trypan blue dye exclusion assay. DNA transfection was done if the cells were >90% viable and the cell density was ~1 x 10^6 cells per ml. For DNA transfection, plasmid DNA at 1 μg per 1 million cells was mixed with appropriate volume of OptiMEM containing 293Fectin/PEI

(Thermo Fisher Cat# 12347019). The DNA and 293Fectin mixture (1:4) was incubated at RT for 20 mins to facilitate the formation of DNA lipid complexes and was added to the cells. The cells were incubated for 4 days on a shaking platform following which they were pelleted at 8000xg for 20 mins at 4ºC. Cell pellets and the clarified culture medium were checked for protein expression as described below by SDS-PAGE and Western blotting.

2.6. zDIII-F protein purification

The clarified culture medium was filtered through a 0.2 μm filter and buffer exchanged with TN50 buffer containing 20 mM Tris pH 7.5, 50 mM NaCl. The buffer exchange was done using a tangential flow filtration system with a Pellicon® 2 Mini Cassette with an Ultracel® 30 kDa Membrane (Millipore). Protein was then purified from this buffer exchanged media using a 5 ml HiTrap Q FF column (GE Healthcare) and an ÄKTApure system (GE Healthcare). The column was rinsed with 10 CV of TN50 buffer, and then a 20 CV elution gradient from 50-1000 mM NaCl was utilized for elution of the protein. Peak fractions were tested for the presence of the protein by SDS-PAGE, and fractions containing the ZDIII-F protein were pooled and concentrated using a Amicon Ultra centrifugal filter unit with a 100 kDa cut off (Millipore). This was followed by separation of the pooled fractions by size exclusion chromatography (SEC) using a Superdex 200 16/600 pg column (GE healthcare). The elution of the purified protein was done in PBS and fractions were examined by SDS-PAGE. The eluted protein fractions were stored at -80ºC until use. For thermostability analysis, several aliquots of

the purified zDIII-F protein were stored at 4ºC for the indicated lengths of time (refer to Fig. 3.6 C and D)

2.7. SDS-PAGE and gel staining

Elution fractions from ion exchange and size exclusion chromatography were subjected to SDS-PAGE analysis to determine the presence of the purified protein. Protein estimation was done by determining the absorbance at 280 nm with 1 absorbance unit corresponding to 1 mg/ml protein. Briefly, ~1 μg of protein from each fraction was loaded per well on a 4-12% precast polyacrylamide gel and electrophoresed at 200 V for 30 mins. After electrophoresis, the gels were stained with either SimplyBlue SafeStain (Novex Biologicals) for 20 mins or Oriole fluorescent gel stain (BioRad) for 90 mins. Following staining, the gels were washed with deionized water and imaged using a Biorad gel imager.

2.8. Western blotting

For the detection of solE-F, zDIII-F and ZIKV E proteins, western blotting analysis was performed as described (Sahoo et al., 2020). For the preparation of cell lysates, cells were washed with cold PBS, trypsinized, and harvested by pelleting at 500xg for 5 min at 4°C. The cell pellet was resuspended in radio-immunoprecipitation assay (RIPA) buffer (25 mM Tris-HCl, pH 7.6, 150 mM NaCl, 1% Triton X-100, 1% sodium deoxycholate, 0.1% SDS) supplemented with the protease and phosphatase inhibitor cocktail and incubated on ice for 15 min with intermittent vortexing after which the lysates were clarified by centrifugation at 10,000xg for 5 min, 4° C. Total protein

quantification was done using the bicinchoninic acid (BCA) assay kit (Thermo Fisher). Twenty μg of total protein was separated by electrophoresis as described (section 2.7). The separated proteins were transferred onto polyvinylidene difluoride (PVDF) membranes using a Bio-Rad semi-dry transfer system and blocked with 5% non-fat milk in 1X tris-buffered saline (TBS) containing 0.2% Tween 20 (TBS-T). The membranes were incubated with primary antibody against respective proteins: anti-ZIKV E (Genetex Cat # GTX1333325) and anti-ZIKV E DIII (ZV-57; monoclonal antibody obtained from Michael S. Diamond, School of Medicine, Washington University, St. Louis). The primary antibodies were used at a dilution of 1:1,000 in 5% non-fat milk in TBS-T and the membranes were incubated at 4ºC overnight. The membrane was washed three times in TBS-T and incubated for 2 hours at room temperature with HRP-conjugated secondary antibodies, either goat anti-rabbit (Sigma Cat # A6154) or goat anti-mouse (Sigma Cat# 12-349) at a dilution of 1:10,000, in 5% non-fat milk in TBS-T. The membrane was washed three times in TBS-T and bands were detected using enhanced chemi-luminescence (ECL) western blotting substrate (Biorad cat # 1705061) using a Biorad imager.

2.9. Transmission electron microscopy (TEM) imaging of zDIII-F nanoparticles

A 30 ul (100ng/μl) droplet of purified zDIII-F was placed on parafilm and the surface of a carbon-formvar coated copper grid was placed upside down to contact the samples for 1-2 min. After excess specimen was wicked away by touching a piece of filter paper to the edge of the grid surface, the grid with the sample side up was air-dried for ~2 min. The grid was placed upside down on to a drop (30 ul) of 1% phosphotungstic

acid solution for ~2 min. Excess stain solution was wicked from the grid following the staining and air-dried for at least 30 min. Samples were examined and different magnifications of images were collected using a Hitachi H7500 TEM (at 80 KV).

2.10. Molecular modeling and *in silico* screening

The ZIKV RdRp structure was modeled based on sequence homology using the DENV-3 RdRp structure (PDB: 2J7U) (Yap et al., 2007) as a template in Modeller 9 program (Webb and Sali, 2014). *In silico* screening was performed using Molegro Virtual Docker (MVD) software (Molegro ApS, Aarhus, Denmark). The docking site was defined using a ray-tracing algorithm. This resulted in a cavity with a volume of approximately 1034 cubic Å. A receptor grid was built within this cavity with a resolution of 0.2 Å and a radius of 13 Å from the geometric center of the cavity in the ZIKV RdRp model. Structure based docking was done using a library of 100,000 compounds from ChemBridge (Chembridge DIVERSet™ Chemical Library, ChemBridge Corporation, San Diego, California) and the top 10 compounds were selected based on docking scores for experimental validation. All structural modelling and analysis were conducted in the Discovery Studio 4.0 (Biovia, San Diego, CA).

2.11. Preparation of stocks of ZIKV inhibitors

Ten lead compounds (Table 4.1) were purchased from Hit2Lead Company (ChemBridge Corporation, San Diego, California). Each compound was dissolved in dimethyl sulfoxide (DMSO) to prepare stock solutions of 10 mM and 1 mM and was stored at -20º C. The compound 1 (c1) used in this study is 3-chloro-N-[((4-[4-(2-

thienylcarbonyl)-1-piperazinyl]phenyl)mino)carbonothioyl]-1-benzothiophene-2-carboxamide (TPB). Based on 1H NMR and LC-MS (ELSD, DAD 200–400 nm, MSD APCI positive) analyses by the provider, the compound is ≥ 95% pure. Mycophenolic acid (MPA) and Ivermectin (IVM) were purchased from Sigma (St. Louis, MO) and resuspended in DMSO to prepare stock solutions. All the compounds used have ≥ 95% purity. Small-molecule ligands, Braco-19 and TMPyP4, were purchased from Sigma, dissolved in water and DMSO, respectively, for preparation of stock solutions, and stored at -20º C until further use.

2.12. Prediction of putative G-quadruplex (GQ)-forming sequences from the ZIKV genome

A total of 247 complete genome sequences of ZIKV were retrieved from the NCBI Genome database (https://www.ncbi.nlm.nih.gov/genomes). The FASTA sequences of the ZIKV genomes were then used for the prediction of the putative GQ-forming sequences with the help of in-house GQ prediction tool (Lim *et al*, 2017). The search was based on the following algorithm: $G_{\geq 2}N_{1\text{-}7}G_{\geq 2}N_{1\text{-}7}G_{\geq 2}N_{1\text{-}7}\ G_{\geq 2}$ where G corresponds to guanine and N corresponds to any base including guanine. Though the ZIKV is a positive-sense RNA virus, we also sought to find the probable GQ sequences in the anti-sense strand of the viral genome. Further, the consensus sequences for each of the ZIKV GQs studied were generated using the WebLogo software (Crooks *et al*, 2004).

2.13. Plaque assay

Virus stock titration was performed by plaque assay using Vero cells as described

in Annamalai *et al*, 2017. One day before the assay, cells were plated on a 12 well plate at a density of 2x 10^5 cells per well. On the assay day, cells became 90-100% confluent. Serial 10-fold dilutions of virus stock were prepared using VGM and kept on ice. The cell monolayer was washed with 1X PBS and 100 µl of each dilution was added to the monolayer. Virus adsorption was done as described above. Following the virus adsorption, the inoculum was removed, the cell monolayer was washed with 1X PBS and overlaid with 1ml of a 1:1 ratio of 2% low gelling temperature (LGT) agarose (w/v) in water and 2X VGM. After a 5 day incubation at 37°C, the cells were fixed in 10% formaldehyde in 1X PBS for 30 minutes, the agarose plugs were removed, and the monolayers were stained with 0.1% crystal violet in 30% methanol in water. Excess staining solution was washed with water and the plaques were counted manually and expressed as PFU/ml.

2.14. Plaque reduction neutralization (PRNT) test

Vero cells were seeded in 12 well plates 1 day prior to the assay to have a confluency of 90-100% at the time of infection. Serum samples obtained from control and zDIII-F immunized mice at 28 days post vaccination were heat inactivated at 56°C for 30 min. The sera were diluted 1/100 followed by serial 1/2 dilutions. A 50 µl volume containing ~200 plaque-forming units
(PFU) of ZIKV (rMR, PRVABC59 or MEX1-7) was mixed with an equal volume of diluted serum sample and incubated at 37°C for 1 hr. After incubation, the mixture was applied to Vero cell monolayers and the cells were incubated at 37°C for 1 hr with intermittent shaking every 15 min. After the incubation, the inoculum was discarded and

the cells were overlayed with 1 ml of 1% LGT agarose in VGM and incubated for 5 days at 37ºC in a humidified CO_2 incubator. The cells were fixed using 10% formaldehyde in PBS for 30 min and the agarose overlays were removed. The cell monolayers were stained with 0.1% crystal violet in 30% methanol. Plaques were counted manually, and antibody titer was determined as the reciprocal of the serum dilution that inhibited 50% of the infectivity ($PRNT_{50}$).

2.15. Virus inhibition assay

Virus inhibition assays were performed in two ways. In the first approach, Vero cells were seeded in a 96-well plate at a density of 6000 cells per well. A mixture of the compound (1 μM) and the virus (0.1 PFU/cell) was made in VGM and was added to the cells. The cells were incubated for 72 hr at 37º C in a humidified incubator containing 5% CO_2. In a separate experiment, Vero cells were seeded in a 12 well plate at a density of 40,000 cells per well and were infected with the virus at MOI 0.1 and following adsorption, the cells were washed twice in 1X PBS and incubated in VGM containing 1 μM concentrations of the drugs. The cell culture media were collected at 96 hr post-infection and assayed for infectious virus yield by plaque assay. Viral genome copies were determined by quantitative RT-PCR (qRT-PCR). In all subsequent studies, cells in 12-well plates were infected with ZIKV at an MOI of 0.1 PFU/cell and following virus adsorption for 1 h at 37º C, VGM containing various concentrations TPB was added to the cells and incubated as above. Clarified supernatants from the infected cells were then used to determine infectious virus or genome copies as above.

To assess the effect of GQ binding ligands, Braco-19 or TMPyP4, on ZIKV replication, Vero cells were infected with the virus at an MOI of 1. Following adsorption at 37º C for 1 hr, the inoculum was removed and replaced with VGM containing various concentrations of Braco-19 or TMPyP4. Infected cells were incubated at 37º C and small aliquots of infected cell culture supernatants were collected every 24 hr post infection (hpi) till 96 hpi, clarified, and stored at -80°C for virus titration at a later time. To determine the amount of cell-associated infectious virus, after collecting culture supernatants, the cells were subjected to two cycles of freeze-thaw at -80º C in the presence of the same volume of growth medium followed by centrifugation at 20,000xg for 10 min at 4º C. The clarified supernatants were then used to quantify the cell-associated virus by plaque assay.

2.16. Quantitative real time RT-PCR

ZIKV viral RNA was detected using qRT-PCR on a C100 Thermal Cycler and the CFX96 Real-Time system (Bio-Rad). Viral RNA (vRNA) was extracted from culture supernatant, sera, or tissue samples from infected mice using a QIAamp Viral RNA Mini kit (Qiagen). Tissue samples were homogenized using metal beads in 1X DMEM in Bullet Blender® (Next Advance, Inc., New York) with a speed setting of 10 for 5 min at 4ºC. This was followed by clarification of the homogenized tissues by centrifugation at 14,000xg for 15 min at 4ºC and the clarified supernatants were used for viral RNA isolation. TaqMan Fast Virus 1-Step Master Mix (Life technologies) was used, and the determination of viral genome copies was done following manufacturer's recommendation. ZIKV primers and probe used are as follows (ZIKV_F:

CCGCTGCCCAACACAAG; ZIKV_R: CCACTAACGTTCTTTTGCAGACAT; PCR Probe: ZIKV-P: AGCCTACCTTGACAAGCAATCAGACACTCAA). The cycling conditions used were: 50°C for 30 min, and 95°C for 5 min followed by 40 cycles of 95°C for 30 secs, and 58°C for 1min. RNA standard concentrations were determined based on the back calculation with OD values and molecular weights and were generated through serial dilution with $R2 > 0.95$.

For the GQ binding ligands studies**,** total RNA from infected cells at 72 or 96 hpi were isolated using TRIzol RNA isolation reagent (Thermo Fisher Scientific) and viral genomic copy numbers were determined using specific probes and primers. The forward primer (5'-GTC GTTGCCCAACACAAG-3') and the reverse primer (5'-CCAC TAATGTTCTTTTGCAGAC-3') along with the fluorescent probe 5' -/56-FAM (5' -6-carboxyfluorescein)/AGCCTACCT/ZEN/TGACAAGCAATCAGACACTCAA/3IABkFQ (3' -Iowa black fluorescent quencher)/-30 were used to determine the standard curve with an oligonucleotide template spanning E gene sequences at positions 1191to 1268. The real-time PCR assays involved two steps. The first step included the cDNA synthesis from the viral RNA using the SuperScript II (Thermo Fisher Scientific, Waltham, MA, USA). The synthesized cDNAs were then used as templates in the qPCR. The qPCR cycling conditions used were as follows: initial denaturation at 95º C for 10 mins; 35 cycles of 95º C for 30 s, 55.3º C for 30 s, and 72º C for 30 s; and a melt curve from 65° C to 95º C with 0.5º C increments for 5 secs. The reactions were run in CFX Connect instrument (Bio-Rad, Hercules, CA, USA). Viral-genome copy numbers were determined in parallel reactions using RNA samples in duplicate and expressed as copy numbers per mg of total cellular RNA and expressed as $\log_{10}$ copies per µg of total cellular RNA.

2.17. ATP-based cell viability assay

A modified ATP based cytopathic effect (CPE) assay was used for this study based on the CPE method for anti-DENV drug development described previously (Che et al., 2009). Vero cells were seeded at a density of 30,000 cells per well in a black bottomed 96-well plate 24 hr before the experiment. Cell monolayers were treated with various concentrations of the drugs and incubated for 96 hr at 37º C in a humidified incubator containing 5% CO_2. The ATP concentration was measured following manufacturer's recommendations using CellTiter-Glo kit from Promega (Madison, Wisconsin). Luminescence was recorded using a Veritas Microplate Luminometer at 420 nm. The 50% cytotoxic concentration (CC_{50}) was calculated by a non-linear regression analysis of the dose-response curves.

2.18. Determination of cell viability by flow cytometry

Vero cells were seeded in 12-well plates at a density of 20,000 cells per well. They were left untreated or treated with 0, 1, 10 and 100 µM of Braco-19 or TMPyP4 and incubated for 96 hrs. Cell culture supernatant was discarded and the cell monolayer was washed with 1X PBS, trypsinized and pelleted at 500xg for 10 mins. The pellet was re-suspended in staining solution containing propidium iodide (PI, 1 µg/ml, Sigma Aldrich, P4170), and monochlorobimane (mBCl, 10 µM, Molecular Probes, M1381MP) in PBS and incubated at room temperature for at least 20 mins. Cell viability was determined by flow cytometry (FACS, Fluorescence Activated Cell Sorting) using Cytek-DxP-10 (BD Biosciences). PI was detected using the BluYel FL-3 channel (488 nm excitation, 695/40 nm emission) and mBCl was detected using the VioFL1 channel (389 nm excitation and

483 nm emission). 10,000 events were recorded, and dead cells were gated as mBCl positive (-) and PI negative (+). The data analysis was done in FlowJo 7.6.5 software.

2.19. Mouse studies

2.19.1. ZDIII-F vaccination and challenge studies

Three-week old interferon (IFN) α/β receptor knockout mice (A129) were purchased from the Jackson Laboratory (Bar Harbor, ME, USA) and acclimatized for 4 days at the mouse facility at University of Nebraska-Lincoln. zDIII-F (10 μg) in 100 μl of PBS was mixed with 100 μl of Addavax (Invivogen Cat# vac-adx-10) and administered in mice using a 22 gauge needle by the subcutaneous route. PBS was injected to mice in the control group. Following this, the mice were observed daily till 28 days when they were infected with ZIKV (rMR, 10,000 pfu/mouse) by the subcutaneous route. The mice were kept under observation for the development of disease symptoms for 7-10 days during which blood samples were drawn by retro-orbital puncture under anesthesia (isoflurane treatment) on days 2, 4, and 6 post-infection for determination of viral genome copies. For passive transfer experiment, 4-week old A129 mice were injected intravenously with 200 μl of naïve or zDIII-F immunized mice serum. Four hours later, the mice were given a lethal dose of ZIKV (rMR, 10,000 pfu/mouse) and were monitored for the development of disease symptoms for 7-10 days during which blood samples were drawn by retro-orbital puncture on days 2, 4, and 6 post-infection for determination of viral genome copies. Some animals were euthanized at day 4 post lethal challenge and organs (brain, liver, and spleen) were harvested for determination of tissue viral load.

2.19.2. Pharmacokinetic (PK) study

For PK studies, groups of Balb/C mice (n = 6) obtained from the Jackson Laboratory (Bar Harbor, ME, USA) and acclimatized for four days were injected intraperitoneally (IP) with doses of 5 mg/kg or 25 mg/kg of body weight of TPB in 5% dextrose. The animals were bled under anesthesia (as described above) using the retro-orbital route at every 2 hr and plasma was harvested and stored at -80° C. TPB concentrations were analyzed by LC-MS/MS. Plasma drug levels were subjected to non-compartmental analysis (WinNonlin ver. 6.4 Certera Inc., Princeton, N.J.). The predicted steady-state levels > 500 ng/ml were estimated using a 12 hr dosing at 25 mg/kg dose for three doses of the compound in mice.

2.19.3. Viral inhibition test in mice

Four-week old Balb/C mice were obtained from the Jakson Laboratory (Bar Harbor, ME, USA). After acclimatization for four days, groups of animals (n = 6) were injected IP with saline alone or 25 mg/kg body weight dose of TPB diluted in saline. Following three injections at 12 hr intervals, the mice were infected with 500 PFU of PRVABC59 virus diluted in 100 μl 1X PBS by the subcutaneous (SC) route. Blood was collected by retro-orbital bleeding under anesthesia on days 2, 3, 4, 5, and 6 post infection. Viral genome copies in the plasma were determined by qRT-PCR.

2.20. Determination of drug concentration in plasma

TPB was dissolved in DMSO at 1 mg/ml. Working standard solutions were then prepared in 50% methanol in water from the stock solution. Standards (an eight-point

calibration curve) and quality controls (at three levels) were prepared by spiking the working standard solutions to blank mouse plasma. One hundred microliter aliquot of plasma was mixed with 25 µl of internal standard spiking solution (rilpivirine 1000 ng/ml in 50% acetonitrile in water), 1.5 ml ethyl acetate was added and vortexed vigorously for 15 min. The tubes were centrifuged at 1700×g for 5 min and 1.3 ml supernatant was evaporated to dryness under a stream of nitrogen at 40°C. The dried extract was reconstituted with 0.1 ml of 50% acetonitrile in water and 5 µl was injected into the LC-MS/MS instrument. The dynamic range of the method was 25–4000 ng/ml.

An Agilent 1200 HPLC system (Agilent Technologies, CA, USA) coupled with AB Sciex API 3200 Q Trap with an electrospray ionization source (Applied Biosystems, Foster City, CA, USA) was used. The mass transitions m/z 541.2 → 330.2 and 541.2 → 212.2 for analyte and m/z 367.2 → 195.2 for internal standard were monitored. Chromatographic separation was carried out on Phenomenex Synergi Polar-RP (150 × 2.0 mm, 4µ) column with isocratic mobile phase consisting of 0.1% formic acid in water (A) and 0.1% formic acid in acetonitrile (B) (20:80 v/v) at a flow rate of 0.5 ml/min. The retention times of analyte and internal standard were 2 and 1.2 min respectively.

2.21. Statistical analysis

Data were analyzed using GraphPad Prism software version 6.0. Unpaired two-tailed Student's t-test for pairwise comparison between the groups to determine significant differences in viral loads (RNA levels and infectious titer) was performed. Two-way ANOVA was used to determine significant differences between untreated and

drug-treated samples for viral loads (RNA copies, infectious titer) for GQ binding ligand studies. Data were represented as mean ± SEM.

2.22. Ethics statement

All procedures involving animals were conducted in accordance with the guidelines established in the Guide for Care and Use of Laboratory Animals of the National Institutes of Health, USA. The protocol was approved by the Institutional Animal Care and Use Committee at the University of Nebraska-Lincoln. Animals were housed in Life Sciences Annex building at the University. Mice were anesthetized with isoflurane prior to inoculation or blood collection and all efforts were made to minimize animal suffering.

Primer Name	Sequence (5′ to 3′)	Application
A_F	GATCCGCTAGCGCCGCCACCATGGATGCAATGAAGA GAGGGCTCTGCTGTGTGCTGCTGCTGTGTGGAGCAG TCTTCGTTTCG**ATTAGATGTATTGGAGTCAGCAAC AG**	Amplification of tPA-solE-F
B_F	GATCCGCTAGCGCCACCATGGGGATCCTTCCCAGCC CTGGGATGCCTGCGCTGCTCTCCCTCGTGAGCCTTCT CTCCGTGCTGCTGATGGGTTGCGTAGCTGAAACCGG T**ATTAGATGTATTGGAGTCAGC**	Amplification of μ-phosphatase signal sequence-solE-F
C_R	AGAGTCGCGGCCGC**TTAGGATTTTC**	Amplification of solE-F
D_F	GCAGCTCCCGGG**CTGTGTCTTACAGCCTGTGCAC**	Amplification of zDIII-F
495_F	GTCGTAACAACTCCGCCC	Primers used to sequence pIRES-solE-F/zDIIIF
1191_F	GGCCTTGACTTTTCAG	
1856_F	GGAAATGCAGTCTTCC	
2403_R	TCAGGTTCAGGGGGAG	

Table 2.1. Primers used for solE-F/zDIII-F construction. Restriction enzyme sites are underlined. E protein/zDIII/Ferritin sequences are shown in bold letters. F- Forward primer, R- Reverse primer. In A_F/B_F primers NheI site was incorporated. In C_R primer NotI site was incorporated. In D_F SmaI/XmaI site was incorporated.

CHAPTER III: CONSTRUCTION AND CHARACTERIZATION OF A NANOPARTICLE-BASED VACCINE CANDIDATE AGAINST ZIKV

3.1. Abstract

ZIKV recently emerged in Brazil and caused a variety of diseases including microcephaly in infants and GBS in adults. The virus spread expeditiously to many countries and became a worldwide public health concern. Substantial strides have been made in developing vaccine candidates against ZIKV infections. However, no FDA-approved and licensed vaccines are currently available for ZIKV. Herein, we describe the development of a bacterial ferritin-based nanoparticle vaccine candidate for ZIKV and highlight its potential as a safer and efficacious vaccine in comparison to existing approaches. Since the domain III (DIII) of the envelope (E) protein of ZIKV induces strong neutralizing antibody responses without causing antibody-dependent enhancement (ADE) of infection, we chose to use DIII as a proof-of-principle of the approach. In this approach, the DIII of ZIKV E protein was fused at the amino-terminus of the *Helicobacter pylori* ferritin with a flexible linker (Ser-Gly-Gly). The fusion construct (zDIII-F) also contained a secretion signal at its amino-terminus to allow secretion of the protein (or nanoparticle) from transfected mammalian cells. Following expression and purification, the nanoparticle vaccine candidate displaying the DIII on the particle surface was found to induce higher levels of humoral responses in vaccinated animals compared to the DIII antigen alone. A single dose of zDIII-F induced high levels of neutralizing antibody responses in vaccinated A129 ($IFNAR^{-/-}$) mice, and conferred protection against lethal ZIKV challenge. Passive transfer of sera from mice vaccinated with

zDIII-F protected A129 mice against subsequent lethal ZIKV challenge. The results point to a promising and potentially more efficacious vaccine candidate based on the ferritin nanoparticle platform.

3.2. Introduction

The recent re-emergence and spread of ZIKV in the Americas and its association with microcephaly and other neurological symptoms in infants and Guillain-Barre syndrome in adults posed a significant threat to human health (Coyne and Lazear, 2016; Cugola et al., 2016; Pattnaik et al., 2018). While several drug and vaccine candidates are in clinical testing phases, none have been approved for use in treating ZIKV infections. Vaccines based on conventional live attenuated viruses have safety concerns given the potential for reversal to virulence, especially in immunocompromised individuals (Lopez-Sagaseta et al., 2016; Plotkin, 2014). Inactivated virus-based vaccines, on the other hand, are comparatively less efficient in promoting protective immune responses. The development of a vaccine platform involving self-assembling protein nanoparticles that have the ability to display multiple copies of the antigen on the surface has emerged as an alternative to conventional strategies. Such a platform can be instrumental in overcoming the issues associated with conventional vaccine platforms and aid in the development of safer and more efficacious vaccines (Lopez-Sagaseta et al., 2016; Plotkin, 2014). Furthermore, the observations that our immune system responds more efficiently to immunogens of the sizes in the nanometer range (Gause et al., 2017; Link et al., 2012) suggest that the efficacy of nanoparticles displaying multiple copies of an antigen as vaccines is likely to exceed that of a soluble monomeric antigen.

The advantage of nanoparticle based vaccines lies in the fact that multiple copies of the immunogen can be displayed on the surface of the nanoparticle as an ordered antigenic array that results in multivalent B-cell receptor (BCRs) binding events (Fig. 3.1A). This is in contrast to monovalent binding events associated with conventional vaccine approaches and leads to an immune response that is multitudes of magnitude higher than traditional vaccines (Bachmann and Jennings, 2010; Lopez-Sagaseta et al., 2016). Furthermore, the suitability of nanoparticle-based vaccines for large scale production adds to the growing interest in this approach.

Several naturally occurring proteins can self-assemble to form stable and structurally organized nanoparticles with optimum dimensions that make them suitable to serve as vaccine delivery platforms (Lee and Wang, 2006; Lopez-Sagaseta et al., 2016). One such example is ferritin, a protein found in all living organisms and functions in iron storage and protects cells from damage caused by reactive oxygen species generated by exposure to excess iron (Cho et al., 2009; Lopez-Sagaseta et al., 2016). The mammalian and insect ferritins are multimeric proteins composed of 24 subunits of any combination of heavy and light chains that are secreted by cells (Hamburger et al., 2005). However, the bacterial ferritin nanoparticle is composed of 24 identical subunits that are structurally organized to form an octahedral structure and is reported to be resistant to thermal and chemical degradation (Fig. 3.1B) (Cho et al., 2009; He and Marles-Wright, 2015; Lopez-Sagaseta et al., 2016). The first report of using ferritin nanoparticles as a vaccine platform demonstrated that influenza virus hemagglutinin (HA) could be displayed on the surface of a ferritin nanoparticle in its native trimeric form. Inoculation of these particles resulted in higher induction of neutralizing antibodies, thus providing

evidence for more potent immune responses (Kanekiyo et al., 2013). This strategy has been used successfully in the development of a universal influenza vaccine, which has shown promising results with heterotypic protection (Yassine et al., 2015), as well as in the development of vaccines against Epstein-Barr virus and HIV (Kanekiyo et al., 2015; Zhou et al., 2014). Most recently, ferritin nanoparticle-based vaccine candidates have been developed for SARS-CoV-2 using the full-length spike (S) protein or the receptor binding domain of the S protein (Kalathiya et al., 2021; Kim et al., 2021).

In this study, we sought to generate plasmid constructs encoding either the full length or the DIII of ZIKV E protein as immunogens in association with ferritin. Transfection of the plasmid constructs into eukaryotic cells resulted in the production of the recombinant proteins that were secreted by the cells. The fusion protein encoding the ZIKV DIII (zDIII-F) was then purified to homogeneity by ion exchange and size exclusion chromatography. Under transmission electron microscopy, the ZDIII-F protein was seen to form typical nanoparticle like structures. The recombinant protein or the nanoparticle (zDIII-F) was found to be stable for prolonged periods of time. In animal studies, this vaccine candidate was seen to induce significantly higher levels of neutralizing antibody response compared to soluble DIII antigen alone and conferred protection against lethal challenge. Furthermore, sera obtained from the immunized mice also protected naïve mice from lethal challenge with ZIKV. The results provide support for the use of the ferritin nanoparticle vaccine candidate for ZIKV for further clinical evaluation.

3.3. Results

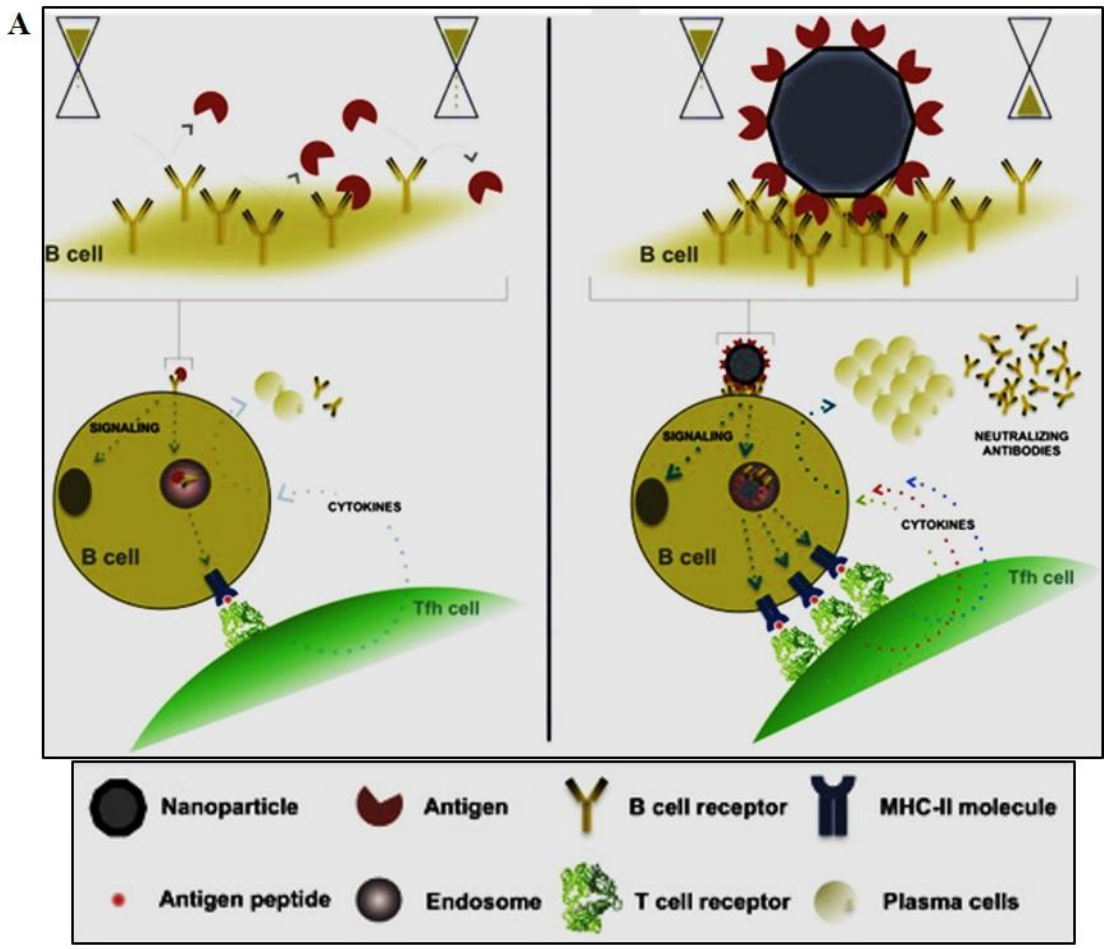

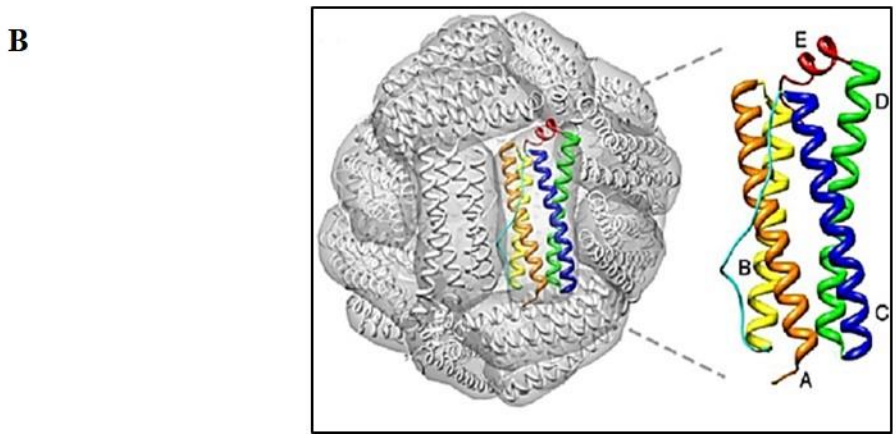

Fig. 3.1. Basic principle of nanoparticle-based enhancement of immune response.

(A) Monovalent recombinant antigens as in traditional vaccine platforms bind to fewer

BCRs resulting in weaker immune response (left). In nanoparticle-based vaccine platform, multiple immunogens can be structured on the surface leading to tighter and prolonged binding with several BCRs (right). This enables the clustering of BCRs for multiple and simultaneous engagement with the antigen epitopes. The B cells trap the antigen-loaded nanoparticle to establish a durable, localized, and strong recognition that translates into B-cell intracellular signaling, internalization, and processing of the antigen for presentation via molecules of the MHC complex to the T follicular helper cells (Tfh) within the germinal centers. Image adapted from López-Sagaseta et al, 2016. **(B)** Organization of a ferritin nanoparticle showing each of the subunits and the structure of a single subunit. Image adapted from Zhang and Orner et al, 2011.

3.3.1. Construction and expression of full-length soluble E protein fused in-frame with ferritin

The coding sequence of ferritin (aa residues 5-167) from *Helicobacter pylori* (*H. pylori*) was synthesized using commercial gene synthesis service from GenScript (New Jersey). The coding sequence of ferritin was then subcloned into the CMV-promoter driven mammalian expression vector, pIRES-2-eGFP after removing the eGFP sequences. Subsequently, the coding sequence of ZIKV E protein spanning residues 1 to 404 was PCR amplified from the full length infectious clone (Annamalai et al., 2017) of ZIKV as the template. The amplified product thus lacked the carboxy-terminal transmembrane and cytoplasmic domains. The E protein coding region was strategically placed at the N terminus of ferritin for it to be exposed on the outside of the nanocage. It has been reported that removal of the first 4 amino acids from the amino-terminus of ferritin and immunogen fusion at that site results in the exposure of the immunogen to the outside leading to better visibility of the antigen to BCRs (Kanekiyo et al., 2013).

To allow for secretion of the E-ferritin chimeric protein from the transfected cells, we also inserted a consensus signal sequence, called secrecon signal (Guler-Gane et al., 2016), at the amino-terminus of the chimeric protein that is known to drive efficient secretion of proteins. Additionally, the linker, Ser-Gly-Gly (SGG) was also inserted between the soluble E and ferritin coding regions as shown (Fig 3.2.A-B) to allow for flexibility of the E protein to fold into its correct conformation and structure. Once the construct was generated, the authenticity of the cloned sequences was confirmed by DNA sequencing. The resulting chimeric protein, solE-F (Fig. 3.2.B) is expected to be about 68 kDa after removal of the signal sequences. To examine the expression and secretion of

the solE-F protein, HEK293T cells were mock-transfected (no plasmid) or transfected with two different concentrations of the plasmid (1 µg and 2.5 µg) encoding solE-F. The cell culture supernatants collected on day four post-transfection were subjected to Western blotting with an antibody to detect the solE-F protein. A 68 kDa protein was specifically detected in the culture supernatants of cells transfected with the plasmid encoding solE-F (Fig. 3.2.C, lanes 4 and 5) that was absent in mock-transfected cells (lane 3). While the cells transfected with 1 µg plasmid DNA expressed lower amounts of the protein (lane 4), transfection with 2.5 µg of the plasmid DNA led to higher level of expression and secretion of the protein into the cell culture medium (lane 5).

Although the secrecon signal sequence in our construct resulted in good levels of secretion of the solE-F protein into the supernatants of transfected cells, in order to obtain more efficient secretion of the protein for large scale purification purposes, we examined if other secretion signal sequences would allow for more efficient secretion. Several signal sequences have been shown to drive efficient secretion of proteins (Dalton and Barton, 2014). Therefore, we constructed similar plasmids (as shown in Fig. 3.2.A) containing signal sequence from tissue plasminogen activator (tPA) (Kou et al., 2017) or from the µ-phosphatase signal sequence present in the pHLvector (Aricescu et al., 2006). Examination of the relative levels of secretion of solE-F from transfected cells directed by these signal sequences revealed that although the other signal sequences directed secretion of the protein (Fig. 3.2D, lanes 4-7), the secrecon signal sequence that we used initially in our construct (Fig. 3.2.A) appeared to be most efficient in promoting secretion

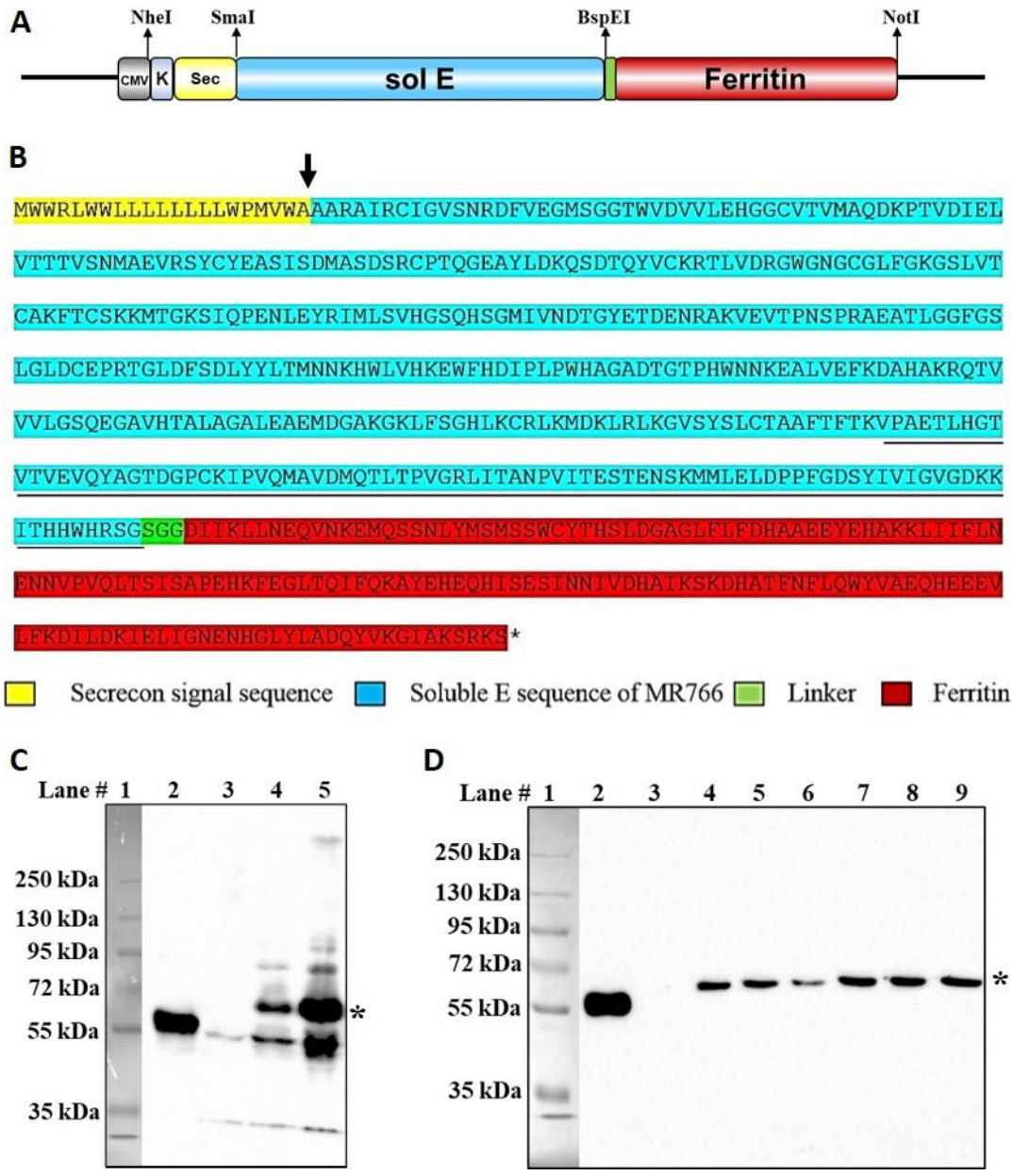

Fig. 3.2. Construction of the plasmid encoding solE-F fusion protein and expression in transfected cells. (**A**) Schematic of the plasmid showing various coding regions and regulatory elements for expression of the protein. CMV, cytomegalovirus promoter; K, Kozak sequences; Sec, secretion signal sequences, solE, coding region of ZIKV E protein from residues 1-404; and ferritin coding sequences from residues 5-167. The flexible

linker SGG is shown as a green rectangle between solE and ferritin sequences. Unique restriction enzyme sites in the plasmid are shown at the top. (**B**) Amino acid sequence of the solE-F fusion protein. The arrow shows the cleavage site following the secretion signal sequences. (**C**) Expression of solE-F in 293T cells. Culture supernatants of cells from mock-transfected (lane 3) or transfected with 1 μg (lane 4) or 2.5 μg (lane 5) of the plasmid were analyzed by Western blotting for ZIKV E. solE-F (identified with an asterisk) migrates as a ~68 kDa protein as compared to ~55 kDa ZIKV E protein (lane 2) from virus-infected Vero cells. Molecular masses of marker proteins are shown on left. **(D)** Secretion of solE-F from transfected cells directed by secretion signal sequences. Supernatants of cells transfected with plasmids containing tPA signal sequence (lanes 4 and 5), μ-phosphatase signal sequence (lanes 6 and 7) and secrecon signal sequence (lanes 8 and 9) were analyzed by Western blotting for solE-F secretion. Lane 2: ZIKV E. Asterisk identifies the secreted solE-F protein.

of solE-F protein (lanes 8 and 9). Therefore, the secrecon signal sequence was used in our constructs.

3.3.2. Construction and expression of DIII domain of E protein fused in-frame with ferritin

While conducting our studies, it became clear that immunization with full length ZIKV E protein may contribute to antibody dependent enhancement (ADE) of infection leading to more severe disease (Shukla et al., 2020a; Shukla et al., 2020b). To overcome this and avoid ADE, parts of the ZIKV E protein can be used as an antigen. ZIKV E protein consists of three domains. It has been reported that of the three domains, DIII elicits a strong neutralizing antibody response in mice without inducing ADE (Cabral-Miranda et al., 2019). Therefore, we generated an expression plasmid that replaced the solE coding sequences with the coding sequence of ZIKV E protein DIII (Fig. 3.3.A), spanning amino acid residues 303 to 404. Following sequence confirmation of the DIII region within the plasmid, we examined expression and secretion of the chimeric protein, zDIII-F. HEK293T cells were transfected with the plasmid and culture supernatant and cell lysates were harvested on day four post-transfection and subjected to Western blotting. A protein band of approximately 27 kDa was detected in the supernatant (Fig. 3.3.B, lane 3) by using an antibody directed against DIII of ZIKV E protein. This protein was also detected in the transfected cell lysates (lane 2). Interestingly, a slower migrating band of ~30 kDa was also observed in the cell pellet (lane 2), which is likely the signal sequence-uncleaved version of the same protein.

3.3.3. Large scale expression and purification of zDIII-F

Large scale expression using a suitable expression system and subsequent purification of a recombinant protein is critical for the development and testing of vaccine candidates. Expression of recombinant proteins in mammalian cell culture systems is widely accepted for their ability to incorporate post translational modifications such as addition of glycan moieties that are key to the proper folding and functioning of proteins.

Although, widely accepted, this system is associated with a strict bottleneck while purifying the recombinant protein due to the presence of serum-borne adventitious agents that pose a risk of contamination. To overcome this bottleneck, the use of serum-free cell culture medium has provided researchers with a system that allows for increased production of the recombinant protein while getting rid of the issues associated with using serum. Therefore, we used the 293FreeStyleSystem from ThermoFisher that involves the use of 293FS suspension cell culture in a serum free medium to scale up the production of zDIII-F and subsequent purification and experimentation. In initial pilot experiments, we transfected 1 µg of the plasmid construct encoding zDIII-F per one million 293FS cells in suspension using 293Cellfectin or polyethylenimine (PEI) transfection reagents. Small aliquots of cell suspension were collected at days 2, 3, 4, and 5 post-transfection (dpt) and the presence of ZDIII-F protein in the supernatants was examined by Western blotting. From the pilot experiments, we inferred that maximal secretion of the protein occurred at 4 dpt and approximately 0.6-0.8 µg of the protein

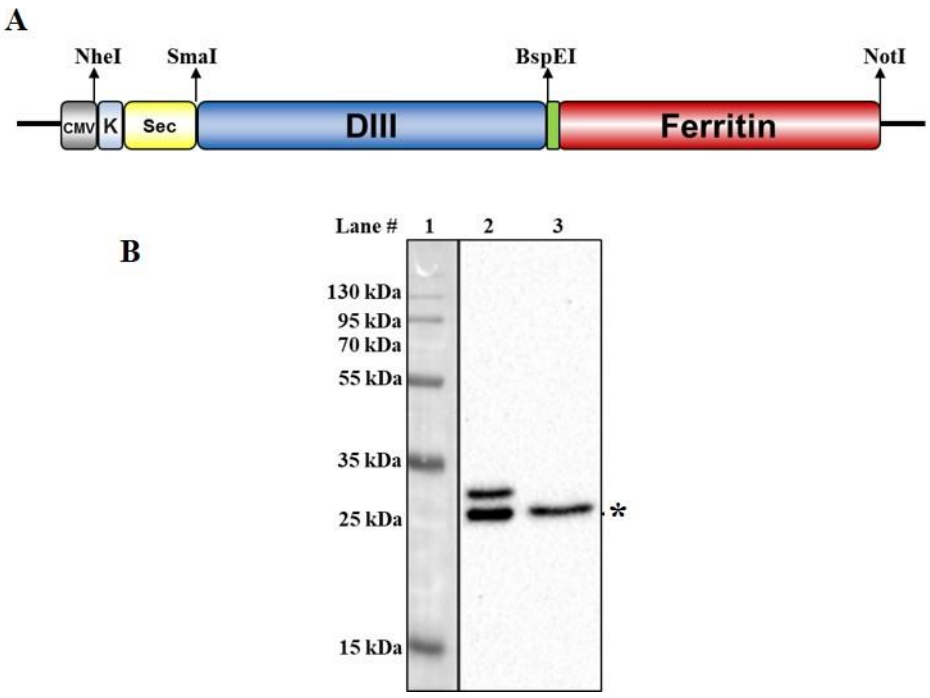

Figure 3.3. Construction and expression of zDIII-F. (A) Schematic of the plasmid encoding zDIII-F showing coding regions and regulatory elements for expression of the protein similar to the plasmid described in Fig. 3.2. ZIKV domain III (DIII) sequences span residues 303-404. **(B)** Expression of zDIII-F in 293T cells. Cells were transfected with the above plasmid and 96 after transfection, cell lysates (lane 2) and supernatants (lane 3) were analyzed by Western blotting for zDIII-F using an antibody against DIII. Molecular masses of marker proteins are shown on left. The secreted zDIII-F protein of ~ 27 kDa is identified by an asterisk on right.

was present in one ml of the culture supernatant as judged by oriole staining of the protein band. Therefore, we used these transfection conditions for large scale expression and purification of ZDIII-F,.

For large scale expression and purification of ZDIII-F, a 500 ml culture of 293FS cells at a density of 1 million cells per ml was transfected with 500 µg of plasmid DNA encoding zDIII-F. Following incubation for 4 days, the clarified cell culture supernatant was subjected to ion exchange chromatography to isolate zDIIIF. Since the zDIII-F chimeric protein carries a calculated net charge of -13.84 at the physiologically relevant pH of 7.4, we used an anion exchange column with a quaternary capto matrix to purify zDIII-F from the culture medium. Using a combination of Tris buffers (pH 7.4) containing 50 mM and 1000 mM NaCl, majority of presumed zDIII-F protein was eluted in a relatively pure form (as judged by Coomassie staining) in pooled fractions corresponding to NaCl concentration of 107-158 mM (Fig. 3.4.A, lane 2). Although higher concentration of NaCl eluted the protein from the column, the amount of other contaminating proteins was either significant or there was less zDIII-F (lanes 3-6). Western blot analysis of the pooled fractions showed that the major band in the 107-158 mM NaCl pooled fraction was indeed zDIII-F protein (Fig. 3.4.B, lane 2). Based on Coomassie staining, we estimated that the purity of the zDIII-F protein was approximately 80-85%. To further purify the protein, we pooled the fractions corresponding to 107-158 mM NaCl concentration and applied to a size exclusion chromatography column. We confirmed the purity of the eluted protein to be approximately 90-95% by SDS-PAGE analysis followed by Coomassie staining of the gel (Fig. 3.5.C) and its identity by Western blot analysis using an antibody against DIII of

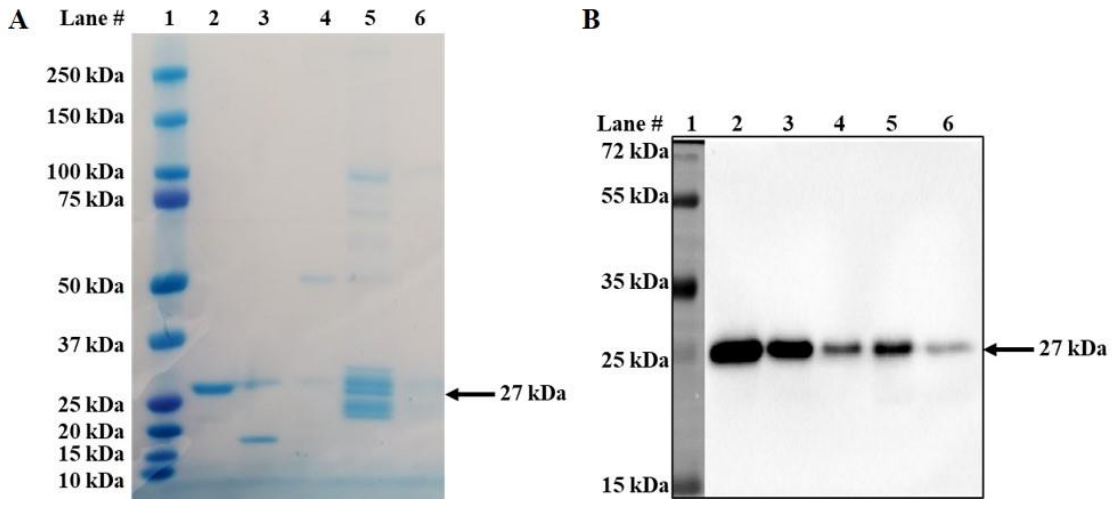

Fig. 3.4. Anion exchange chromatograpy for purification of zDIII-F. SDS-PAGE and Coomassie staining **(A)** and Western blot analysis **(B)** of various pooled fractions from anion exchange column chromatography. Eluted zDIII-F protein detected in pooled fractions from concentrations of NaCl ranging from 107-158 mM (lane 2), 159-214 mM (lane 3), 215-271 mM (lane 4), 272-379 mM (lane 5) and 380-422 mM (lane 6) are shown. Approximately 1 µg of total protein in panel A and 100 ng of total protein in panel B were analyzed. Molecular masses of marker proteins are shown on left side of each panel.

ZIKV E (Fig 3.5.C).

3.3.4. zDIII-F forms stable nanoparticles as visualized by transmission electron microscopy (TEM)

Since ferritin spontaneously self-assembles into nanoparticles, resembling a cage like structure with 24 units (Lopez-Sagaseta et al., 2016), my expectation was that we will observe the purified zDIII-F chimeric protein as a nanoparticle with the zDIII region protruding out from the surface of the nanoparticle. Indeed, structural prediction of zDIII-F chimeric protein based on the known structures of ferritin (PDB ID: 3BVE) and the ZIKV E DIII protein (PDB ID: 5JHM) revealed that the DIII region of the E protein folds independently and protrudes from the amino-terminal end of ferritin molecule (Fig. 3.6.A). Two dimensional TEM images of purified zDIII-F show the formation of spherical structures about 12-15 nm in diameter with protruding structures indicating that the recombinant protein is able to form a nanocage-like structure with the zDIII likely protruding from its surface (Fig. 3.6.B). We attempted to perform cryo-EM structural analysis of a highly purified preparation of zDIII-F. However, our collaborator Dr. Terje Dokland, University of Alabama at Birmingham was unable to detect any density on the surface of ferritin particles and suggested that the presence of the highly flexible linker (SGG) between ferritin and DIII might have contributed to the inability to detect density of DIII. Therefore, future chimeric protein constructs may be designed without the use of the flexible linker sequences.Ferritin is a stable protein and is known to be resistant to degradation even when exposed to high temperatures. Indeed, a study reports that a vaccine candidate using the ferritin platform is thermally stable and retains its potency

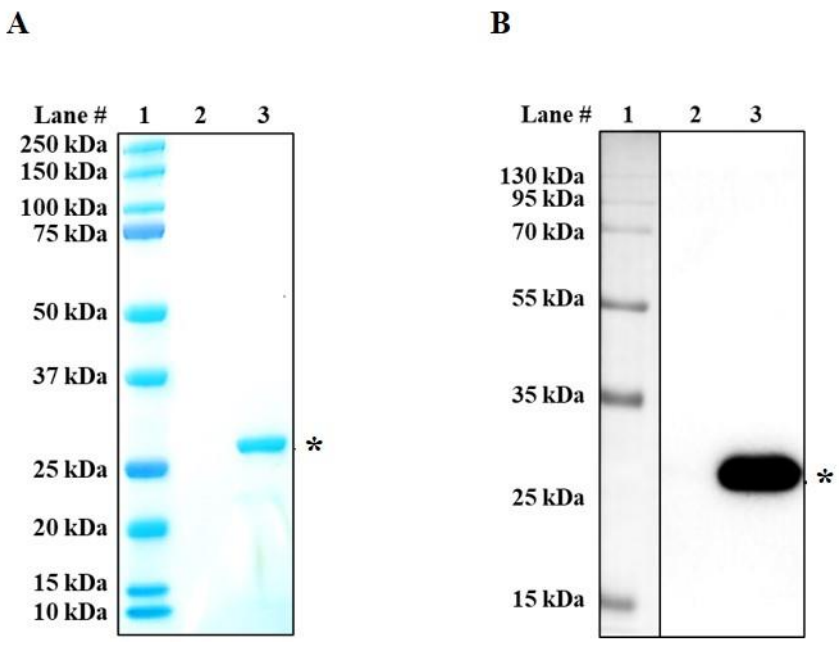

Fig. 3.5. Examination of purity of zDIII-F following size exclusion chromatograpy. SDS-PAGE followed by Coomassie staining **(A)** and Western blot analysis **(B)** of zDIII-F after purification using size exclusion column chromatography. Approximately1 µg of total protein in panel A and 100 ng of total protein in panel B were analyzed. Asterisk on right identifies the zDIII-F protein. Molecular masses of marker proteins are shown on left.

even after exposure to high temperatures for prolonged periods of time (Lopez-Sagaseta et al., 2016). Consistent with the known stability of proteins fused to ferritin, we observed that the zDIII-F chimeric protein was stable as judged by SDS-PAGE analysis of zDIII-F samples taken every 15 days post storage at 4ºC, showing minimal or no degradation of the protein (Fig. 3.6.C). Additionally, TEM images of particles in samples taken at every 30 days show intact nanoparticles that appear similar to those observed on the day of isolation (Fig. 3.6.D). These data demonstrate that the zDIII-F nanoparticles are stable at 4ºC for up to 90 days.

3.3.5. Mice immunized with zDIII-F are protected from lethal ZIKV challenge

To evaluate the efficacy of the zDIII-F nanoparticle vaccine compared to soluble DIII domain of ZIKV as a vaccine, we acquired the soluble DIII antigen from ProSpec (Cat# ZKV-008). Three-week-old Ifnar1$^{-/-}$ A129 mice were divided into three groups: PBS group (n=6), DIII group (n=7), and zDIII-F group (n=7). Mice were injected with either PBS (PBS group), 4 μg of soluble ZIKV DIII protein per animal (DIII group), or 10 μg of the zDIII-F nanoparticle vaccine (equivalent to 4 μg of zDIII antigen) per animal (zDIII-F group) formulated with Addavax adjuvant. We monitored the mice for 28 days and then challenged them subcutaneously with 10,000 pfu of ZIKV (infectiousclone derived rMR virus) per mouse. The mice were monitored and scored for clinical signs, weight loss, and survival for 10 days at which time the surviving mice were euthanized (Fig 3.7.A).

At 2-3 dpi, the mice in the PBS group and infected with rMR, began showing

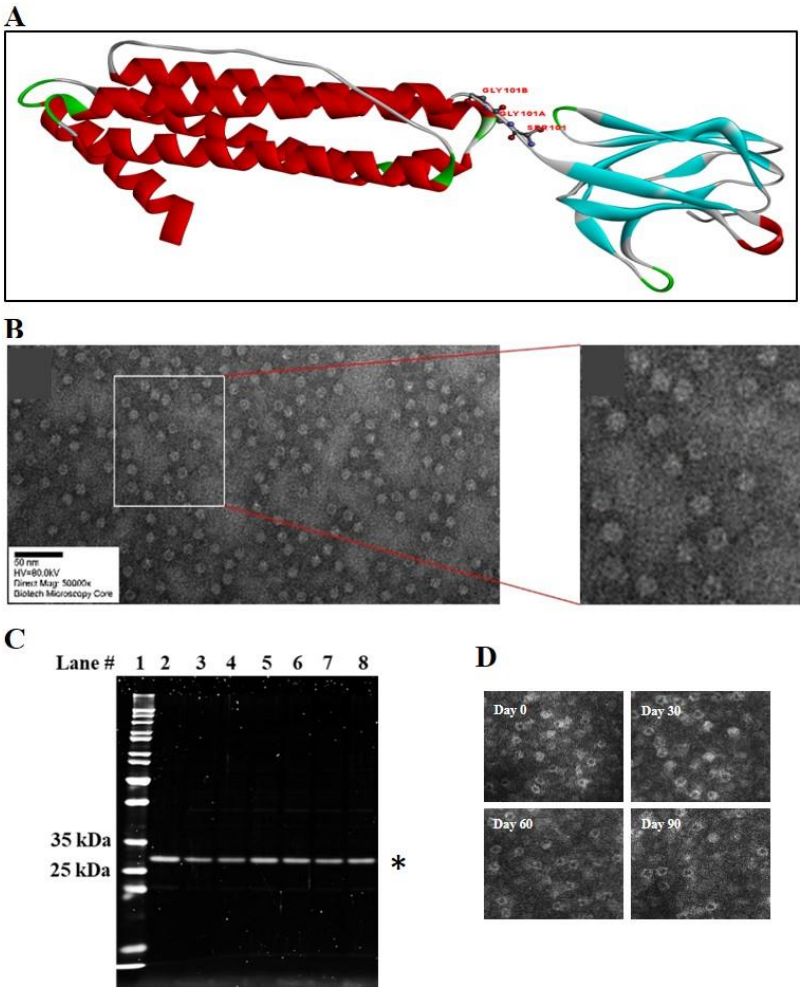

Fig. 3.6. Characterization of zDIII-F fusion protein and nanoparticles. (**A**) Predicted structure showing folding of zDIII-F fusion protein as two separate domains linked by the SGG linker. The ribbon structure was generated by Dr. Santosh Behera (NIPER, India) using PyMOL software and PDB IDs: 3BVE (*H pylori* ferritin) and 5JHM (ZIKV E DIII). (**B**) TEM image of purified zDIII-F nanoparticles. (**C**) Stability of zDIII-F fusion protein following incubation at 4^{o}C with time. Two hundred ng aliquots of the protein were taken from a purified preparation at every 15 day intervals and stored at -80^{o}C before analysis. Following SDS-PAGE, protein bands were visualized by oriole staining. Lanes 2-8 contain proteins from day 0, 15, 30, 45, 60, 75, and 90 post-incubation at 4^{o}C, respectively. (**D**) TEM images of particles after 0, 30, 60, and 90 days of storage at 4^{o}C.

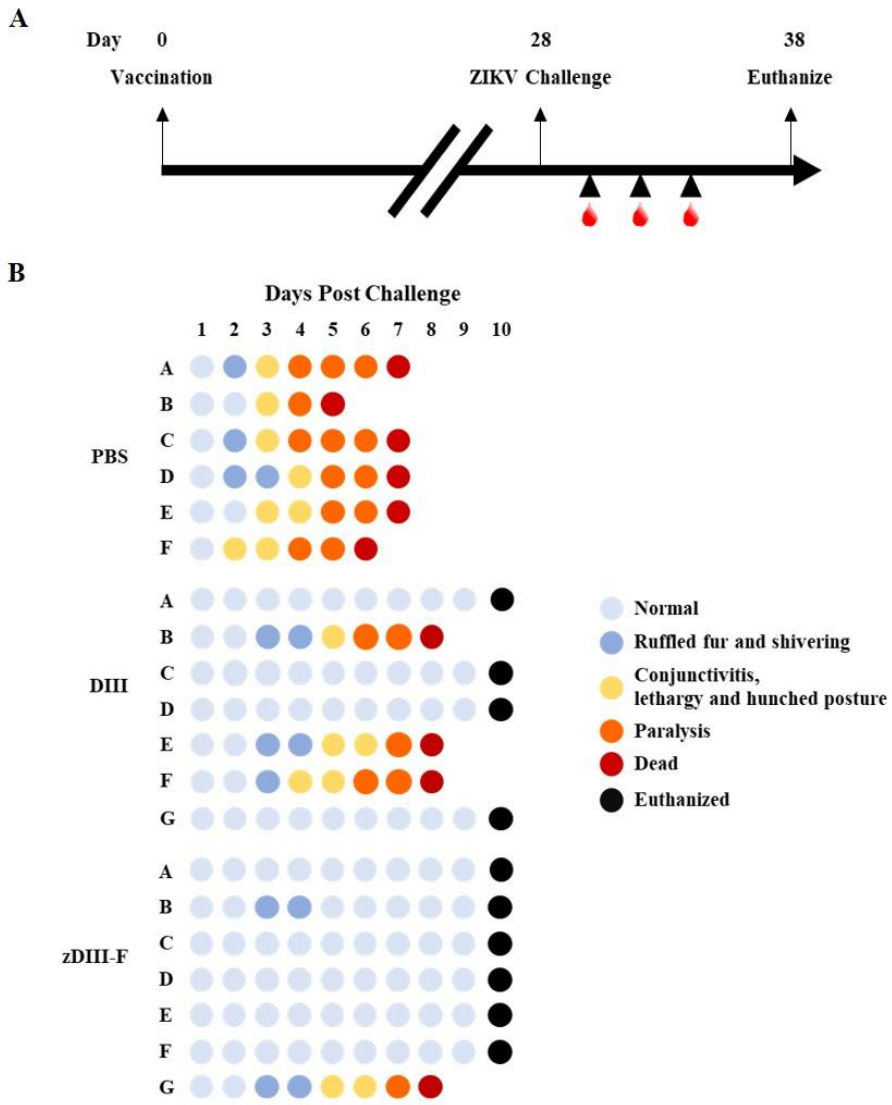

Fig. 3.7. zDIII-F vaccinated animals are protected from lethal ZIKV challenge. (**A**) Strategy for vaccination and lethal challenge using four-week-old A129 mice. Mice were injected with PBS (n=6), 4 µg of DIII (n=7) or 10 µg of zDIII-F (n=7) subcutaneously (s.c.) on day 0 and challenged with rMR (10^4 PFU/mouse) on day 28. Blood samples were collected on days 2, 4, and 6 post challenge. (**B**) Clinical symptoms developed in individual mouse (identified as A to F/G in various groups) following lethal ZIKV challenge.

signs of disease such as shivering and ruffled fur which by day 3-4 progressed to conjunctivitis, lethargy, and hunched posture (Fig 3.7.B). Additionally, some mice presented with both fore limb and hind limb paralysis beginning at 4 dpi which extended till day 6. All the mice in this group developed severe disease signs and succumbed to virus infection by 7 dpi with one mice each dying at 5 dpi and 6 dpi (Fig 3.7.B, PBS group). Mice in soluble DIII-vaccinated group appeared healthy for 3 dpi but 3 mice developed clinical symptoms exhibiting ruffled fur, conjunctivitis, followed by limb paralysis by day 6 and ultimately succumbing to infection by day 8. All other mice in this group were healthy until day 10, at which time they were euthanized. In contrast, 5 out of 7 mice in the zDIII-F group showed no symptoms of disease at even at 10 dpi. Two mice presented ruffled fur and shivering on 3 dpi which continued till 4 dpi but one mouse recovered completely while the other mice exhibited more severe symptom and succumbed on day 8 (Fig 3.7.B). At the end of the experiment on day 10 when they were euthanized, all mice (except one that died on day 8) in this group appeared healthy. Weight loss was observed in all mice administered with PBS and infected with rMR by 2 dpi (Fig 3.8.A) and this trend continued until they succumbed to virus infection. One mouse each succumbed to infection on day 5 and 6 (Fig 3.8.B) and by 7 dpi, all mice in this group had perished (Fig 3.8.B). On the other hand, mice vaccinated with soluble DIII or zDIII-F and infected with rMR virus did not exhibit any weight loss. In fact, most mice in these groups began to gain weight after about 3 dpi and the trend continued up to 10 dpi (Fig. 3.8.A). Three mice from soluble DIII vaccinated group died on day 8, whereas 6 out of 7 mice in zDIII-F vaccinated group survived the virus infection until 10 dpi when all the mice were euthanized (Fig 3.8.B).

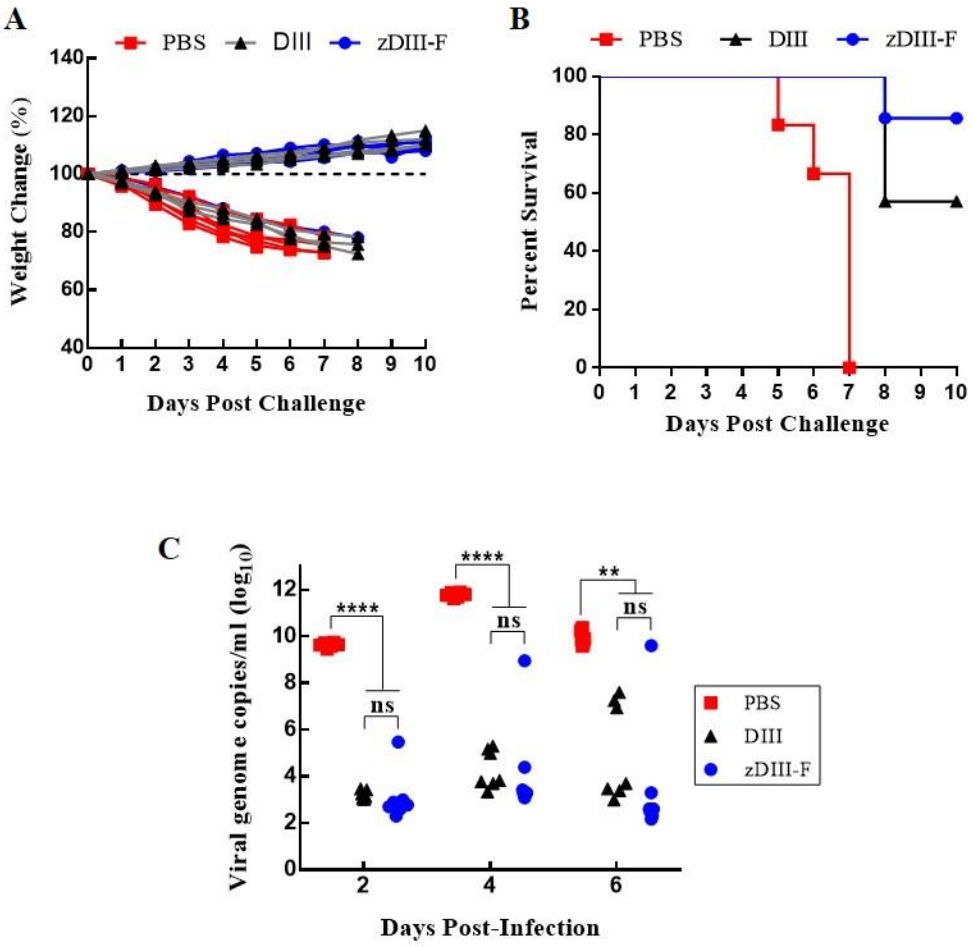

Fig. 3.8. zDIII-F vaccinated animals are protected from lethal ZIKV challenge. (A) Weight change and **(B)** Percent (%) survival of mice in PBS or DIII or zDIII-F vaccinated groups. **(C)** Viral genome copies in serum at days 2, 4, and 6 post-challenge as measured by qRT-PCR. Data presented as ± SEM. Two-way ANOVA was used to determine significance. Ns, non-significant; **, $p < 0.01$, ****, $p < 0.0001$.

Viral genome copy numbers in the serum of the infected mice were significantly reduced genome copies in the soluble DIII-vaccinated and zDIII-F-vaccinated groups at 2 dpi in comparison to mice in the PBS group (Fig 3.8.C). At days 4 and 6 post-infection, significantly lower number viral genome copy numbers were detected in the majority of the animals in the two vaccinated groups. On the other hand, high levels of viral genomes were detected in all animals administered with PBS. These results indicate that the nanoparticle based zDIII-F vaccine protects Ifnar1$^{-/-}$A129 mice from lethal challenge and that zDIII-F appears to be a more efficacious vaccine candidate in protecting the animals and reducing viremia than the soluble DIII antigen.

3.3.6. Vaccination with zDIII-F elicits high levels of neutralizing antibody

To determine if zDIII-F nanoparticle induces neutralizing antibody responses against ZIKV infection, we examined the presence of neutralizing antibodies in the serum samples of zDIII-F vaccinated A129 mice collected at 28 days post-vaccination. Results show significantly higher neutralizing antibody titers ($PRNT_{50}$) in sera from zDIII-F nanoparticle vaccinated animals in comparison to sera from animals from PBS administered group (Fig. 3.9.A). Interestingly, the antibody titers elicited by zDIII-F was significantly higher than those elicited by soluble DIII antigen (Fig. 3.9.A). Overall, these results indicate that vaccination with zDIII-F elicits a strong neutralizing antibody response that protects mice from lethal ZIKV (rMR) challenge whereas vaccination with soluble DIII confers protection to a lesser degree. To determine if the antibodies induced by zDIII-F vaccination can neutralize different ZIKV strains from recent outbreaks, we performed a $PRNT_{50}$ assay with the serum from zDIII-F vaccinated mice. We used the

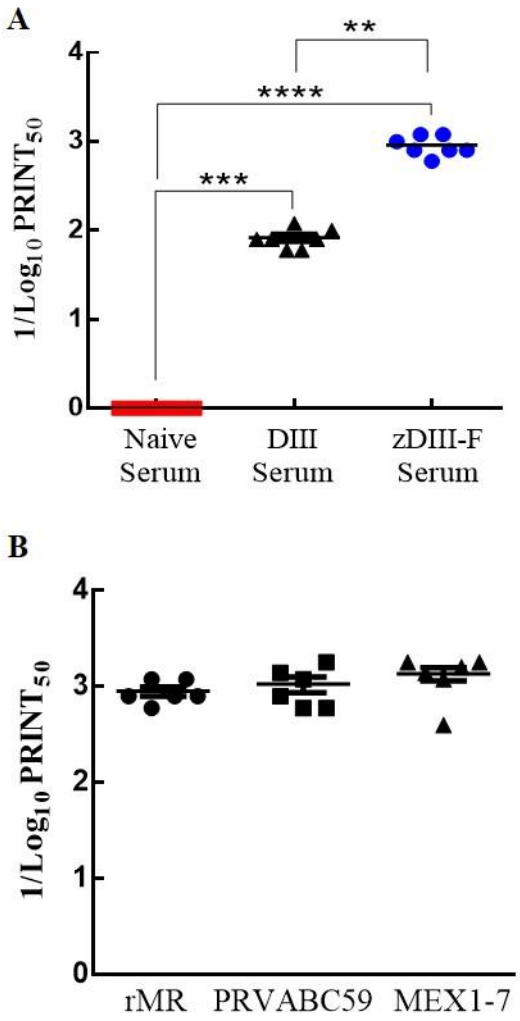

Fig. 3.9. Neutralizing antibody titers in the sera of zDIII-F vaccinated animals. (A) The ZIKV neutralizing antibody titers in serum [expressed as reciprocal of 50% plaque reduction neutralization test ($PRNT_{50}$) values] from naïve or zDIII-F vaccinated mice at 28 dpi. **(B)** $PRNT_{50}$ titer of serum samples from individual animals vaccinated with zDIII-F against PRVABC59 and MEX1-7 strains of ZIKV. **(A)** Data in panel A are presented as ± SEM. Two-way ANOVA was used to determine significance. **, $p \leq 0.01$; ***, $p \leq 0.001$; ****, $p \leq 0.0001$.

PRVABC59 and MEX1–7 strains of ZIKV that are currently in our laboratory. The results show potent inhibition of all ZIKV strains with similar $PRNT_{50}$ values, suggesting that the zDIII-F vaccine candidate may confer protection against other ZIKV strains (Fig. 3.9.B).

3.3.7. Passive transfer of antibodies from animals vaccinated with zDIII-F protects mice from lethal challenge

To explore the possibility that serum antibodies from zDIII-F vaccinated animals could protect mice form lethal ZIKV infection, we conducted a passive antibody transfer experiment in A129 mice. Mice were divided into two groups: one group (n=10) received sera obtained from mice that were administered with PBS while the other group (n=10) received sera from mice vaccinated with zDIII-F. The sera were collected at 28 days post-vaccination (as shown in Fig. 3.7.A) and the pooled sera were administered to mice by the intravenous route using the tail vein. The mice were challenged with 10,000 pfu ZIKV at 4 hours post sera administration and were monitored for disease progression for 10 days (Fig. 3.10.A). The mice that received sera from PBS-administered animals developed disease with half of them showing ruffled fur and shivering at 2 dpi. By 3 dpi, some mice (n=3) developed conjunctivitis, lethargy, and hunched posture (Fig. 3.10.B). In contrast, 8 out of 10 mice that received sera from zDIII-F-vaccinated animals appeared healthy until termination of the experiment, while one animal progressively exhibited symptoms and succumbed to infection on day 9 and the other exhibited symptoms early but recovered (Fig. 3.10.B). At 4 dpi, we sacrificed 5 mice from each group. The remaining 5 mice that received sera from PBS-administered animals developed severe

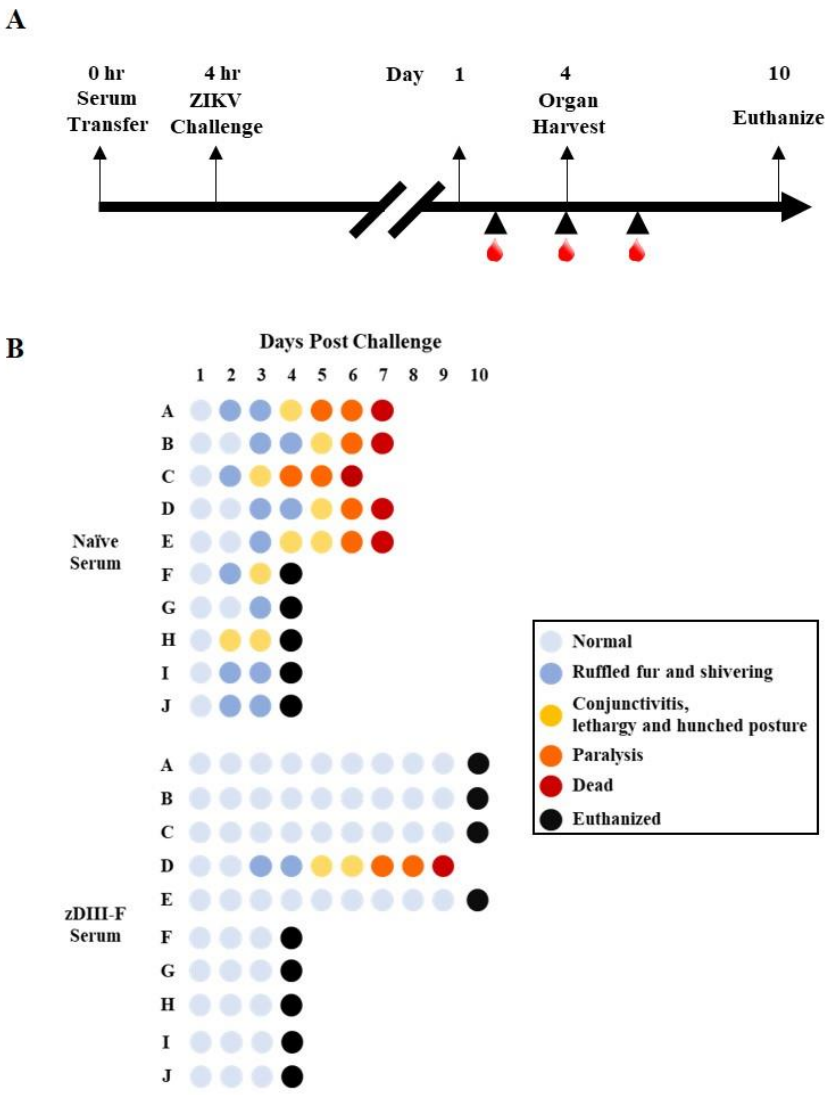

Fig. 3.10. Passive transfer of sera from zDIII-F vaccinated animals protects naïve animals from lethal ZIKV challenge. (**A**) Strategy for passive transfer of immune sera and lethal ZIKV challenge in four-week-old A129 mice. Mice were injected with 200 µl of PBS (n=10) or pooled sera from zDIII-F vaccinated animals (n=10) intravenously at 0 hr and challenged with rMR (10^4 PFU/mouse) at 4 hr. Blood samples were collected on days 2, 4, and 6 post lethal challenge. **(B)** Clinical symptoms developed in individual mouse (identified as A to J in each group) following lethal ZIKV challenge are shown.

disease and by 6-7 dpi, all five mice succumbed (Fig. 3.11.B) while 4 out of the remaining 5 mice that received sera from zDIII-F-vaccinated mice did not exhibit any clinical signs of disease and survived (Fig. 3.10.B). However, one mouse from this group died on day 9. The mice that received sera from PBS-administered animals also began to lose weight and by 4 dpi, weight loss was significant while the mice in the other group continued to gain weight (Fig. 3.11.A). These results suggest that passive transfer of sera from zDIII-F-vaccinated animals protected the mice against rMR virus lethal challenge**.**

Determination of viral genome copies in serum samples collected from mice in both groups showed that the mice that received the sera from zDIII-F vaccinated animals had significantly lower viral genome copies in comparison to the mice that received the sera from PBS-administered mice (Fig. 3.11.C). Additionally, viral genome copies in the brain, spleen, and the liver were also greatly reduced in mice that received the sera from zDIII-F-vaccinated animals (Fig. 3.11.D). These results demonstrate that passive transfer of sera obtained from mice vaccinated with zDIII-F confers solid protection against lethal ZIKV challenge.

3.4. Discussion

The emergence of ZIKV in the western hemisphere and its association with neurological disease in infants as well as adults poses a serious concern to public health. Licensed vaccines or antiviral drugs to treat ZIKV infections are not available thereby necessitating the development of countermeasures against this viral epidemic. Although several different vaccine strategies have been developed and are being tested (Pattnaik et al., 2020), none have been approved for clinical use. Therefore, an efficacious vaccine is

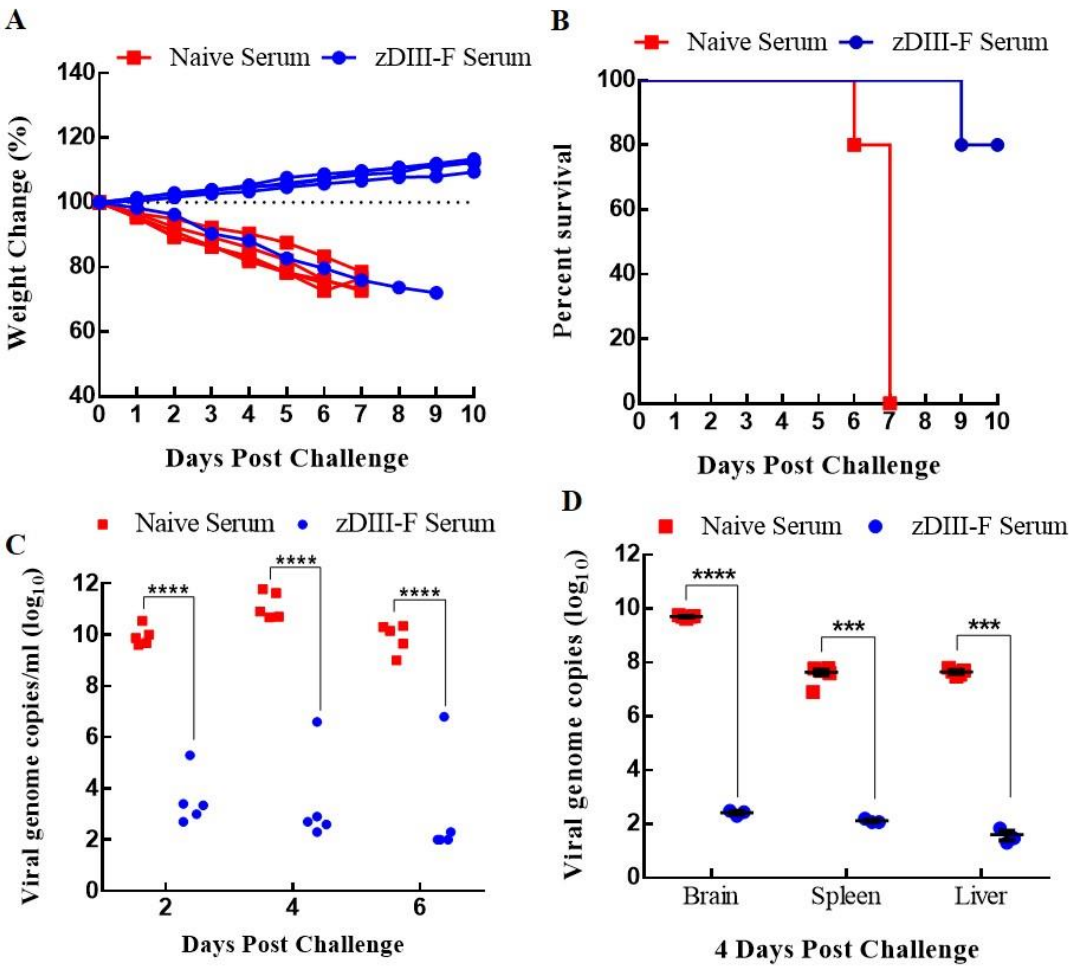

Fig. 3.11. Passive transfer of sera from zDIII-F vaccinated animals protects naïve animals from lethal ZIKV challenge. Percent weight change (A) and survival (B) of mice injected with immune sear from naïve or zDIII-F vaccinated animals. **(C)** Viral genome copies in serum at days 2, 4, and 6 post challenge. **(D)** Viral genome copies per gram of tissues as measured by qRT-PCR. Data presented as ± SEM. Two-way ANOVA was used to determine significance in panels C and D. ***, $p \leq 0.001$; ****, $p \leq 0.0001$.

still much sought after. Since ZIKV infections have occurred in DENV endemic areas and the observations that cross-reactive antibodies can cause ADE (Kawiecki and Christofferson, 2016; Stettler et al., 2016; Zimmerman et al., 2018), attention must also be paid in the development of efficacious ZIKV vaccines that do not induce ADE of DENV or ZIKV infections. Furthermore, due to detection of ZIKV infections in many countries, particularly in resource-limited developing countries, rapid production of vaccines in a cost-effective manner would be highly desirable.

Although our initial plan was to use the ectodomain of E protein as the target for development of a vaccine candidate based on the studies showing that neutralizing antibodies that are protective against ZIKV infections are mostly directed against the E protein, it has become clear that such antibodies have the potential to induce ADE. Therefore, we focused on using the DIII domain of the ZIKV E protein, which has been shown to not induce ADE (Cabral-Miranda et al., 2019; In et al., 2020; Shukla et al., 2020c; Yang et al., 2017b) .

Nanoparticles provide an improved vaccine platform for the delivery of antigens and have been in clinical development against several infectious diseases (Lopez-Sagaseta et al., 2016). Ferritin is a stable protein that has the ability to self-assemble into nanoparticles and this property has been exploited in the development of vaccine candidates against several pathogenic viruses. In this study, we have developed the bacterial ferritin-based vaccine candidate that displays the ZIKV E DIII as the antigen that has been shown to self-assemble into nanocage like structure with the antigen displayed on its surface. The zDIII-F protein and the nanoparticles were found to be resistant to degradation and maintained structural integrity when left at 4ºC for up to 3

months, demonstrating a desirable property of thermostability of a vaccine candidate.

While designing our nanoparticle construct, we rationalized that by adding a flexible linker between DIII and ferritin sequences would allow the DIII to be displayed on the surface of the nanoparticle in its native structure for it to be recognized efficiently by the B cells. However, attempts to determine its structure by cryo-EM was compromised due to the presence of the flexible linker sequences. Insertion of a less flexible linker sequence or direct fusion of DIII with ferritin may allow determination of the DIII structure that would be visible by the immune cells. It would be interesting to see if a construct such as the one without a flexible linker would induce stronger immunological response as compared to the one I have described here. The use of the consensus secrecon signal sequence in the plasmid construct for this vaccine candidate greatly enhances the ability of the synthesized protein to be secreted into the culture medium from which it can be purified in a simple and easily up-scalable purification process.

Previous studies have shown that HA-ferritin nanoparticles induce neutralizing antibody response against a number of pathogens including influenza virus (Kanekiyo et al., 2013), HIV-1 (Sliepen et al., 2015), and Epstein Barr virus (Kanekiyo et al., 2015). Most recently, ferritin nanoparticles have also been used for multivalent display of SARS-CoV-2 spike protein RBD domain (Kalathiya et al., 2021) resulting in induction of potent neutralizing antibodies that could protect ferrets from the virus challenge (Kim et al., 2021). In line with these observations, we have demonstrated that immunization of mice with ferritin-based nanoparticles (zDIII-F) displaying ZIKV E DIII elicits a strong antigen specific neutralizing antibody response which correlates with protection of

animals against lethal ZIKV challenge. The neutralizing antibody response was approximately ten-fold higher than those obtained with the conventional soluble DIII antigen.

The results reported in this study demonstrate that immunization of mice with zDIII-F markedly reduces viral load, alleviates disease symptoms, and protects mice against lethal ZIKV infection. Additionally, passive transfer of sera from immunized animals confers protection in mice by decreasing viral load in serum as well as in tissues. Furthermore, the neutralizing potency of zDIII-F induced antibodies against two other recent ZIKV isolates (PRVABC59 and MEX1-7, both belonging to Asian strain) from recent outbreaks was found to be very similar to the homologous strain (rMR, belonging to African strain), whose DIII sequence was used for vaccine construction, suggesting that the zDIII-F vaccine candidate may protect both African and Asian strains of the virus.

In the vaccination regimen used here, we found that a single dose of zDIII-F nanoparticles induced significantly higher neutralizing antibody response as compared to the soluble DIII. Although I only used one dose (10 µg) of the nanoparticle vaccine, the possibility exists that increasing the antigen dose and/or employing a prime-boost strategy may further enhance the levels of neutralizing antibody responses. In a previous study, a ZIKV vaccine candidate displaying the E-DIII domain on an immunologically optimized cucumber mosaic virus-derived VLP was shown to induce high levels of specific IgG after a single injection that could neutralize ZIKV *in vitro* (Cabral-Miranda et al., 2019). It should be noted that most DIII-based vaccine candidates in the form of soluble antigens, nanoparticles, in tandem repeats, or having been displayed on the

surface of VLPs were shown to induce neutralizing antibody responses to varying degrees that were protective against ZIKV (Chen et al., 2020; Cibulski et al., 2021; In et al., 2020; Shukla et al., 2020c; Yang et al., 2017a; Yang et al., 2017b). However, an exception to this was reported in a study (Lopez-Camacho et al., 2020) showing that DIII conferred limited protection against ZIKV and suggested that the DIII may not be an appropriate vaccine candidate for induction of immune responses against ZIKV. The reason(s) for this discrepancy is not known at this time and clearly further research is necessary. Our results showing that zDIII-F induces high levels of protective neutralizing antibody responses are consistent with the majority of the previous studies.

In attempts to understand the mechanism(s) of protection conferred by zDIII-F vaccine, we have found significantly higher levels of total IgG and IgG2a, which may indicate that Th1 type cellular response likely contributes to the generation of specific antibody classes for protection (preliminary findings). Additionally, IFN-γ^+ CD4 and CD8 cells were also significantly increased, indicating a strong cellular immune response as well. Although these results are preliminary and not included here, our overall data suggest that both humoral and cellular responses are likely contributing factors for protection induced by the zDIII-F vaccine candidate. We realize the limitations of the data presented here such as the use of a single dose of the zDIII-F vaccine candidate, single immunization, and examining the efficacy in immunocompromised mice. Therefore, we have to be cautious in extrapolating our data from the mice model to ZIKV infections in humans. Nevertheless, collectively, this study provides a proof-of-principle for the feasibility of developing an efficacious ZIKV vaccine that uses a multivalent delivery platform for enhanced immunological response against the virus.

CHAPTER IV: IDENTIFICATION AND CHARACTERIZATION OF A NON-NUCLEOSIDE INHIBITOR OF ZIKV RNA POLYMERASE

Part of the studies described in this chapter was published in **Antiviral Research**, **2018**. **Pattnaik, A.,** Palermo, N., Sahoo, B.R., Yuan, Z., Hu, D., Annamalai, A.S. Vu, H.L., Correas, I., Prathipati, P.K., Destache, C.J., Li, Q., Osorio, F.A. Pattnaik, A.K. and Xiang, S.-h. (2018). Discovery of a non-nucleoside RNA polymerase inhibitor for blocking ZIKV replication through *in silico* screening. **Antiviral Research, 151: 78-86. doi.org/10.1016/j.antiviral.2017.12.016**

4.1. Abstract

ZIKV, an emerging arbovirus, has become a major human health concern globally due to its association with congenital abnormalities and neurological diseases. Licensed vaccines or antivirals against ZIKV are currently unavailable. Studies reported here describe our attempt to identify and characterize a small molecule inhibitor of ZIKV replication. At the time these studies were undertaken, the structure of the ZIKV RNA-dependent RNA polymerase (RdRp) was not known. Therefore, we first predicted the structure of the viral RdRp through homology modeling using the known structure of the RdRp of dengue virus (DENV), which is closely related to ZIKV. Subsequently, by employing a structure-based approach targeting the ZIKV RdRp, we conducted *in silico* screening of a library of 100,000 small molecules and tested the top ten lead compounds for their ability to inhibit the virus replication in cell-based *in vitro* assays. One compound, 3-chloro-N-[((4-[4-(2-**t**hienylcarbonyl)-1 **p**iperazinyl]phenyl)amino) carbonothioyl]-1-**b**enzothiophene-2-carboxamide (TPB), potently inhibited ZIKV replication at submicromolar concentrations. Molecular docking analysis suggested that TPB binds to the catalytic active site of the RdRp and therefore likely blocks the viral RNA synthesis by an allosteric effect. The inhibitory concentration 50 (IC_{50}) and the cytotoxicity concentration 50 (CC_{50}) of TPB in Vero cells were found to be 94 nM and 19.4 μM, respectively, yielding a high selective index of 206. In *in vivo* studies using immunocompetent mice, TPB reduced ZIKV viremia significantly, indicating TPB as a potential drug candidate for ZIKV infections.

4.2. Introduction

ZIKV has a single positive-strand RNA genome of ~11 kilobases and replicates using the viral RNA-dependent RNA polymerase (RdRp). Since the RdRp is a key enzyme for ZIKV replication, it is an attractive target for antiviral drug development (Duan et al., 2017; Ramharack and Soliman, 2018; Wang et al., 2017). During replication, the viral positive-sense RNA genome is translated into a single polypeptide that is subsequently cleaved by viral and host proteinases to generate three structural proteins and seven non-structural (NS) proteins (Baronti et al., 2014; Perera and Kuhn, 2008). The NS5 is the most conserved among the NS proteins and contains two domains (Fig. 4.1): the methyltransferase (MTase) domain at the N-terminus (residues 1–264) and the RdRp domain at the C-terminus (residues 275–903). The MTase is required for mRNA capping and stabilization to facilitate translation process, to escape detection of the viral mRNA by the host innate immune sensors as well as for cap-independent methylation with yet unknown functions (Coutard et al., 2017), whereas the RdRp domain is required for RNA synthesis. The structure of ZIKV RdRp, like other RdRps of flaviviruses, adopts a typical right-hand shape architecture which includes three subdomains: fingers, thumb and palm (Duan et al., 2017; Godoy et al., 2017; Upadhyay et al., 2017; Zhao et al., 2017). A large cavity is formed at the junction of the three subdomains. The palm subdomain contains several conserved motifs (A, B, C, D, and E), one of which (motif C), contains the catalytic site residues, GDD (residues 664-666), while the thumb subdomain contains the priming loop (Fig. 4.1). The cavity contains the catalytic site for RNA polymerization, RNA entry and exit channels, and NTP entry channel as well as the large priming loop which plays an important role in regulating

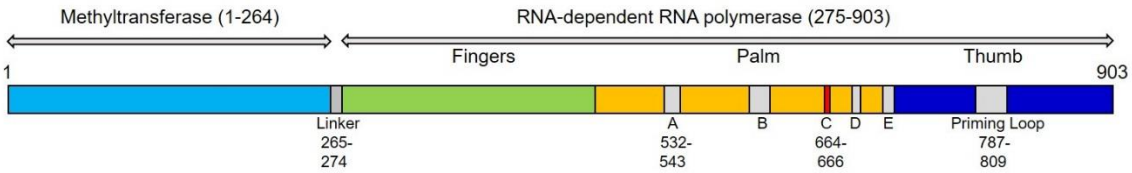

Fig 4.1. The NS5 protein of ZIKV showing the amino-terminal methyltransferase and carboxy-terminal RNA-dependent RNA polymerase (RdRp) domains. Various subdomains in RdRp such as fingers, palm, and thumb subdomains as well as some key structural motifs in palm and thumb subdomains with residue numbers spanning these motifs have been identified. Motif C contains the catalytic active site residues, GDD. Adapted from Zhao, B. et al. (2017), Nature Communications, 8:14762.

RNA synthesis and elongation. This large cavity in the RdRp of other viruses has become a major target for antiviral drug development (Choi and Rossmann, 2009; Duan et al., 2017; Shi and Gao, 2017).

In this chapter, we sought to generate a predicted three-dimensional model of ZIKV RdRp for virtual drug screening. At the time I initiated this project, the three-dimensional structure of the ZIKV RdRp was not known. Since dengue virus (DENV) is closely related to ZIKV, we used the known DENV RdRp structure to perform homology modeling for prediction of the structure of the ZIKV RdRp. Following that, the large cavity containing the active site and the priming loop in ZIKV RdRp was chosen as a target for the structure-based drug screening. *In silico* screening approach was employed to search for compounds that target this large cavity and a library containing about 100,000 small molecule compounds was screened. Subsequently, we identified 10 small molecule compounds with top scores for their ability to bind to this large cavity and then tested their activity to inhibit virus replication in *in vitro* assays. Amongst these top 10 small compounds, one compound, 3-chloro-N-[((4-[4-(2-**t**hienylcarbonyl)-1-**p**iperazinyl]phenyl)amino) carbonothioyl]-1-**b**enzothiophene-2-carboxamide (TPB), was found to inhibit ZIKV replication in cell based assays with high potency at submicromolar concentration and reduced viremia in immunocompetent mice. Hence, we propose its potential as a drug candidate for further development against ZIKV.

4.3. Results

4.3.1. Generation of 3-D structure of RdRp domain of NS5 protein

In 2016, when this project was initiated, the crystal structure of ZIKV NS5 protein (the viral RdRp) was not available. To generate a 3-D model of RdRp, we first aligned the amino acid sequences of ZIKV RdRP with the amino acid sequences of the RdRp of the closely related DENV strain 3 (DENV-3). The RdRp amino acid sequence of the historical strain MR766, 1947 Uganda isolate (accession number: KU720415) and sequence of DENV-3 (accession number: AY662691) were selected from the NCBI database. The sequence alignment was done by using Clustal Omega (EMBL-EBI) and I found that RdRp of ZIKV sequence was highly homologous with RdRp of DENV-3 (Fig. 4.2), with 68% identity and 75% similarity. Since the high resolution (1.8 Å) crystallographic structure of RdRp of DENV-3 was available (Yap et al., 2007), we used this structure as a template to generate a predicted structure of ZIKV RdRp.

Like RdRp structures in other flaviviruses, the ZIKV RdRp structure model showed a very similar right-handed architecture with fingers, palm, and thumb subdomains (Fig. 4.3). The crystallographic structure of RdRp domain of ZIKV NS5 protein of the BeH819015 strain (Brazilian isolate) at 1.8 Å resolution (Duan et al., 2017) was described after we predicted the structure through homology modeling. We compared both the RdRp structures of ZIKV to determine the accuracy of our predicted structure and was found to be superimposable with the reported crystal structure of ZIKV RdRp (Fig. 4.3) with C-alpha atom root mean square deviation (RMSD) of 2.519. The target site appeared to fit well and the relative larger RMSD value should be mainly from the flexible loops and the outer layers of the three domains. This comparison result was very satisfactory and confirmed that our predicted structure was in line with the actual crystallographic structure (Duan et al., 2017).

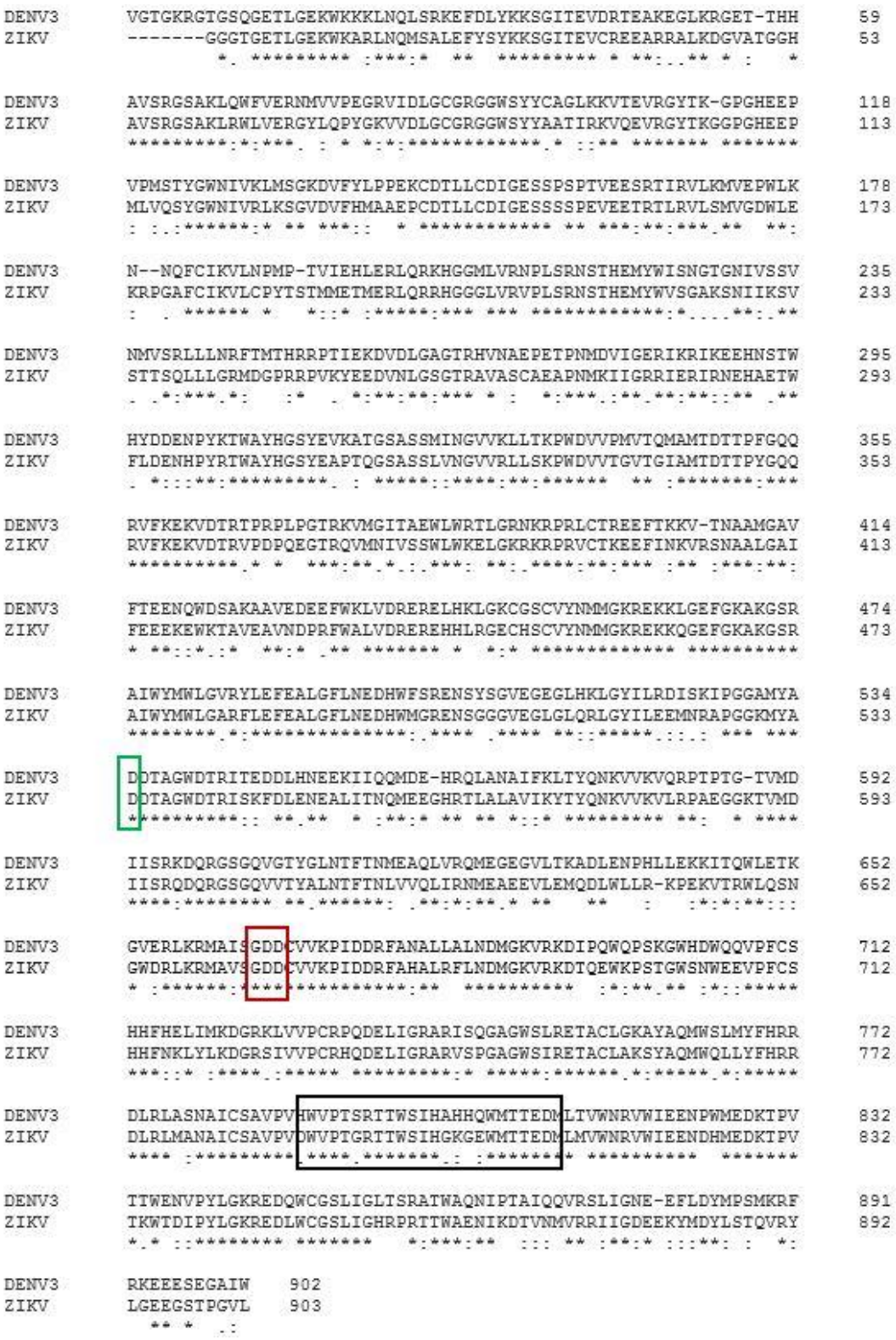
DENV3 VGTGKRGTGSQGETLGEKWKKKLNQLSRKEFDLYKKSGITEVDRTEAKEGLKRGET-THH 59
ZIKV -------GGGTGETLGEKWKARLNQMSALEFYSYKKSGITEVCREEARRALKDGVATGGH 53
DENV3 AVSRGSAKLQWFVERNMVVPEGRVIDLGCGRGGWSYYCAGLKKVTEVRGYTK-GPGHEEP 118
ZIKV AVSRGSAKLRWLVERGYLQPYGKVVDLGCGRGGWSYYAATIRKVQEVRGYTKGGPGHEEP 113
DENV3 VPMSTYGWNIVKLMSGKDVFYLPPEKCDTLLCDIGESSPSPTVEESRTIRVLKMVEPWLK 178
ZIKV MLVQSYGWNIVRLKSGVDVFHMAAEPCDTLLCDIGESSSSPEVEETRTLRVLSMVGDWLE 173
DENV3 N--NQFCIKVLNPMP-TVIEHLERLQRKHGGMLVRNPLSRNSTHEMYWISNGTGNIVSSV 235
ZIKV KRPGAFCIKVLCPYTSTMMETMERLQRRHGGGLVRVPLSRNSTHEMYWVSGAKSNIIKSV 233
DENV3 NMVSRLLLNRFTMTHRRPTIEKDVDLGAGTRHVNAEPETPNMDVIGERIKRIKEEHNSTW 295
ZIKV STTSQLLLGRMDGPRRPVKYEEDVNLGSGTRAVASCAEAPNMKIIGRRIERIRNEHAETW 293
DENV3 HYDDENPYKTWAYHGSYEVKATGSASSMINGVVKLLTKPWDVVPMVTQMAMTDTTPFGQQ 355
ZIKV FLDENHPYRTWAYHGSYEAPTQGSASSLVNGVVRLLSKPWDVVTGVTGIAMTDTTPYGQQ 353
DENV3 RVFKEKVDTRTPRPLPGTRKVMGITAEWLWRTLGRNKRPRLCTREEFTKKV-TNAAMGAV 414
ZIKV RVFKEKVDTRVPDPQEGTRQVMNIVSSWLWKELGKRKRPRVCTKEEFINKVRSNAALGAI 413
DENV3 FTEENQWDSAKAAVEDEEFWKLVDRERELHKLGKCGSCVYNMMGKREKKLGEFGKAKGSR 474
ZIKV FEEEKEWKTAVEAVNDPRFWALVDRERERHHLRGECHSCVYNMMGKREKKQGEFGKAKGSR 473
DENV3 AIWYMWLGVRYLEFEALGFLNEDHWFSRENSYSGVEGEGLHKLGYILRDISKIPGGAMYA 534
ZIKV AIWYMWLGARFLEFEALGFLNEDHWMGRENSGGGVEGLGLQRLGYILEEMNRAPGGKMYA 533
DENV3 DDTAGWDTRITEDDLHNEEKIIQQMDE-HRQLANAIFKLTYQNKVVKVQRPTPTG-TVMD 592
ZIKV DDTAGWDTRISKFDLENEALITNQMEEGHRTLALAVIKYTYQNKVVKVLRPAEGGKTVMD 593
DENV3 IISRKDQRGSGQVGTYGLNTFTNMEAQLVRQMEGEGVLTKADLENPHLLEKKITQWLETK 652
ZIKV IISRQDQRGSGQVVTYALNTFTNLVVQLIRNMEAEEVLEMQDLWLLR-KPEKVTRWLQSN 652
DENV3 GVERLKRMAISGDDCVVKPIDDRFANALLALNDMGKVRKDIPQWQPSKGWHDWQQVPFCS 712
ZIKV GWDRLKRMAVSGDDCVVKPIDDRFAHALRFLNDMGKVRKDTQEWKPSTGWSNWEEVPFCS 712
DENV3 HHFHELIMKDGRKLVVPCRPQDELIGRARISQGAGWSLRETACLGKAYAQMWSLMYFHRR 772
ZIKV HHFNKLYLKDGRSIVVPCRHQDELIGRARVSPGAGWSIRETACLAKSYAQMWQLLYFHRR 772
DENV3 DLRLASNAICSAVPVHWVPTSRTTWSIHAHHQWMTTEDMLTVWNRVWIEENPWMEDKTPV 832
ZIKV DLRLMANAICSAVPVDWVPTGRTTWSIHGKGEWMTTEDMLMVWNRVWIEENDHMEDKTPV 832
DENV3 TTWENVPYLGKREDQWCGSLIGLTSRATWAQNIPTAIQQVRSLIGNE-EFLDYMPSMKRF 891
ZIKV TKWTDIPYLGKREDLWCGSLIGHRPRTTWAENIKDTVNMVRRIIGDEEKYMDYLSTQVRY 892
DENV3 RKEEESEGAIW 902
ZIKV LGEEGSTPGVL 903

Fig. 4.2. Pairwise amino acid sequence alignment of ZIKV and DENV3 RdRp domains. Sequence alignment was performed by Clustal Omega software. Amino acid sequence of RdRp domain (residues 275-903) of ZIKV (accession #: KU720415) was aligned with the corresponding sequences of DENV-3 RdRp domain (accession #: AY662691). The catalytic motif (GDD) of the viral RdRp is boxed with a red rectangle, conserved residue D535 is boxed with green rectangle, and the catalytic cavity used for screening is boxes with a black rectangle.

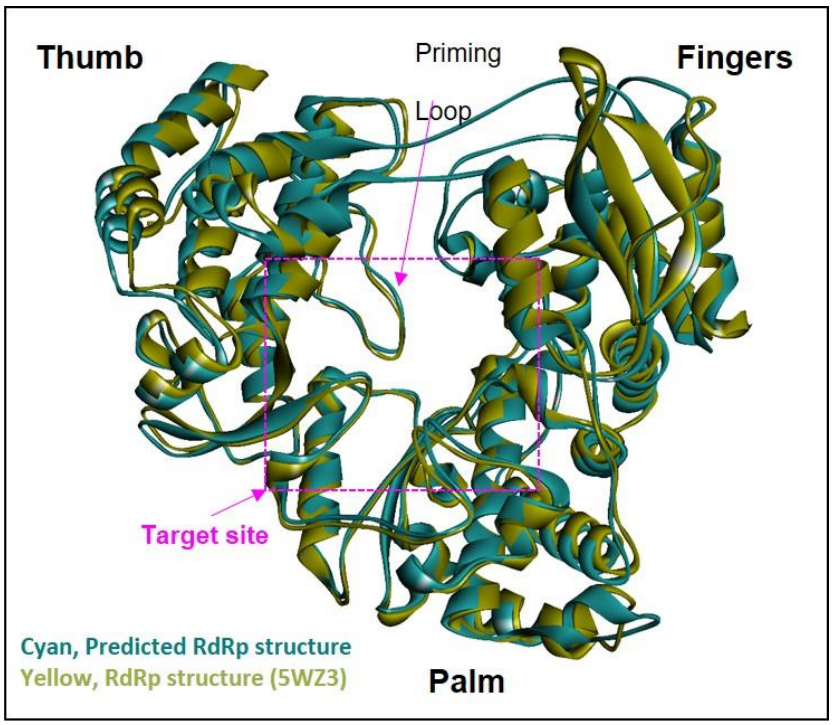

Fig. 4.3. Superimposition and alignment of 3-D structures of ZIKV RdRp domain. The predicted RdRp structure (depicted in cyan) is generated based on the DENV-3 RdRp structure. The actual crystal structure of ZIKV RdRp (PDB ID: 5WZ3), shown in yellow, is superimposed on the predicted structure. The thumb, fingers, palm subdomains and priming loop are shown. The drug target site is marked by pink box. The superimposed ribbon structure was generated using PyMOL software.

4.3.2. Virtual screening of a compound library against RdRp loops

In silico screening of a library of 100,000 small molecule compounds against the catalytic active site on the ZIKV RdRp molecule was conducted. The active site is in the palm sub-domain which is critical for *de novo* RNA synthesis performed by ZIKV RdRp (Duan et al., 2019). Based on the *in silico* screening data, the top 10 compounds with highest docking scores are shown in Table 4.1. The docking score represents how well the compound fits into the cavity and binds to the residues surrounding the cavity. A compound with a lower negative score would suggest its higher binding affinity to the residues surrounding the cavity. The molecular weights of these ten compounds are also similar, ~ 500 Da, which are in the appropriate range of druggable compounds. To test their ability to inhibit virus replication in *in vitro* assays, we purchased these top 10 compounds with the lowest docking scores from Hit2Lead Company (ChemBridge Corporation). Following manufacturer's recommendations, the compounds were dissolved in DMSO to prepare stocks and were stored at -20^{o} C until use. Each of these compound's chemical structures with names are shown in Table 4.1. The compounds were named c1-c10 for sake of convenience.

4.3.3. Cell-based inhibition test of the lead compounds against ZIKV infection

To determine inhibitory effect of the compounds (c1-c10) on ZIKV replication, we infected Vero cells with PRVABC59 ZIKV at an MOI of 1 followed by treatment of the infected cells with 1 μM concentration of the compounds as shown in Fig. 4.4A**.** All the compounds I tested did show some level of inhibition of ZIKV replication, however, the compound c1, 3-chloro-N-[((4-[4-(2-**t**hienylcarbonyl)-1-**p**iperazinyl]phenyl)amino)

Compound	Name	Structure	Mol. Weight	Score
c1	3-chloro-N-[((4-[4-(2-thienylcarbonyl)-1-piperazinyl]phenyl)amino)carbonothioyl]-1-benzothiophene-2-carboxamide	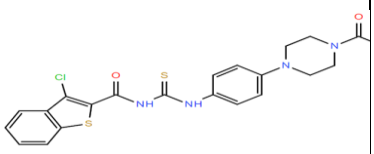	541.108	−118.794
c2	N-(([4-(5,7-dimethyl-1,3-benzoxazol-2-yl)phenyl]amino)carbonothioyl)-3-methyl-1-benzofuran-2-carboxamide	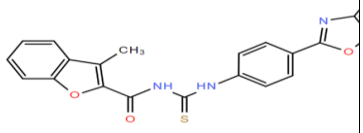	455.528	−118.36
c3	7-[4-(([3-(ethoxycarbonyl)phenyl]amino)carbonothioyl)-1-piperazinyl]-1-ethyl-6-fluoro-4-oxo-1,4-dihydro-3-quinolinecarboxylic acid	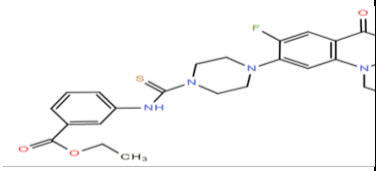	525.572	−118.358
c4	2,2'-[(4,4'-diallyl-4H,4'H-3,3'-bi-1,2,4-triazole-5,5'-diyl)bis(thio)]bis(1-phenylethanone)	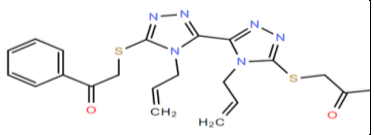	516.638	−118.097
c5	3-(phenoxycarbonyl)benzyl 3-(5-phenyl-1,3,4-oxadiazol-2-yl)benzoate	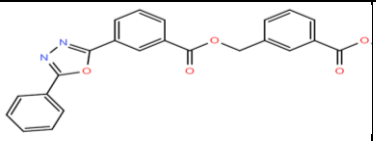	476.480	−117.319
c6	2-[(5-([(4-amino-6,7-dihydro-5H-cyclopenta[4,5]thieno[2,3-d]pyrimidin-2-yl)thio]methyl)-4-phenyl-4H-1,2,4-triazol-3-yl)thio]-N-cyclohexylacetamide	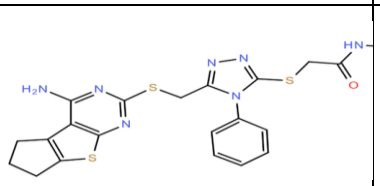	539.61	−116.087
c7	N,N'-[(3-oxo-2,3-dihydro-1H-isoindole-1,1-diyl)di-4,1-phenylene]bis(2-phenylacetamide)	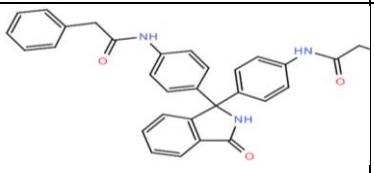	484.618	−115.823

c8	**N-(([3-(3-methyl[1,2,4]triazolo[3,4-b][1,3,4]thiadiazol-6-yl)phenyl]amino)carbonothioyl)-1-benzofuran-2-carboxamide**	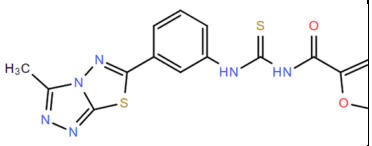	471.592	−115.789
c9	**2-([4-allyl-5-(2-quinolinyl)-4H-1,2,4-triazol-3-yl]thio)-1-(1H-indol-3-yl)ethanone**	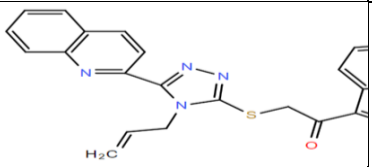	471.574	−115.724
c10	**N-(([5-(5-ethyl-1,3-benzoxazol-2-yl)-2-methylphenyl]amino)carbonothioyl)-1-benzofuran-2-carboxamide**	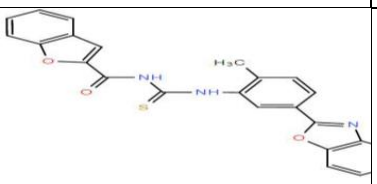	482.443	−114.333

Table 4.1 Top ten compound's chemical structures, names, molecular weight with docking score.

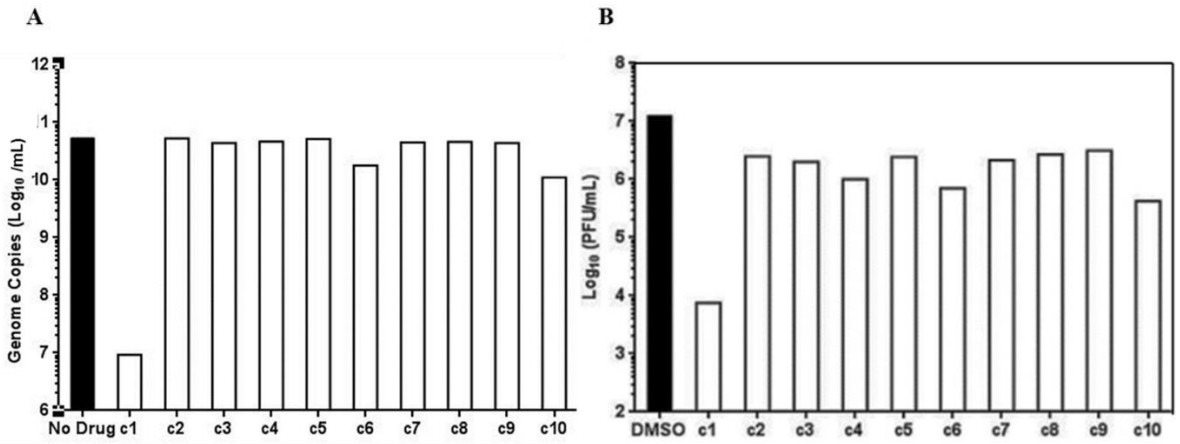

Fig. 4.4. Inhibition of ZIKV replication by the top 10 lead compounds. (A) Viral genome copies in the supernatants of cells infected with PRVABC59 virus in the presence of 1 μM concentration of the ten compounds (c1-c10) or with vehicle (No Drug) alone for 72 hr. The data are expressed as % of DMSO-treated control. The experiment was done in triplicate and bars represent ± SEM. **(B)** Infectious virus titers in the supernatant of cells infected with the virus and incubated with 1 μM concentration of the compounds or with vehicle (DMSO) alone for 96 hr.

carbonothioyl]-1-**b**enzothiophene-2-carboxamide (TPB) exhibited the highest inhibitory activity among the 10 lead compounds. While ZIKV growth was inhibited **(**Fig. 4.4A**)** (as determined by genome copies in the culture supernatants) by ~1000-fold in cells treated with c1 (TPB) compared to the vehicle-only treated cells, c6 and c10 also inhibited virus growth by nearly 10-12 fold. Infectious virus yield was also inhibited by at least 1000-fold in the presence of 1 μM TPB (Fig. 4.4B) whereas c6 and c10 inhibited virus growth by nearly 10-fold at the same concentrations. Although all the compounds readily bound to the target site as per *in silico* docking analysis, c1, c6, and c10 appeared to show additional contacts with the priming loop as well as other regions in the RdRp target site resulting in possibly stronger interactions and better binding (Fig. 4.5A and B). These initial studies thus demonstrated that three compounds, c1, c6, and c10 exhibited significant inhibitory activity on ZIKV growth under *in vitro* conditions, with c1 being the most potent.

4.3.4. Characterization of compound 1 (TPB) interaction with RdRp

From molecular docking analysis, it appears that c1 (named TPB from here onwards), interacts with residues in the target site of the ZIKV RdRp (Fig. 4.6A-C). Three hydrogen bonds of TPB are in direct contact with two aspartic acid residues (D535 in motif A and D665 in motif C) in RdRp (Fig. 4.6A). Since these two aspartic acid residues as well as D666 are highly conserved residues in the target and the active site of all RdRps of flaviviruses and play critical roles in coordinating divalent metal ions (Mg++), TPB could potentially be a highly promising anti-ZIKV as well as anti-flavivirus drug candidate. So, from the initial cursory screening studies, TPB was shown

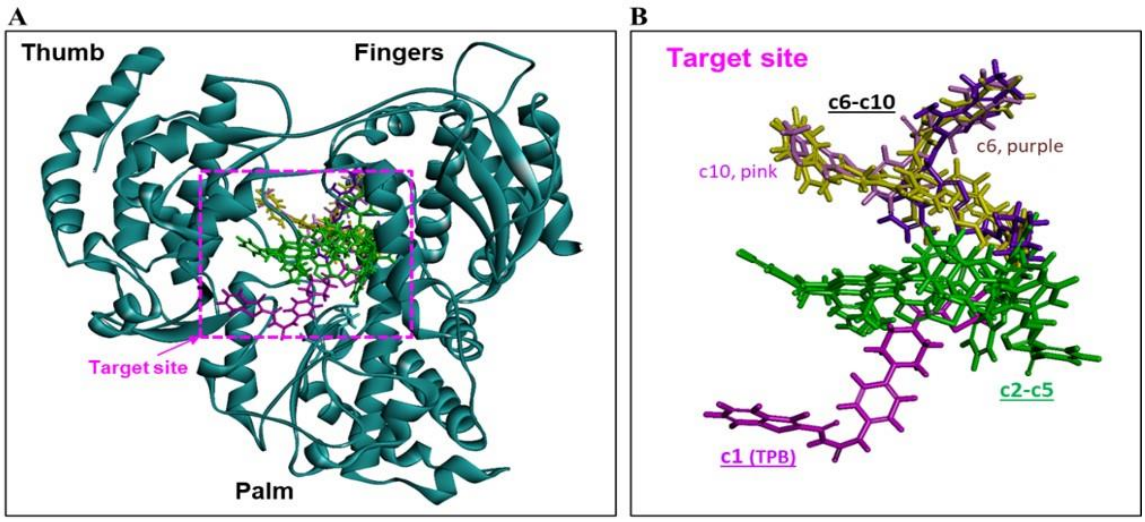

Fig. 4.5. Docking of compounds c1-c10 in the catalytic cavity of the RdRp of ZIKV. **(A)** The drug target site is marked by pink square box. The binding sites and the top 10 compounds are shown in ribbon (protein) and stick (drug) representation. **(B)** Close-up view of stick representation of top 10 compounds within the RdRp target site. The image was generated by PyMol.

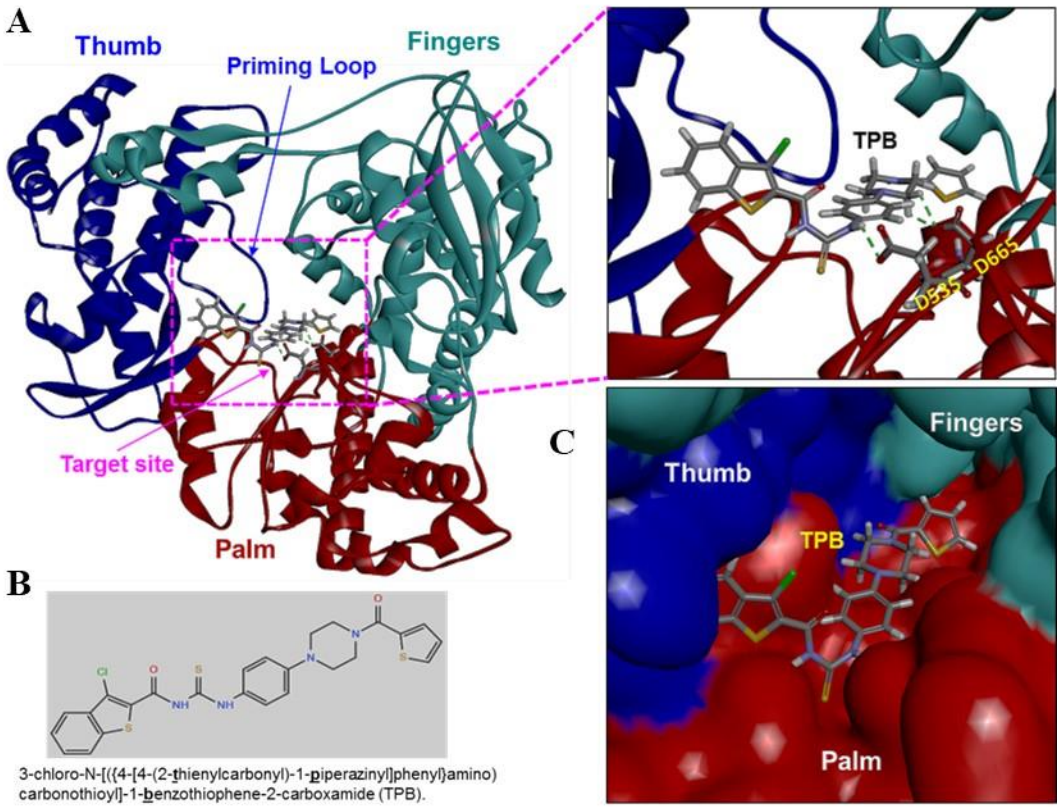

Fig. 4.6. Interaction of TPB with the residues within the target site of RdRp. (A) Structure of ZIKV RdRp generated by homology modeling. The three subdomains are colored separately: fingers (cyan), thumb (blue), and palm (red). The catalytic active site and the priming loop are labeled. Docking of TPB on the active site of RdRp and the contacts with the two aspartic residues (D535 and D665) along with the three hydrogen bonds are indicated. A magnified view of the target site with TPB is shown on the right. The hydrogen bonds (dashed lines) and the two aspartic acid residues are identified. **(B)** The chemical structure of TPB (molecular weight of 541.108 Da). **(C)** The space-filing model of the boxed area in A is shown along with the bound TPB. TPB binding at the palm subdomain is shown.

to inhibit ZIKV replication significantly.

4.3.5. TPB inhibits ZIKV replication in a dose-dependent manner

We then tested the inhibitory activity of TPB in a dose-dependent manner in the μM range. Vero cells were infected with ZIKV at an MOI 1 and treated with different concentrations (0, 0.5, 1, 2, 4, 8 and 16 μM) of TPB for 96 hr. Culture supernatants were then examined for viral genome copy numbers as well for infectious progeny. The results showed that even at 0.5 μM concentration of TPB, significant inhibitory activity against ZIKV replication was observed. Both genome copy numbers (Fig. 4.7A) and infectious virus (Fig. 4.7B) in the supernatants were reduced by over 100-fold at this concentration of TPB. Although TPB at 1 μM reduced virus growth by over 1000-fold, further increase in TPB concentration did not result in further inhibition.

4.3.6. Inhibition of ZIKV protein synthesis by TPB

Since TPB inhibits ZIKV virus replication significantly in cell based assay, we investigated to find out if the inhibitory effect of TPB on ZIKV replication is due to lower viral protein expression in infected cells. We examined the expression levels of E in ZIKV infected cells by western blotting. The ZIKV genome is translated into a single polypeptide which is cleaved to yield 3 structural and 7 non-structural proteins. We chose to look for the expression of E protein since the E protein antibody was readily available. Vero cells were infected with PRVABC59 virus at an MOI 1 and the cells were treated with 0, 0.5, 1, 2 μM concentrations of TPB for 48 hr. Cell lysates were assessed for viral

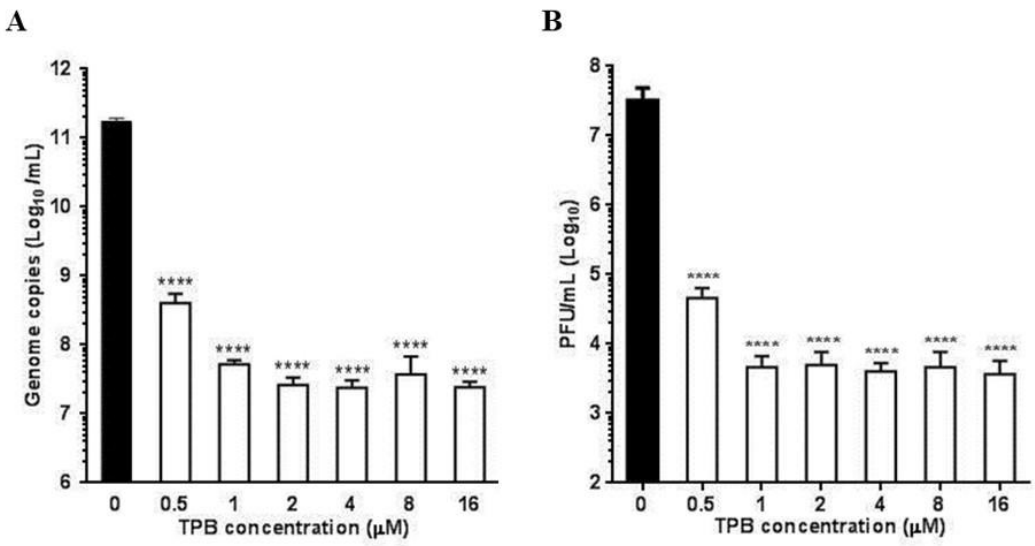

Fig. 4.7. Validation of the antiviral effect of TPB. Cells infected with PRVABC59 virus were incubated in the presence of various concentrations of TPB for 96 h. Culture supernatants were titrated for viral genome copies **(A)** and infectious virus **(B)**. Data are from three independent experiments with error bars showing ± SEM. Statistical analysis was performed using unpaired two-tailed Student'st-test to determine significance of difference. ****, $p \leq 0.0001$.

E protein levels. Results show that the levels of E protein is significantly reduced at 0.5 μM TPB and was undetectable at higher concentrations (Fig. 4.8). These results suggest that TPB inhibits viral protein expression in infected cells.

4.3.7. The growth of the original isolate (MR766) of ZIKV is also inhibited by TPB

Since we used a contemporary isolate of ZIKV (PRVABC59, isolated from a patient in Puerto Rico in 2015) in our initial studies, we wanted to determine if TBP also has antiviral activity against the historical isolate of the virus. In this study, Vero cells were infected with the historical strain of ZIKV, MR766 (isolated in Uganda), at an MOI 1 and treated with different concentrations of TPB for 96 hr. As control, we similarly infected cells with PRVABC59 virus and treated with the same concentrations of TPB. The culture supernatants were collected after 96 hours of infections and assayed for infectious progeny production. Results demonstrated that the MR766 isolate was also inhibited by TPB at the concentrations tested (Fig. 4.9A). The extent of MR766 virus growth inhibition appeared to be similar to that of the PRVABC59 virus (Figs. 4.9B). Overall, it appears that maximal ZIKV growth inhibition by TPB could be achieved at 1-2 μM concentrations and further increase had no significant inhibitory effect, indicating that the TPB inhibitory target is saturable at these concentrations. The results show that both the contemporary and historical isolates of ZIKV are equally inhibited by TPB.

4.3.8. TPB inhibits ZIKV growth in physiologically relevant cell line

Initially all our experiments were conducted using Vero cells. We sought to test whether TPB can inhibit ZIKV replication in physiologically relevant cell lines. ZIKV

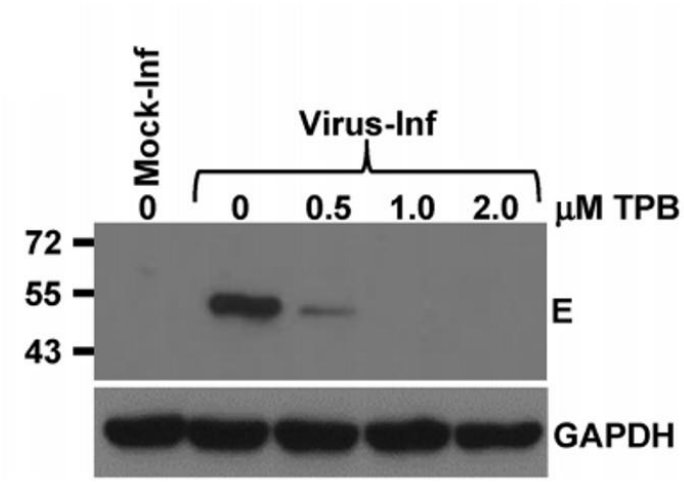

Fig. 4.8. Western blot analysis of E protein expression in the presence of TPB. Vero cells were infected (Virus-Inf) with PRVABC59 virus or mock-infected (Mock-Inf) and subsequently incubated in the presence of various concentrations of TPB. Cell extracts were examined for E protein expression. Relative mobility of molecular mass markers (in kilodaltons) is shown on the left.

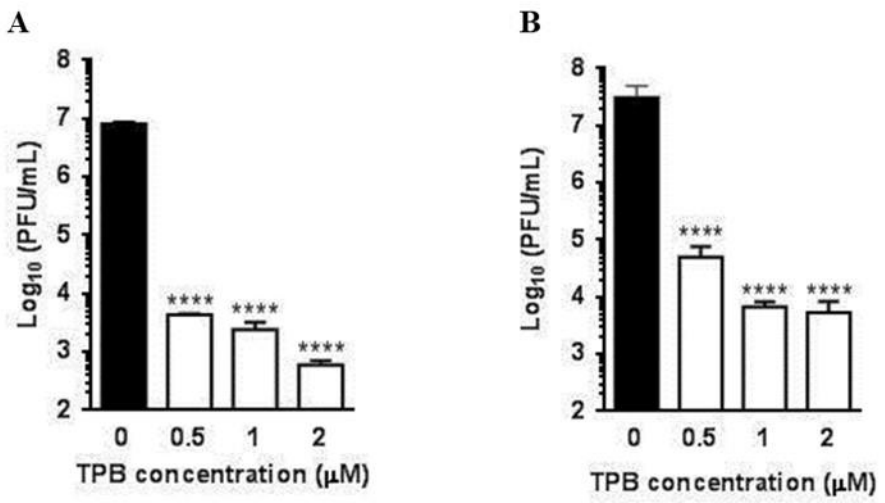

Fig. 4.9. TPB inhibits both African and Asian strains of ZIKV. Cells infected with MR766 (African) or PRVABC59 (Asian) strains of the virus were incubated in the presence of various concentrations (0, 0.5, 1, and 2 μM) of TPB for 96 h. Culture supernatants were titrated by plaque assay. Infectious virus titer of MR766 **(A)** and PRVABC59 **(B)** virus. Data are from three independent experiments with error bars showing ± SEM. Statistical analysis was performed using unpaired two-tailed Student's t-test to determine significance of difference. ****, $p \leq 0.0001$.

has a broad tissue tropism in humans and is known to interact with various cell surface receptors which contributes to its wide cell tropism (Hamel et al., 2015), which in turn may contribute to the clinical manifestation of congenital neurological disorders in infants. ZIKV is known to be transmitted sexually in humans (Allard et al., 2017). Vertical transmission from mother to fetus is also reported (Ciota et al., 2017). Therefore, we choose two cell lines from the human reproductive system, HTR-8 (human trophoblast cell line), and NTERA (human testicular cell line), and SH-SY5Y (neuroblastoma cell line) to check the effect of TPB. A previous study from our lab has shown that the above mentioned cells are permissive to ZIKV infection (Annamalai et al., 2017). My results show that TPB significantly inhibits the virus growth in HTR-8, NTERA, and SH-SY5Y (Figs. 4.10A-C) similar to what was seen in Vero cells. Therefore, our results show that not only TPB inhibits ZIKV growth in Vero cells, but it also inhibits virus growth in several other physiologically relevant cell lines.

4.3.9. Determination of cellular cytotoxicity 50 (CC_{50}) of TPB

Low cytotoxicity is an essential requirement for drug development. It would also suggest whether the drug's inhibitory effect is independent of cellular cytotoxicity due to the presence of the drug. Therefore, we performed a cell viability assay to determine the cellular cytotoxicity 50 (CC_{50}) concentration of TPB. Vero cells were exposed to increasing concentrations of TPB (0.1 μM to 32 μM) and incubated for 96 hr. Subsequently, an ATP-based assay was conducted to determine cell viability and the results showed that cell viability was >95% in the presence of up to 12 μM TPB and

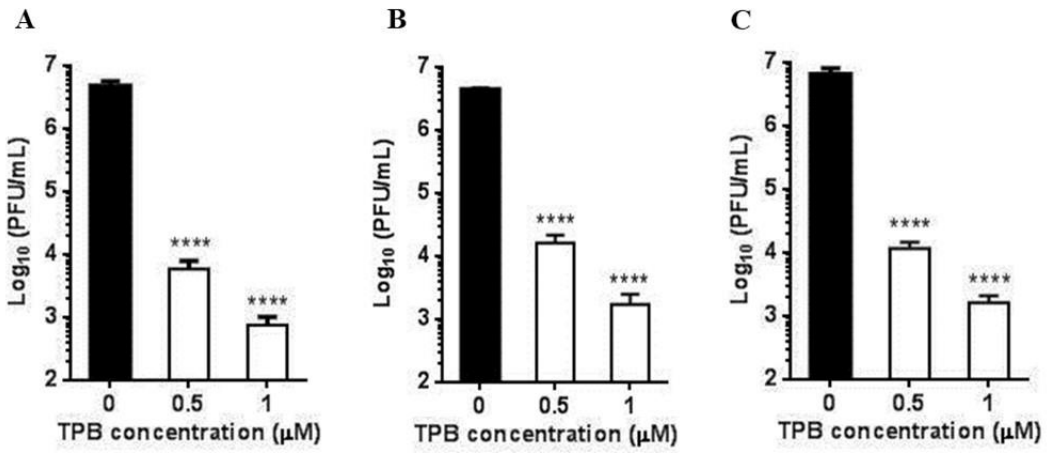

Fig. 4.10. TPB inhibits ZIKV replication in physiologically relevant cell lines. Cells infected with PRVABC59 virus were incubated in the presence of various concentrations (0, 0.5, 1 μM) of TPB for 96 h. Culture supernatants were titrated by plaque assay for infectious virus titers and expressed as PFU/ml. Virus titers in HTR-8 cell line **(A),** in NTERA cell line **(B),** and in SH-SY5Y cell line **(C).** Data are from three independent experiments with error bars showing ± SEM. Statistical analysis was performed using unpaired two-tailed Student'st-test to determine significance of difference. ****, p≤ 0.0001.

further increase in TPB concentration resulted in a gradual loss of viability (Fig. 4.11A). The CC_{50} value for TPB was calculated to be 19.4 μM (Fig. 4.11A).

4.3.10. Inhibitory concentration 50 (IC_{50}) determination

To characterize the anti-ZIKV potency of TPB, we conducted studies to determine the inhibitory concentration 50 (IC_{50}). We used serial 2-fold dilutions of TPB, and treated Vero cells infected with PRVABC59. The culture supernatants were assayed for infectious virus by plaque assay and expressed as % virus yield relative to the virus yield without TPB. The data were statistically analyzed and the IC_{50} concentration was determined to be about 94 nM (Fig. 4.11B). The IC_{50} value of TPB in the 10-100 nM range also suggests that TPB is a strong inhibitor of ZIKV and a potential drug candidate for further development. The selectivity index 50 ($SI_{50} = CC_{50}/IC_{50}$) was calculated to be 206. This high SI_{50} also suggests that TBP is not only a potent inhibitor of ZIKV at submicromolar concentrations but is also nontoxic to the cells.

4.3.11. Comparison of TPB with other known inhibitors of ZIKV

To further compare the potency of TPB relative to other reported ZIKV inhibitors, we examined two compounds that have been recently shown to inhibit ZIKV replication. Mycophenolic acid (MPA) is an immunosuppressant drug and is used to prevent rejection in organ transplantation and was shown to inhibit DENV RNA replication (Diamond et al., 2002). In a screen of FDA-approved drugs for inhibition of ZIKV infection, MPA at 1 μM was found to inhibit infection of cells *in vitro* by ZIKV by over 99% (Barrows et al., 2016). Likewise, ivermectin (IVM), an anti-parasitic drug (Omura and Crump, 2017),

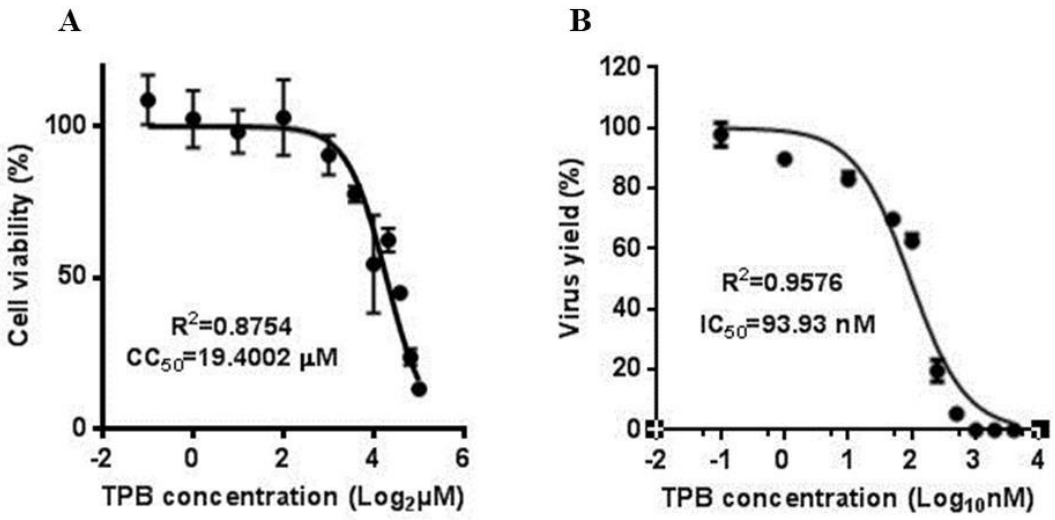

Fig. 4.11. Determination of CC_{50} and IC_{50} of TBP. (A) Vero cells were treated with TPB at various concentrations for 96 hr and cell viability was measured based on ATP assay. The luminescence signals were measured at 420 nm using a Microplate Luminometer. Non-linear regression analysis of the data was employed to determine the CC_{50}. **(B)** For determination of IC_{50} value of TBP, Vero cells were infected with PRVABC59 virus at an MOI of 1 and incubated with various concentrations of TPB as shown. Infectious virus titers in the supernatants of the cells at 96 h post-infection were determined by plaque assay and virus yield was expressed as % of TPB-untreated control. Non-linear-regression was employed to determine the IC_{50}.

which also inhibits YFV infection (Mastrangelo et al., 2012), was found to inhibit ZIKV infection strongly at 10 μM (Barrows et al., 2016). A side-by-side comparison of the inhibitory potency of TPB with MPA and IVM shows that while TPB inhibited ZIKV yield by over 1000-fold, MPA and IVM inhibited virus yield by approximately 10- to 20-fold (Fig. 4.12). These results suggested that TPB is more potent in inhibiting ZIKV as compared to MPA or IVM.

4.3.12. Pharmacokinetic of TPB *in vivo*

Since TPB was found to be a potent inhibitor of ZIKV replication *in vitro*, we wanted to examine if it also inhibits virus replication and viremia in mice. Therefore, we first conducted a pharmacokinetics (PK) analysis of TPB in immunocompetent BALB/C mice to examine the stability and *in vivo* retention of the drug. BALB/C (n=18) were divided into two groups. One group (n=9) was injected with TPB intraperitoneally (IP) at 5mg/kg body weight and the other group (n=9) injected with a dose of 25mg/kg body weight. Blood collection was done every 2 hr to evaluate plasma concentrations of TPB. The results of the PK studies show that TPB is retained in the plasma at approximately 500 ng/ml (corresponding to a concentration of approximately 1 μM) in the initial 2 hr post injection and is gradually reduced to ~100 ng/ml (approximately 0.2 μM concentration) in the next 10-12 hrs at the two doses tested (Fig. 4.13).

4.3.13. Antiviral activity of TPB in vivo

We next tested whether administration of TPB into immunocompetent mice would result in reduced levels of ZIKV viremia. Although immunodeficient mice models

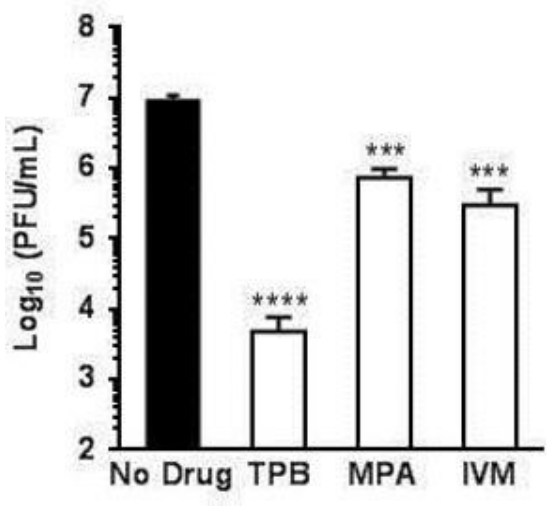

Fig. 4.12. Comparison of TPB inhibitory activity with mycophenolic acid (MPA) and ivermectin (IVM). Vero cells were infected with PRVABC59 virus at an MOI 1 and incubated with TPB (1 μM), MPA (1 μM), or IVM (10 μM). Culture supernatants were collected at 96 h post-infection and assayed for infectious virus. Data presented are from three independent experiments with error bars showing ±SEM. Statistical analysis was performed using unpaired two-tailed Student's t-test to determine significance of difference. ***, $p \leq 0.001$; ****, $p \leq 0.0001$.

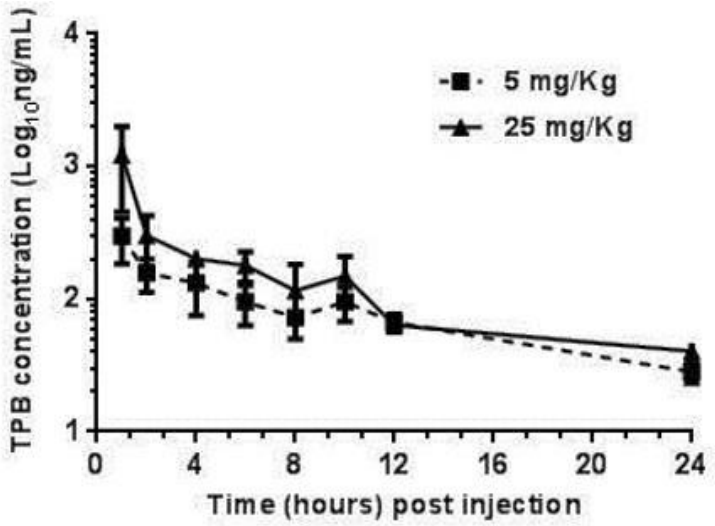

Fig. 4.13. Pharmacokinetics (PK) analysis of TPB in mice. BALB/C mice were divided into two groups. Intraperitoneally, mice in one group (n=9) were injected with TPB (5 mg/kg body weight) while mice in the other group (n=9) were injected with a dose of 25 mg/kg body weight. At every 2 hr intervals, blood was collected from these animals to measure plasma concentrations of TPB. Analysis was done by LC-MS/MS.

have been developed to study ZIKV pathogenesis and drug development (Julander et al., 2017; Lazear et al., 2016; Rossi et al., 2016a; Zmurko et al., 2016), less expensive immunocompetent mice models with limited clinical manifestations have also been used to examine viremia in vaccine studies (Larocca et al., 2016). Based on non-compartment analysis of the pharmacokinetics data, it was estimated that steady-state levels > 500 ng/ml of TPB (~1 μM) could be achieved with three injections at twelve hour intervals at 25 mg/kg dose of TPB in mice. To examine the effect of the drug on ZIKV growth in mice, groups of mice (n = 6) were first injected intraperitoneally with the drug at 25 mg/kg dose and subsequently infected with 500 PFU of ZIKV subcutaneously (Fig. 4.14A). Two more doses of the drug were injected at 0 hr and 12 hr following virus infection. Virus load in the plasma of the animals on days 2, 3, 4, 5, and 6 post-infection was determined. Results of virus growth (genome copies in the serum) in individual animals showed that these immunocompetent mice supported transient ZIKV growth that could only be detected on day 4 (Fig. 4.14B). The level of viral RNA detected on day 4 post-infection was nearly 40-fold lower in mice injected with the drug as compared to the group injected with the vehicle (5% dextrose) alone (Figs. 4.15A). The transient nature of viremia in these animals has also been noted previously (Larocca et al., 2016; Yu et al., 2017). We also examined for the plasma concentration of TPB on 0, 1, and 2 days post-infection and it was found to be on average ~270 ng/ml in the animals on day 2 (Fig. 4.15B). Although this level of TPB was not optimal for maximal virus growth inhibition as observed under *in vitro* conditions, the results suggested that TPB exerts significant growth inhibition of ZIKV *in vivo.*

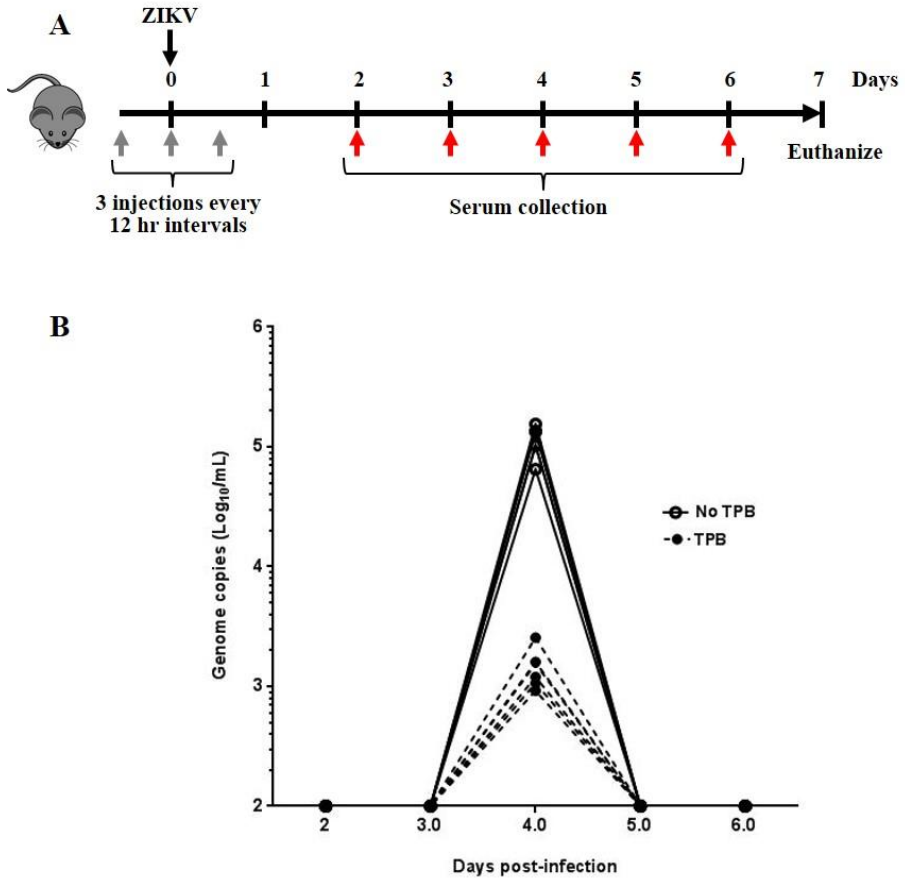

Fig. 4.14. Efficacy of TPB in mice. (A) Schematic diagram showing the experimental plan. BALB/C mice were divided into two groups. Twelve hours prior to virus infection, mice in one group were injected with TPB (25 mg/kg) while mice in the other group were injected with the vehicle (DMSO). All mice were infected subcutaneously with 500 PFU of ZIKV per mouse followed by two additional intraperitoneal injections of TPB at the same dose or DMSO at 0 and 12 hrs after virus infection. **(B)** Genome copies at various days post-infection in the plasma of individual mice treated without (continuous lines) or with (discontinuous lines) TPB.

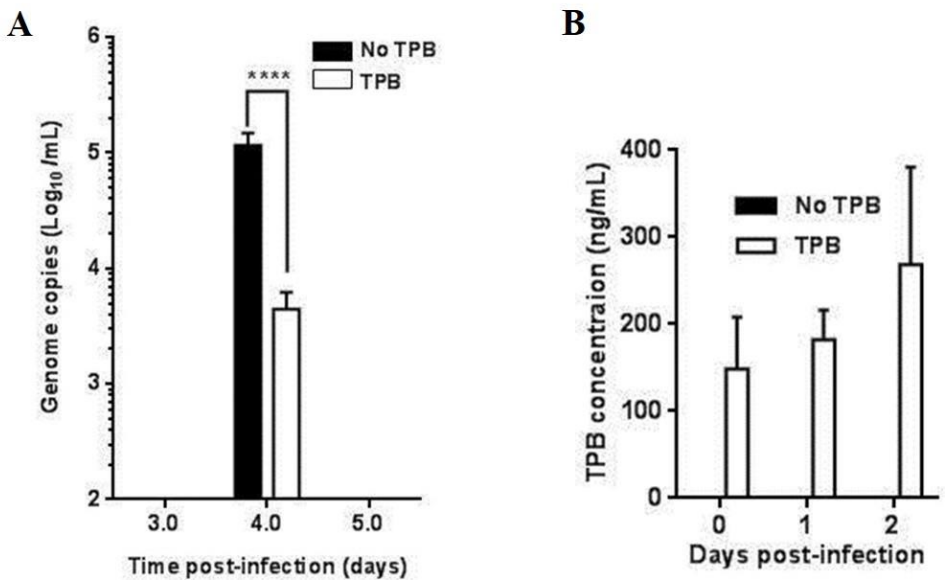

Fig. 4.15. Inhibitory efficacy of TPB in mice. (A) Data from the mice groups in Fig. 14B. Error bars show ±SEM. Statistical analysis was performed using unpaired two-tailed Student's t-test to determine significance of difference. ****, $p \leq 0.0001$. **(B)** TPB mean concentrations in mice plasma (from Fig. 14B) at various days post-injection. Error bars show ±SEM.

4.4. Discussion

Through *in silico* screening of a library of 100,000 small molecules, we identified TPB as a potential anti-ZIKV drug candidate. Subsequent *in vitro* and *in vivo* studies demonstrated that TPB exhibits potent inhibitory activity against ZIKV at submicromolar concentrations. The inhibitory activity was shown to be against both the African and Asian genotypes representing the historical and contemporary isolates of the virus. In addition, the inhibitory effect of TPB is cell-type independent at least in the cells tested in this study. The IC_{50} and CC_{50} of TPB were determined to be 94 nM and 19.4μM, respectively, yielding an SI_{50} value of over 200. Such high SI_{50} value suggests that TPB has a strong potential for an effective anti-ZIKV drug with little to no cytotoxicity.

TPB is a non-nucleoside compound which makes it more valuable in the drug development field since non-nucleoside inhibitors (NNI) of viral RdRps are considered to inhibit through allosteric effect by blocking RNA replication/transcription. Thus, they are more selective for viral targets only and with significantly less side-effects (Lim et al., 2015; Malet et al., 2008). Furthermore, since TPB was docked to the active site of the ZIKV RdRp forming three hydrogen bonds in direct contact with two aspartic acid residues (D535 in motif A and D665 in motif C) in RdRp (Fig. 4.5A and 4.6A), it makes this compound a promising anti-ZIKV drug candidate. The aspartic acid residues (D535/D665 or D535/D665/D666) are highly conserved in the active sites of all RdRps of flaviviruses and play essential roles in coordinating with two divalent metal ions (Mg^{++}) for initiation of ribonucleotide polymerization (Butcher et al., 2001; Choi and Rossmann, 2009; Duan et al., 2017; Godoy et al., 2017; Ng et al., 2008; Yap et al., 2007; Zhao et al., 2017). The binding of TPB to these active site residues and possibly blocking

of this active site are likely very efficient, which may likely explain the potent inhibitory activity of TPB at submicromolar concentrations. However, *in vitro* binding of the polymerase with TPB leading to inhibition of RdRp activity needs to be validated experimentally. Additionally, the binding of TPB to NS5 may alter its interaction with other NS proteins involved in virus genome replication leading to inhibition. Future studies will reveal the mechanism of inhibition of NS5 function by TPB.

We have evaluated TPB toxicity in terms of cell viability using ATP-based assays and found no cellular toxicity. When TPB was administered at 25 mg/kg dose, all mice appeared normal over a six-day period. However, if TPB is to be tested for its potential use as a drug candidate, detailed investigation needs to be conducted to assess its toxicity *in vivo*. Since the ZIKV RdRp model used in this research was generated from homology modeling using the DENV-3 RdRp structure, it is presumed that TPB and other lead compounds could be tested for anti-DENV activity. Additionally, because ZIKV RdRp aa sequence is closest to JEV EdRp (Lu and Gong, 2013; Upadhyay et al., 2017), it is possible that TPB could also be effective against JEV. Although there are some observed structural differences such as in the Ring motif F, the active site is highly conserved in the flavivirus RdRps. Of special note here are the two aspartic acid residues (D535/D665) that are present in the catalytic pocket of RdRp that provide a foundation for TPB binding.

In conclusion, through the *in silico* screening approach, we have identified a non-nucleoside compound, TPB, which shows a potent inhibitory activity against ZIKV infection *in vitro* as well as *in vivo*. TPB is a novel non-nucleoside inhibitor targeting the active site of ZIKV and likely other flavivirus RdRp.

CHAPTER V: INHIBITION OF ZIKV REPLICATION BY G-QUADRUPLEX-BINDING LIGANDS

Part of the studies described in this chapter was published in **Molecular Therapy: Nucleic Acids, 2021**

Majee, P., **Pattnaik, A.**, Bikash R. Sahoo, Uma Shankar, Asit K. Pattnaik, Amit Kumar, and Debasis Nayak (2021). Inhibition of ZIKV replication by G-quadruplex- binding ligands. **Molecular Therapy: Nucleic Acids Vol. 23, 691-701. doi.org/10.1016/j.omtn.2020.12.030**

5.1. Abstract

In recent years, the presence of non-canonical G-quadruplex (GQ) secondary structures in viral genomes has ignited significant attention as potential targets for anti-viral strategy. In this study, we identified several novel conserved potential GQ structures by analyzing published ZIKV genome sequences. Whether these potential GQ structures do actually exist in the genome of ZIKV and whether they play any role in the viral genome replication were addressed in experiments reported here. Bio-physical and biochemical analysis of the RNA sequences suggested the existence of GQs in the ZIKV genomes. Studies with known GQ structure-binding and -stabilizing ligands such as Braco-19 and TMPyP4 provided further support for this contention. In cells infected with ZIKV, the presence of these ligands in culture media led to significant inhibition of infectious ZIKV yield. Furthermore, viral genome replication as well as viral protein production were significantly downregulated in the presence of these drugs. Overall, our results, for the first time, show that ZIKV replication can be inhibited by GQ structure-binding and -stabilizing compounds. Results from our studies will greatly expedite research on the use of GQ-binding ligands as potential therapeutics against ZIKV replication for mitigation and control of infections.

5.2. Introduction

As there are no effective licensed vaccines or drugs currently available, various strategies and approaches are being explored for the development of vaccines and antiviral drugs against ZIKV. These include targeting viral proteins (structural and non-structural) for vaccine development and repurposing of the already approved antivirals and/or anticancer drugs (Zou and Shi, 2019) as potential antivirals. Further research on

alternate strategies for the discovery of new and effective antiviral compounds is warranted. In the previous chapter of this thesis, we explored the possibility of using the viral RdRp as the target to identify and characterize a non-nucleoside inhibitor of the virus replication. In this chapter, we target the viral genome structural features for the purpose of developing an antiviral strategy.

As outlined in the introductory chapter of this thesis, the G-quadruplex (GQ)-forming sequences are being explored extensively as drug targets and have gained significant attention as potential antiviral strategies in recent years (Lavezzo et al., 2018; Ruggiero and Richter, 2018). Several viruses including SARS-CoV-2 (Cui and Zhang, 2020), ZIKV (Fleming et al., 2016), human papillomaviruses (HPV) (Tluckova et al., 2013) herpes simplex virus (HSV) (Artusi et al., 2015) and human immunodeficiency virus (HIV) (Piekna-Przybylska et al., 2014) are reported to bear GQ-forming sequences in their genome. Furthermore, the GQ-binding ligands such as Braco-19 and core-extended naphthalene diimides (NDI) have been shown to have a significant antiviral effect on HIV replication (Perrone et al., 2014; Perrone et al., 2015). Another potent GQ-binding ligand, TMPyP4, was found to stabilize the GQ structure in the Ebola virus polymerase (L) gene, thereby repressing its expression at the RNA transcription level (Wang et al., 2016b). A similar effect of TMPyP4 was also observed in the case of the core gene of hepatitis C virus (HCV) (Wang et al., 2016a). These studies provide a framework for further research on the potential use of GQ-binding and -stabilizing ligands for antiviral strategies (Lavezzo et al., 2018; Ruggiero and Richter, 2018).

In a recent report (Fleming et al., 2016), it was first shown that putative GQ-forming sequences are present in the ZIKV genome that are largely conserved among the

Flaviviridae family, although the functional consequences of the presence of such structures were not examined by the authors. In this study, we have discovered a number of additional GQ-structure-forming sequences that are unique ZIKV in addition to those reported by Fleming *et al*. Taking ZIKV genomic RNA sequences carrying several of these potential GQ structures, and by using various assays such as fluorescence titration assay, nuclear magnetic resonance (NMR) spectral analysis, isothermal titration calorimetric (ITC) assay, and thermal denaturation experiments, our research collaborators in India demonstrated that (1) the GQ structures do in fact exist in these RNA sequences, and (2) that the GQ-binding ligands such as Braco-19 and TMPyP4 bind specifically to these structures and stabilize them. Extending those observations, we conducted studies to show here that treatment of ZIKV-infected cells with these ligands results in significant reduction in infectious virus production, as well as inhibition of viral genome replication and viral protein production in a dose-dependent manner. Thus, GQ-ligand binding strategy displayed in this study stands as a proof of concept and appears promising toward the development of potential antiviral agents against ZIKV infection.

5.3. Results

5.3.1. ZIKV genome has potential GQ structures conserved across the strains

In a previous study, it was reported that Flaviviruses including the ZIKV contain conserved GQ-forming sequences (Fleming et al., 2016). By employing stringent criteria where the number of guanine repeat was kept ≥2 and the loop length was restricted between 1 and 7 nucleotides, we identified four new ZIKV GQs (ZGQ1-4) conserved in the NS genes NS2, NS4B, and NS5 genes of ZIKV genome (Fig.5.1A) in addition to the

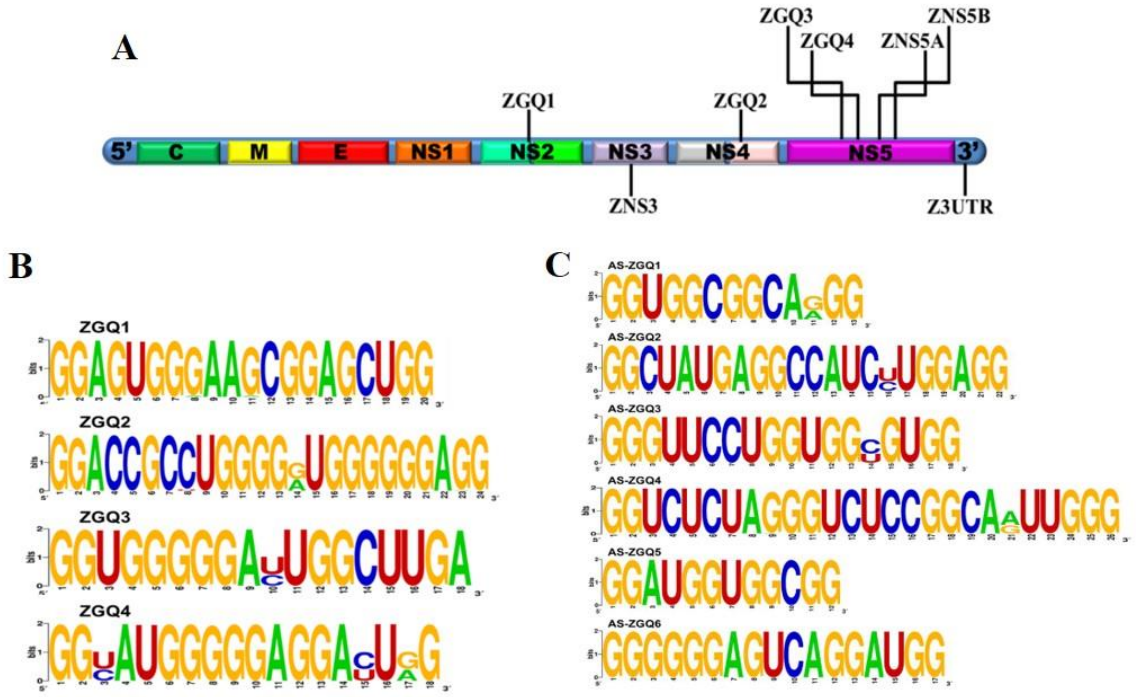

Fig. 5.1. G-quadruplex (GQ) structures are highly conserved in ZIKV genome. (A) Schematic diagram showing the location of the GQ sequences predicted in the ZIKV genome. Seven GQ sequences are distributed in the NS genes, namely, NS2, NS3, NS4B, and NS5, and one in the 3' UTR region. **(B)** WebLogo representation of the four newly predicted ZGQ sequences (ZGQ1-4) showing conservation of the nucleotides among various strains. The height of the letter indicates the relative frequency of that particular nucleotide at that position, therefore reflecting the degree of conservation at that position. **(C)** WebLogo representation of the predicted GQ sequences showing conservation of the nucleotides among different strains in the anti-genomic (negative-sense) RNA.

other ZGQs (ZNS3, ZNS4, ZNS5A, and ZNS5B) identified previously (Fleming et al., 2016). Importantly, the genome-wide mining of 247 ZIKV genomes from the NCBI Genome database revealed that these newly identified ZGQs are highly conserved among >90% of the ZIKV strains (Majee et al., 2021) (Fig. 5.1B). As displayed in Fig. 5.1B, the WebLogo representation of the newly predicted four ZGQ sequences suggests that the guanine residues involved in the GQ formation are highly conserved among the analyzed strains. The residues present in the loop region are mostly divergent. Because ZIKV is an RNA virus, it is prone to a higher mutation rate (Duffy, 2018); thus, the conservation of these ZGQs across the isolates suggests functional importance of these sequences associated with viral life cycle and pathogenesis. Since ZIKV replication occurs through anti-genomic (negative-sense) RNA intermediates, we also examined the presence of ZGQs in the negative-sense RNA. Our search identified several highly conserved ZGQ sequence motifs (AS-ZGQs) in the viral anti-genomic (negative-sense) RNA (Majee et al., 2021) (Fig. 5.1C).

5.3.2. ZIKV growth is inhibited *in vitro* in the presence of GQ-binding compounds Braco-19 and TMPyP4

Biophysical and biochemical characterization of ZGQ1-4 by our collaborators suggested that the predicted ZGQ in ZIKV genome can fold into GQ structures that are be stabilized through the binding of Braco-19, as well as TMPyP4. To determine whether the presence of such structures and stabilizing them through binding with Braco-19 could impact ZIKV growth in cultured cells, we performed experiments to assess ZIKV growth in Vero cells in the presence of varying concentrations of the drug. Vero cells infected

with MR766 isolate of ZIKV were treated with Braco-19 and infectious virus yield in the supernatants at various time points was measured by plaque assay. In response to Braco-19 treatment, the infectious virus yield showed a significant reduction in a dose-dependent manner, at each of the time points examined. The inhibition of virus growth was most significant at 96 hpi in the presence of 100 μM concentration of Braco-19, compared to the untreated control (Fig. 5.2A). At lower concentrations (1 μM and 10 μM), although we reproducibly observed 3-5 fold less infectious
virus compared to untreated controls at all the time points examined, they were not statistically different from the untreated control.

In a similar experiment using a different GQ-binding and -stabilizing drug TMPyP4, we observed that ZIKV growth was also significantly inhibited (Fig. 5.2B). At a concentration of 10 μM, the infectious virus yield in the supernatants at 72 hpi and 96 hpi was reduced nearly 120-fold and 170-fold, respectively, compared to the untreated control (Fig. 5.2B). However, at 100 μM concentration, the infectious virus yield in the supernatant was below the limit of detection at any of the time points studied (Fig. 5.2B).

To determine inhibition of viral replication was due to binding of the drug to GQ structures and not to drug-dependent cytotoxicity, we performed a cell viability assay. This experiment allowed me to determine the overall health of cells in the presence GQ binding ligands. We treated Vero cells with 0, 1, 10 and 100 μM concentrations of Braco-19 or TMPyP4 for 4 days. Four independent experimental replicates with the above mentioned concentrations were done for both the compounds. Four days after drug treatments, cell viability was determined by flow cytometry analysis. In the presence of 100 μM concentration of Braco-19, where virus growth was inhibited by > 80-fold, cell

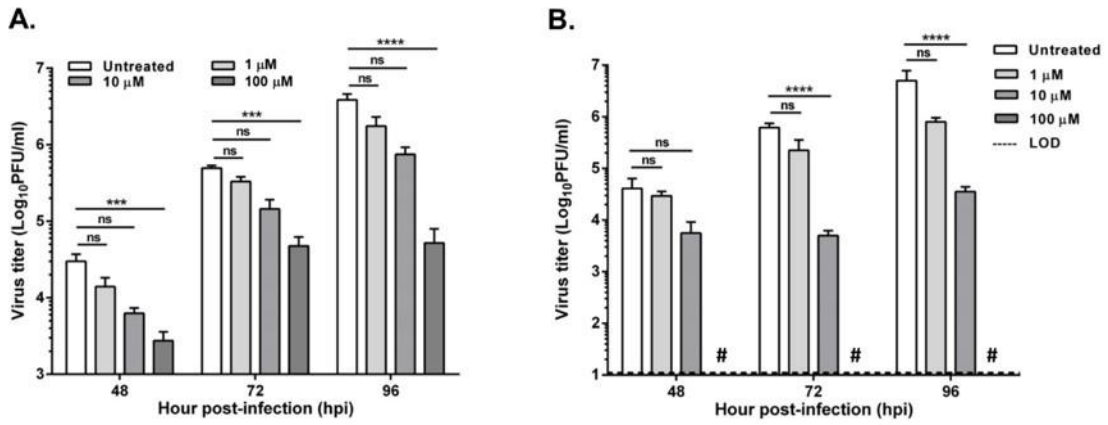

Fig. 5.2. Inhibition of ZIKV growth in cells treated with Braco-19 and TMPyP4. Vero cells infected with ZIKV at an MOI of 1 were incubated in medium containing 0 (untreated), 1 μM, 10 μM, and 100 μM concentrations of Braco-19 (**A**) or TMPyP4 (**B**). Aliquots of culture supernatants were collected at various hour post-infection (hpi) and infectious virus titers were determined by plaque assay. The graphs show mean values of virus titers, with error bars representing standard deviations from the results of four independent experiments. Two-way ANOVA was used to determine significant differences in virus titers between untreated and drug-treated samples. LOD, the limit of detection. # represents values below LOD. ns, nonsignificant; ***$p \leq 0.001$; ****$p \leq 0.0001$

viability was greater than 85% (Fig. 5.3). Unlike Braco-19, TMPyP4 was toxic at 100 μM and cell viability was ~40% (Fig.5.3); however, at 1 μM and 10 μM concentrations where ZIKV growth inhibition was significant, cell viability was shown to be over 85%. Overall, these results show that both Braco-19 and TMPyP4 inhibit ZIKV growth at concentration which are not toxic to the cells and suggest that these GQ-binding ligands directly inhibit ZIKV growth without adversely affecting cell viability.

5.3.3. Intracellular accumulation of infectious virus is not significantly different in the presence or absence of Braco-19 or TMPyP4

It is possible that lower levels of infectious virus in the culture supernatants of infected cells in the presence of Braco-19 and TMPyP4 could be due to increased accumulation of intracellular virus. To investigate such a possibility, we determined the amount of virus present in the cells. For this, following infection of cells in the presence of the drugs for 72 hours, we collected the culture supernatants, washed the cells with PBS and then subjected the cells to three rounds of freeze-thaw in the presence of PBS to break open the cells and release cell-associated virus, after which the clarified cell extracts were assayed for infectious virus by plaque assay. As can be seen (Fig. 5.4), on average, cell-associated virus represented about 17-fold less than the virus released in the supernatants of infected cells under no-drug treatment condition at 72 hpi. In the presence of 100 μM Braco-19 or 10 μM TMPyP4, cell-associated virus represented approximately 14- to 15-fold less than that in the corresponding supernatants. Importantly, the cell-associated virus in drug treated cells were significantly lower than those in untreated cells (Fig. 5.4). These results show that both Braco-19 and TMPyP4 inhibit infectious ZIKV

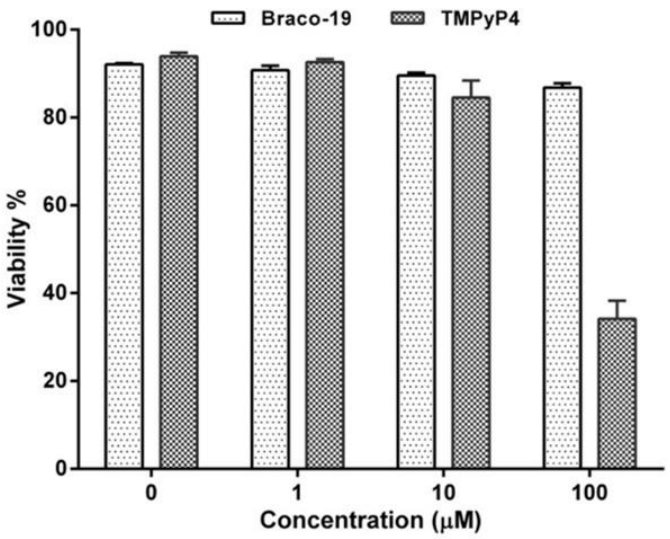

Fig. 5.3. Cell viability in the presence of Braco-19 and TMPyP4. Vero cells were exposed to 0, 1, 10, and 100 μM Braco-19 or TMPyP4 for 4 days. Following exposure, the cells were trypsinized and stained with mBCl and propidium iodide (PI) to measure cell viability and total cell number. Flow cytometric data acquisition was performed using a BD Cytek flow cytometer (Becton Dickinson, Franklin Lakes, NJ) in the VioFL1 and BluYeFL3 channels and data analysis was done using FlowJo software (Becton Dickinson, Franklin Lakes, NJ).

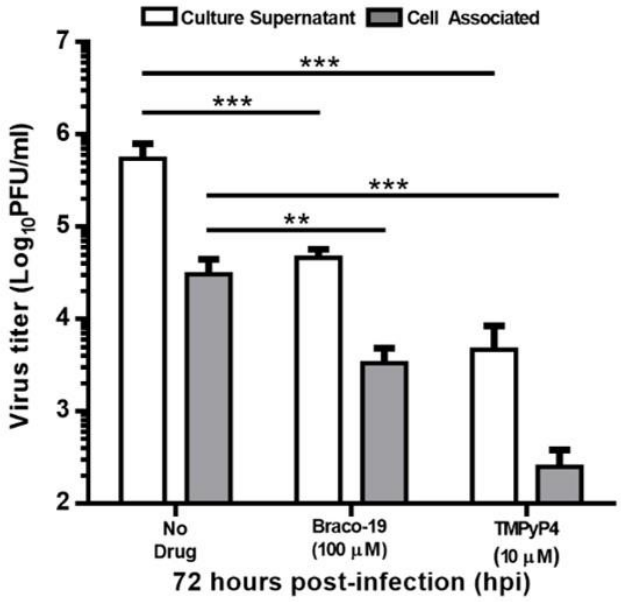

Fig. 5.4. Inhibition of ZIKV progeny virus production in cells treated with Braco-19 and TMPyP4. Vero cells were infected with ZIKV at an MOI of 1 and treated with 100 μM Braco-19 or 10 μM TMPyP4 for 72 hpi. Infectious virus in the supernatants and cells were quantitated by plaque assay. The graphs show mean values of virus titers, with error bars representing standard deviations from the results of three independent experiments. Two-way ANOVA was used to determine significant differences in virus titers between untreated and drug-treated samples. **$p \leq 0.01$; ***$p \leq 0.001$

progeny production.

5.3.4. ZIKV viral protein synthesis is inhibited by Braco-19 and TMPyP4

Since Braco-19 and TMPyP4 treatment reduced infectious ZIKV yield, we next sought to find out whether this is due to lower viral protein expression in infected cells. We examined the E protein expression levels in virus-infected cells in the presence of Braco-19 or TMPyP4. Since the ZIKV genome is translated into a single large polyprotein, which is processed to yield 10 different proteins including the E protein, we picked the E protein as indicator viral protein production. Vero cells, infected with MR766 ZIKV, were treated with varying concentrations of Braco-19 or TMPyP4 immediately after infection. Cell lysates were prepared from the infected cells at 48 or 96 hpi and analyzed for E protein levels by western blotting. Results showed a marked reduction in E protein expression with increasing concentrations of Braco-19 at both 48 hpi and 96 hpi (Fig. 5.5 A-B). The reduction of E protein levels was most pronounced at 100 μM Braco-19 and at 96 hpi, although reduction in the levels of E was reproducibly seen at lower concentrations.

In response to TMPyP4 treatment, E protein levels showed noticeable reduction over time (Fig. 5.6A-B). Interestingly, the electrophoretic mobility of the E protein was altered at 48 hpi time point (Fig. 5.6A), with increasing dose of TMPyP4, resulting in apparently increased molecular mass of the E protein. However, at 96 hpi, the reduced electrophoretic-mobility of E was only observed with 100 μM TMPyP4 (lane 5, Fig. 5.6B) and the mobility difference was less pronounced compared to Braco-19. The reason for the observed electrophoretic mobility shift in E protein in the presence of TMPyP4 is

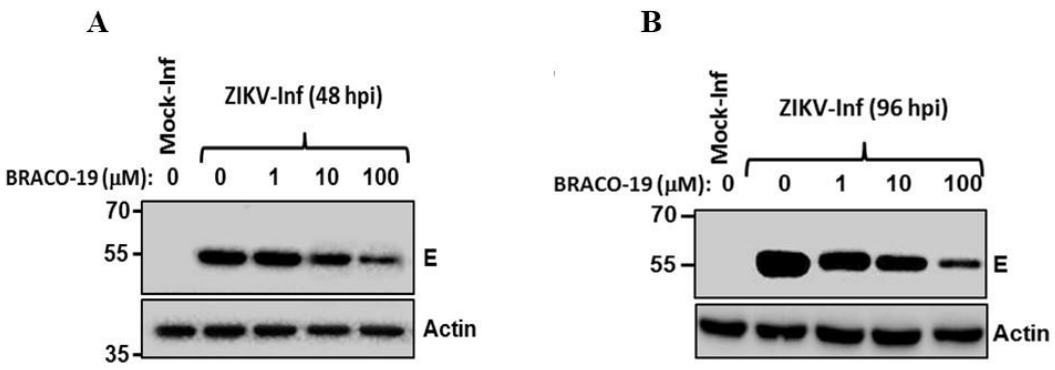

Fig. 5.5. Braco-19 inhibits viral protein synthesis. Vero cells were either mock-infected or infected with ZIKV at an MOI of 1 and subsequently incubated in medium containing 0, 1 μM, 10 μM, and 100 μM concentrations of Braco-19. Cell extracts were prepared at 48 hpi **(A)** and 96 hpi **(B)**. Twenty μg of proteins from each sample were analyzed by SDS-PAGE and western blotting with ZIKV E antibody to detect viral E protein. Levels of actin detected in the blots using anti-actin antibody served as the loading control. Molecular mass markers (in kDa) are shown on the left. Representative data are shown in each panel.

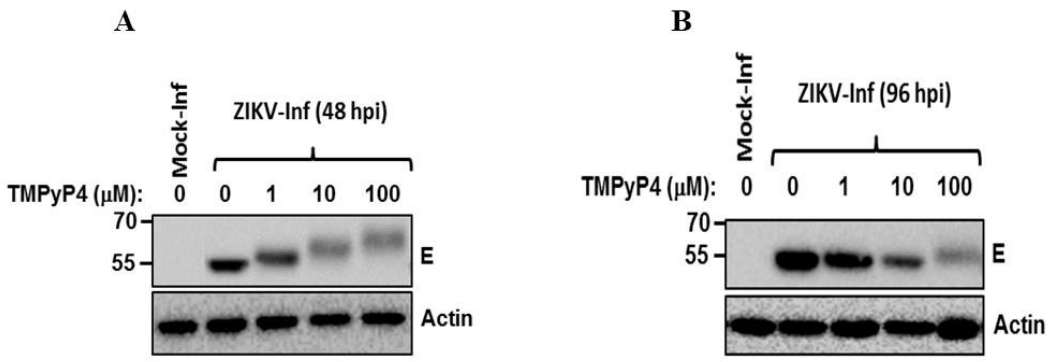

Fig. 5.6. TMPyP4 inhibits viral protein synthesis. Vero cells were either mock-infected (M) or infected with ZIKV at an MOI of 1 and subsequently incubated in medium containing 0, 1 μM, 10 μM, and 100 μM concentrations of TMPyP4. Cell extracts were prepared at 48 hpi (**A**) and 96 hpi (**B**). Twenty μg of proteins from each sample were analyzed by SDS-PAGE and western blotting with ZIKV E antibody to detect viral E protein. Levels of actin detected in the blots using anti-actin antibody served as the loading control. Molecular mass markers (in kDa) are shown on the left. Representative data are shown in each panel.

unclear at this time but it is possible that metabolic byproducts of TMPyP4, known to be generated in cells could bind to the E protein in a time- and concentration-dependent manner to reduce the mobility of the E protein. Nevertheless, our results suggest that both Braco-19 and TMPyP4 inhibit viral protein expression in infected cells.

5.3.5. ZIKV genome replication is inhibited by Braco-19 and TMPyP4

Since the GQ binding ligands directly target the GQ structures in the viral genomic and anti-genomic RNAs, these drugs are likely to impede progress of the viral RdRp during genome replication and ribosomal movement during translation. As we have already demonstrated reduction in viral protein levels in the presence of these ligands, we next sought to determine whether intracellular replication of the ZIKV genome is negatively affected by the GQ-binding ligands. Vero cells, infected with ZIKV MR766, were treated with Braco-19, TMPyP4, or left untreated and total RNA from the cells was extracted at 72 and 96 hpi. Total RNA was subjected to qRT-PCR with ZIKV-specific primers and probes to determine the copy numbers of the viral positive-sense genome. In these experiments, we used 100 μM Braco-19 and 10 μM TMPyP4 because these concentrations of the ligands exhibited maximum inhibition without adversely affecting cell viability. Results from the experiment showed that ZIKV genome copies were significantly lower in cells treated with Braco-19 or TMPyP4 at both 72 and 96 hpi (Fig. 5.7), suggesting that these GQ-binding molecules inhibit ZIKV genome replication in infected cells.

5.4. Discussion

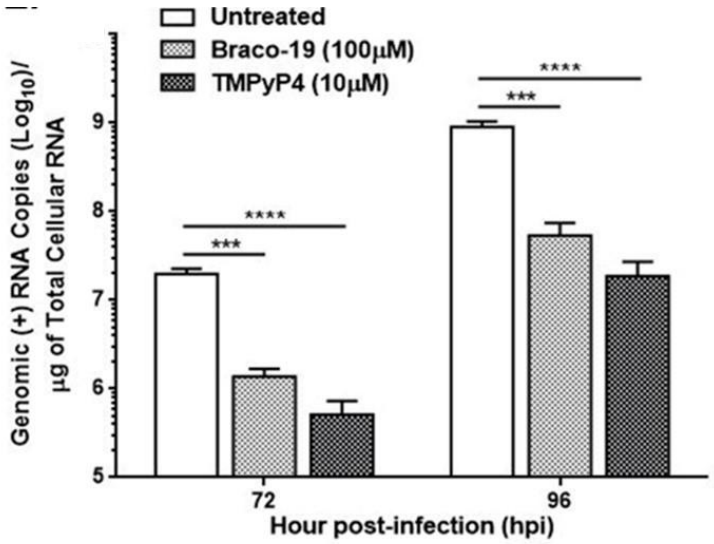

Fig. 5.7. Braco-19 and TMPyP4 inhibit ZIKV genome replication. Levels of viral genome in the presence of Braco-19 or TMPyP4. Vero cells infected with ZIKV at an MOI of 1 were incubated in medium without drug (untreated) or in medium containing 100 μM Braco-19 or 10 μM TMPyP4. Viral genome copies in the cells at 72 and 96 hpi were quantitated and expressed as copies per mg of total cellular RNA from the cells. The graphs show mean values of genome copy numbers with error bars representing standard deviations from the results of three independent experiments. Two-way ANOVA was used to determine significant differences between untreated and drug-treated samples. ***$p \leq 0.001$; ****$p \leq 0.0001$

Due to the unavailability of commercial vaccines or antiviral drugs, control and mitigation strategies for ZIKV infection remain a huge challenge to date. The unpredictable nature of ZIKV outbreaks and the global prevalence of its arthropod vector have further worsened the situation. Although attempts to repurpose the drugs like Sofosbuvir, (Barrows et al., 2016), Niclosamide (Xu et al., 2016) and Galidesivir (Lim et al., 2017) have shown pronounced anti-Zika activity, these drugs also come with certain shortcomings such as poor bioavailability, poor liberation, and improper mode of administration. If infection takes place during pregnancy, ZIKV can cause detrimental effects on the fetus and eventually on the newborn. Prognosis of newborn babies infected with ZIKV is unfavorable and infections could lead to permanent congenital defects. Thus, utmost precaution and precision should be taken while strategizing therapeutic countermeasures against ZIKV infection.

In recent years, GQ structures, which are non-canonical nucleic acid secondary structures, are being discovered in almost all organisms including many viral genomes and thus have been considered as potential targets for antiviral strategies (Ruggiero and Richter, 2018). ZIKV and other Flaviviruses have been reported to possess conserved GQ structures (Fleming et al., 2016). By expanding the analysis to all the available ZIKV genome sequences published in the NCBI Genome database and employing an in-house algorithm (Mishra et al., 2016), we were able to predict four additional highly conserved GQ structures in ZIKV. Some GQ-forming sequences were also found to be conserved in the anti-genomic strand of the ZIKV. However, further studies will be required to validate whether the predicted GQs in the anti-genomic RNA actually form GQs. The current study mainly focused on the GQ structures formed in the genomic RNA (positive-

sense) of the ZIKV. The observation that these GQ structures are highly conserved suggested to us that they may play a specific role in the life cycle and/or pathogenesis of the virus. Two of the GQs were found to be located in the coding region of NS5 gene, i.e., the RNA-dependent RNA polymerase coding gene, while the other two were present in the NS2 and NS4B genes. These GQs were characterized by CD and NMR spectra analysis and were found to form parallel GQ structures. Moreover, it has been previously shown that RNA GQ structures are more stable compared to their DNA counterparts due to the presence of the 2'hydroxyl group in the ribose sugar.

Following CD and NMR spectra studies, our collaborators at the Indian Institute of Technology, Indore, India evaluated whether these GQ structures would interact with the known GQ-binding ligands. GQ-binding ligands such as Braco-19, TMPyP4, etc. have been widely studied to measure the stability of the GQ structures and are presently being explored as an antiviral strategy (Ruggiero and Richter, 2018). The ligands bear certain characteristics like basic aromatic rings, electron-deficient cationic core, and positively charged side chains, which facilitate the efficient interaction of these ligands with the GQ secondary structures (Vy Thi Le et al., 2012). The mode of interaction of these ligands may be through end-stacking, groove binding, or interaction with the backbone or loop sequences. The molecules fit themselves within these GQ structures and bind through various non-covalent bonds thus stabilizing the structure. Further biophysical studies including the fluorescence titration assay, ITC, and thermal denaturation assays carried out by our collaborators conclusively demonstrated that Braco-19 and TMPyP4 bind selectively and preferentially to the GQ-forming sequences in comparison to the non-GQ linear RNA sequences. These studies unequivocally

demonstrated the existence and formation of GQ structures in the genome of ZIKV.

We reasoned that the binding of the Braco-19 or TMPyP4 could potentially impact the function(s) of the viral RNA containing the GQ structures. The *in vitro* studies that I conducted in cells infected with ZIKV and treated with Braco-19 or TMPyP4 suggested that both of these compounds inhibit the activities of the RNA template. Viral protein synthesis was substantially reduced in a dose-dependent manner as evidenced by the reduced levels of the E protein in the cells compared to control cells. Additionally, it is possible that binding of these compounds to the GQ structures inhibited the movement of the viral RNA polymerase, resulting in overall reduction of viral RNA copy numbers as we have observed in our experiments. Although our studies revealed the existence of multiple functional GQ structures in the viral genome, it would be interesting to examine whether a particular GQ structure functions more prominently than the other structures.

Examination of E protein in ZIKV-infected cells treated with TMPyP4 revealed slower migrating forms of the protein (Fig. 6A-B). The molecular basis for the reduced mobility of E compared to that in TMPyP4-untreated cells is not clear at this time. However, it is known that TMPyP4 becomes metabolized in cells through oxidation by hemeoxygenase enzymes (HO-1 and HO-2) to produce 4-formyl-1-methylpyridinium (4F-MP) and 4-carboxyl-1-methylpyridinium (4C-MP). Since these metabolites can bind to certain cellular proteins such as acetylcholinesterase (Fujiwara et al., 2015), it is possible that 4F-MP and/or 4C-MP bind specifically to the viral E protein in a time- and concentration-dependent manner to reduce its mobility. Although our results are consistent with such an interpretation, further research is needed to determine the molecular basis of the observed mobility shift in the E protein.

Taken together, our studies provide the first evidence that highly conserved GQ structures present in ZIKV genome and the ligands that bind and stabilize these GQ structures can potently inhibit ZIKV growth, genome replication, and viral protein expression in cultured cells. However, the two ligands evaluated here are the most common GQ-specific ligands used regularly to characterize these secondary structures and are not highly specific to the particular ZIKV GQs. Moreover, the toxicity and bioavailability of these ligands pose a hindrance for their potential use as antiviral drugs. Although the results of my studies presented here stands as a proof of concept for using GQ-binding ligands as anti-ZIKV drugs, development of sequence-specific ligands needs further research. Moreover, the availability of ligands that can potentially target ZIKV GQ sequences and that have the ability to distinguish them from the host GQs can address the problem of off-target effects of the ligands. Thus, our results open the possibility for understanding the role of GQ structures in ZIKV life cycle and pathogenesis, as well as for use of these structures as targets for development of innovative and efficacious antiviral strategies.

CHAPTER VI: SUMMARY, CONCLUSIONS, AND FUTURE DIRECTIONS

6.1. Summary

In 2015, ZIKV, a mosquito-borne flavivirus, re-emerged in Brazil and rapidly spread in the Americas. In addition to causing previously known mild self-limiting symptoms of flavivirus infections such as fever, headache, joint pain and rash, the outbreak was implicated in the development of severe neurological and developmental deficits in infants and demyelination and development of GBS in adults. Eventually, global travel led to spread of the virus to other parts of the world and increasing reports of such serious clinical manifestations of ZIKV infections were documented from many countries. Owing to such serious pathological consequences, the World Health Organization (WHO), declared the outbreak a global public health emergency in 2016. While multiple antiviral drugs and vaccine candidates are being developed for use against ZIKV infections, none have been approved for clinical use yet. The objectives of my research described in this thesis were to develop and characterize vaccines and antiviral therapeutics to mitigate ZIKV infections.

We used a nanoparticle-based vaccine platform, which utilizes ferritin, a ubiquitous, self-assembling and naturally occurring protein that forms a nanoparticle to display an organized array of an antigen on the surface of the nanoparticle. Such an approach presents multiple copies of the antigen to BCRs leading to a stronger interaction resulting in enhanced immune response in comparison to conventional strategies where the soluble antigen interacts with BCRs with low affinity. In my studies, we demonstrated formation of stable nanoparticles displaying the DIII domain of ZIKV E

protein. Such nanoparticles induced much higher levels of neutralizing antibody response and protected animals from lethal ZIKV challenge as compared to DIII alone as antigen. These results provide a proof-of-principle for the approach to develop an efficacious vaccine against ZIKV.

Additionally, we characterized an anti-ZIKV drug candidate, TPB that has shown promising results in my studies. TPB was identified from a library of 100,000 compounds that bound to the viral RdRp domain. TPB was shown to significantly reduce viral replication *in vitro* and its administration significantly reduced viremia in infected mice. With the IC_{50}, and CC_{50} in the submicromolar and micromolar range, respectively and a high selective index of over 200, TPB is a strong candidate for its development as an antiviral drug against ZIKV infections.

The observation that ZIKV RNA genome may form non-canonical secondary structures, called G-quadruplexes, prompted me to explore the possibility of re-purposing anti-cancer drugs, BRACO-19 and TMPyP4, as anti-ZIKV agents. BRACO-19 and TMPyP4 are small molecule G-quadruplex binding ligands that stabilize the G-quadruplex structures, and this leads to inhibition of cellular processes such transcription, translation, and genome replication, etc. We found that exposure of ZIKV-infected cells to either BRACO-19 or TMPyP4 led to a dose-dependent inhibition of ZIKV replication in cells. Although, concerns about the bioavailability and toxicity of both compounds exist at this time, further research on developing G-quadruplex binding ligands as antiviral agents is needed.

Taken together, my dissertation focused on developing therapeutics (vaccines and antivirals) to combat ZIKV infections. Fig. 6.1 summarizes the three objectives of my

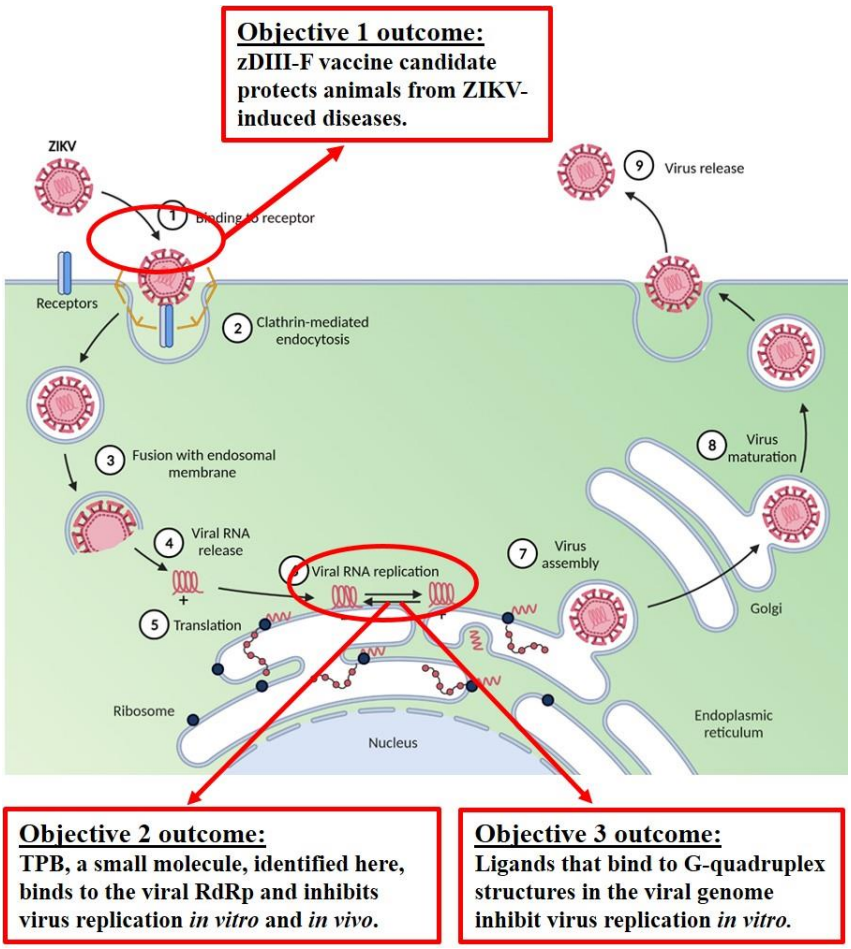

Fig. 6.1. Objectives and summary of results of the studies presented in my dissertation.

dissertation research identifying the viral replication steps for therapeutic intervention and the results of the studies to achieve these objectives.

6.2. Conclusions

The following conclusions are drawn from the studies reported in this thesis.

1. A ferritin-based nanoparticle carrying the DIII of ZIKV (zDIII-F) is stable and induces high levels of neutralizing antibody response in vaccinated mice.
2. Vaccination with zDIII-F protects mice from challenge with lethal dose of ZIKV.
3. Passive transfer of antibodies from zDIII-F-vaccinated mice into naïve animals confers protection against ZIKV challenge.
4. ZIKV RdRp structure-based *in silico* screening led to identification of a small molecule, TPB that potently inhibits the virus replication in cells in culture.
5. TPB inhibits viremia in mice infected with ZIKV. TPB should be further investigated for its potential as an antiviral against ZIKV/flavivirus infections.
6. Targeting G-quadruplex structures present in the genome of ZIKV by ligands that bind and stabilize these secondary structures results in inhibition of ZIKV replication *in vitro*.
7. G-quadruplex binding ligands should be explored further as potential anti-ZIKV therapeutics.

6.3. Future Directions

6.3.1. Characterization of the dynamics of germinal center (GC) development induced by zDIII-F vaccination

In preliminary studies, we observed higher levels of lymph node germinal center development in zDIII-F nanoparticle vaccinated mice by immunohistological staining in comparison to mice vaccinated with DIII. GC development indicates generation of high affinity antibody-secreting plasma cells and memory B cells that contribute to humoral immunity (Laidlaw and Cyster, 2021). Therefore, it would be interesting to characterize the development of GC with time after vaccination and assess the appearance of specific B and T cells in response to zDIII-F. Using fluorescently tagged zDIII-F, we intend to track the dynamics zDIII-F specific GC-associated B cell and T follicular helper cell populations in secondary lymphoid tissues by cell imaging as well as by flow cytometry. Transcriptomics and proteomics analysis of B and T cells isolated from GCs may identify critical cellular factors that regulate enhanced GC development in the presence of zDIII-F vaccine compared to DIII vaccine. This may provide an understanding of the possible mechanism(s) of the development of a robust humoral immunity in response to zDIII-F vaccination.

6.3.2. Investigation of other naturally occurring proteins as nanoparticle-based vaccine delivery platforms.

While ferritin nanoparticle is composed of 24 subunits, other proteins such as lumazine synthase, obtained from *Aquifex aeolicus*, can form nanoparticles that are composed of 60 subunits (Ra et al., 2014). This property of lumazine synthase nanoparticles can be exploited to display even higher number of antigenic epitopes on its surface. Therefore, the strategy described in the construction of the ferritin-based nanoparticle vaccine could be used for the development of a lumazine synthase

nanoparticle-based ZIKV vaccine. Such a strategy may lead to higher number of BCRs interacting with the epitopes exposed on the surface of the lumazine synthase nanoparticle thereby leading to stronger immune response. The expectation is that the efficacy of such a vaccine candidate will be significantly higher.

6.3.3. Development of a ferritin nano-particle based peptide vaccine using immunoinformatics.

With the use of immunoinformatics, a developing field in vaccine research (Oli et al., 2020), a small protein carrying multiple B and T cell immunodominant epitopes in tandem found in the ZIKV proteins could be synthesized as a vaccine candidate. Several such epitopes have been reported in ZIKV E and NS1 proteins (Prasasty et al., 2019). Ferritin nanoparticles can be engineered to display an array of multiple copies of such epitopes on the surface that can result in a better and more efficient B- and T- cell responses thereby leading to a more efficacious nanoparticle-based vaccine.

6.3.4. Development of TPB as an anti-flaviviral drug

The structure of ZIKV RdRp was modelled based on the structure of DENV3 RdRp and it was found that TPB effectively inhibited ZIKV replication by allosteric inhibition (Fig. 4.6A). Furthermore, the protein sequence of JEV, another flavivirus, is known to be homologous to the protein sequence of ZIKV and DENV RdRp (Pattnaik et al., 2018). Therefore, the possibility exists that TPB may also inhibit DENV and JEV replication. Studies directed at examining the effect of TPB on DENV/JEV replication may reveal if TPB could be developed as an anti-DENV and/or anti-JEV drug.

6.3.5. Enhancement of the bio-availability of TPB.

Pharmacokinetics studies of TPB in mice revealed that it is cleared from circulation with a short half-life and only ~100 ng/ml is detected after 10-12 hours. Although this level of TPB was shown to inhibit ZIKV viremia in mice, increasing the bioavailability of TPB may enhance its protective efficacy. It is known that physical modifications such as nanomilling (Li et al., 2016b), micronisation (Chaumeil, 1998) or the development of a TPB NanoSol (Lai et al., 2015) or chemical modifications such as conjugation with cell penetrating peptides (Foged and Nielsen, 2008) can result in significant increase in bioavailability of compounds. Therefore, studies to explore these possibilities may result in enhanced bioavailability of TPB.

6.3.6. Studying the effect of other lead compound(s) identified from our screen on ZIKV replication.

This dissertation focused on one compound (c1; TPB) from a list of ten lead compounds that had high docking scores in *in silico* screening. Out of the ten compounds that I examined initially, apart from TPB, c10 was also found to inhibit ZIKV replication by ~80% at 1 μM (Fig. 4.4). Further characterization of this compound may reveal whether it can function as an anti-ZIKV/flavivirus.

6.3.7. Validation and targeted inhibition of specific G-quadruplex forming motifs.

Although many G-quadruplex structures were predicted to exist in ZIKV genome and specific ligands that bind to these structures were shown to inhibit the virus

replication, it is unknown which G-quadruplex structures play significant role in the process. It has been reported that the formation of stable G-quadruplex structures leads to suppression of transcription and translation of protein coding sequences that are downstream of such motifs (Hershman et al., 2008; Verma et al., 2008). Therefore, insertion of a particular G-quadruplex forming sequence upstream of the coding sequence of a reporter protein, for instance, a fluorescent protein like GFP or RFP, and examining its expression in the absence or presence of G-quadruplex binding ligands may suggest if that particular structure contributes to the observed ligand-mediated inhibition of ZIKV replication. Subsequently, conjugation of complementary DNA sequences upstream or downstream of that particular G-quadruplex structure with a specific ligand may direct the ligand to bind specifically to that particular G-quadruplex structure to inhibit virus replication. Such an approach can be extended to other G-quadruplex structures and binding ligands which can also be explored for their antiviral activities.

6.3.8. Exploration the molecular basis of the mobility shift in the viral E protein with TmPyP4 treatment.

It was interesting to find that upon TMPyP4 exposure, there was a significant concentration-and time-dependent mobility shift in the migration pattern of ZIKV E protein as observed by Western blot analysis. TMPyP4 is known to be oxidized by cellular heme-oxygenase enzymes (HO-1 and HO-2), to form 4-formyl-1-methylpyridinium (4F-MP) and 4-carboxyl-1-methylpyridinium (4C-MP). Both 4F-MP and 4C-MP are known to bind to certain intracellular proteins (Fujiwara et al., 2015). It is possible that these metabolites also bind specifically to E protein of ZIKV and alter its

mobility. While this may explain the shift in the observed migration pattern of ZIKV E protein, experimental evidence is still lacking. Other yet unknown modifications induced by the presence of TMTyP4 may also account the mobility shift. Experiments using mass spectrometric analysis of isolated E proteins may suggest the type of modification(s) occurring in E protein. Further, proteolytic digestion and mass spec studies may reveal the site of modification in the protein.

REFERENCES

2016. WHO statement on the first meeting of the International Health Regulations (2005) (IHR 2005) Emergency Committee on ZIKV and observed increase in neurological disorders and neonatal malformations. World Health Organization.

Abbink, P., Larocca, R.A., De La Barrera, R.A., Bricault, C.A., Moseley, E.T., Boyd, M., Kirilova, M., Li, Z., Ng'ang'a, D., Nanayakkara, O., Nityanandam, R., Mercado, N.B., Borducchi, E.N., Agarwal, A., Brinkman, A.L., Cabral, C., Chandrashekar, A., Giglio, P.B., Jetton, D., Jimenez, J., Lee, B.C., Mojta, S., Molloy, K., Shetty, M., Neubauer, G.H., Stephenson, K.E., Peron, J.P., Zanotto, P.M., Misamore, J., Finneyfrock, B., Lewis, M.G., Alter, G., Modjarrad, K., Jarman, R.G., Eckels, K.H., Michael, N.L., Thomas, S.J., Barouch, D.H., 2016. Protective efficacy of multiple vaccine platforms against ZIKV challenge in rhesus monkeys. Science 353, 1129-1132.

Abbink, P., Larocca, R.A., Visitsunthorn, K., Boyd, M., De La Barrera, R.A., Gromowski, G.D., Kirilova, M., Peterson, R., Li, Z., Nanayakkara, O., Nityanandam, R., Mercado, N.B., Borducchi, E.N., Chandrashekar, A., Jetton, D., Mojta, S., Gandhi, P., LeSuer, J., Khatiwada, S., Lewis, M.G., Modjarrad, K., Jarman, R.G., Eckels, K.H., Thomas, S.J., Michael, N.L., Barouch, D.H., 2017. Durability and correlates of vaccine protection against ZIKV in rhesus monkeys. Sci Transl Med 9.

Adams Waldorf, K.M., Rubens, C.E., Gravett, M.G., 2011. Use of nonhuman primate models to investigate mechanisms of infection-associated preterm birth. BJOG 118, 136-144.

Agrelli, A., de Moura, R.R., Crovella, S., Brandao, L.A.C., 2019. ZIKV entry mechanisms in human cells. Infect Genet Evol 69, 22-29.

Albulescu, I.C., Kovacikova, K., Tas, A., Snijder, E.J., van Hemert, M.J., 2017. Suramin inhibits ZIKV replication by interfering with virus attachment and release of infectious particles. Antiviral Res 143, 230-236.

Aliota, M.T., Caine, E.A., Walker, E.C., Larkin, K.E., Camacho, E., Osorio, J.E., 2016a. Characterization of Lethal ZIKV Infection in AG129 Mice. PLoS Negl Trop Dis 10, e0004682.

Aliota, M.T., Dudley, D.M., Newman, C.M., Mohr, E.L., Gellerup, D.D., Breitbach, M.E., Buechler, C.R., Rasheed, M.N., Mohns, M.S., Weiler, A.M., Barry, G.L., Weisgrau, K.L., Eudailey, J.A., Rakasz, E.G., Vosler, L.J., Post, J., Capuano, S., 3rd, Golos, T.G., Permar, S.R., Osorio, J.E., Friedrich, T.C., O'Connor, S.L., O'Connor, D.H., 2016b. Heterologous Protection against Asian ZIKV Challenge in Rhesus Macaques. PLoS Negl Trop Dis 10, e0005168.

Allard, A., Althouse, B.M., Hebert-Dufresne, L., Scarpino, S.V., 2017. The risk of sustained sexual transmission of Zika is underestimated. PLoS Pathog 13, e1006633.

Alvarado, M.G., Schwartz, D.A., 2017. ZIKV Infection in Pregnancy, Microcephaly, and Maternal and Fetal Health: What We Think, What We Know, and What We Think We Know. Arch Pathol Lab Med 141, 26-32.

Andries, O., Mc Cafferty, S., De Smedt, S.C., Weiss, R., Sanders, N.N., Kitada, T., 2015. N(1)-methylpseudouridine-incorporated mRNA outperforms pseudouridine-incorporated mRNA by providing enhanced protein expression and reduced immunogenicity in mammalian cell lines and mice. J Control Release 217, 337-344.

Annamalai, A.S., Pattnaik, A., Sahoo, B.R., Guinn, Z.P., Bullard, B.L., Weaver, E.A., Steffen, D., Natarajan, S.K., Petro, T.M., Pattnaik, A.K., 2019. An Attenuated ZIKV Encoding Non-Glycosylated Envelope (E) and Non-Structural Protein 1 (NS1) Confers Complete Protection against Lethal Challenge in a Mouse Model. Vaccines (Basel) 7.

Annamalai, A.S., Pattnaik, A., Sahoo, B.R., Muthukrishnan, E., Natarajan, S.K., Steffen, D., Vu, H.L.X., Delhon, G., Osorio, F.A., Petro, T.M., Xiang, S.H., Pattnaik, A.K., 2017. ZIKV

Encoding Nonglycosylated Envelope Protein Is Attenuated and Defective in Neuroinvasion. J Virol 91.
Arias, C.F., Preugschat, F., Strauss, J.H., 1993. Dengue 2 virus NS2B and NS3 form a stable complex that can cleave NS3 within the helicase domain. Virology 193, 888-899.
Aricescu, A.R., Lu, W., Jones, E.Y., 2006. A time- and cost-efficient system for high-level protein production in mammalian cells. Acta Crystallogr D Biol Crystallogr 62, 1243-1250.
Arora, A., Nair, D.R., Maiti, S., 2009. Effect of flanking bases on quadruplex stability and Watson-Crick duplex competition. FEBS J 276, 3628-3640.
Artusi, S., Nadai, M., Perrone, R., Biasolo, M.A., Palu, G., Flamand, L., Calistri, A., Richter, S.N., 2015. The Herpes Simplex Virus-1 genome contains multiple clusters of repeated G-quadruplex: Implications for the antiviral activity of a G-quadruplex ligand. Antiviral Res 118, 123-131.
Atkinson, B., Hearn, P., Afrough, B., Lumley, S., Carter, D., Aarons, E.J., Simpson, A.J., Brooks, T.J., Hewson, R., 2016. Detection of ZIKV in Semen. Emerg Infect Dis 22, 940.
Avelino-Silva, V.I., Alvarenga, C., Abreu, C., Tozetto-Mendoza, T.R., Canto, C., Manuli, E.R., Mendes-Correa, M.C., Sabino, E.C., Figueiredo, W.M., Segurado, A.C., Mayaud, P., 2018. Potential effect of ZIKV infection on human male fertility? Rev Inst Med Trop Sao Paulo 60, e64.
Bachmann, M.F., Jennings, G.T., 2010. Vaccine delivery: a matter of size, geometry, kinetics and molecular patterns. Nat Rev Immunol 10, 787-796.
Bailey, M.J., Duehr, J., Dulin, H., Broecker, F., Brown, J.A., Arumemi, F.O., Bermudez Gonzalez, M.C., Leyva-Grado, V.H., Evans, M.J., Simon, V., Lim, J.K., Krammer, F., Hai, R., Palese, P., Tan, G.S., 2018. Human antibodies targeting ZIKV NS1 provide protection against disease in a mouse model. Nat Commun 9, 4560.
Barbi, L., Coelho, A.V.C., Alencar, L.C.A., Crovella, S., 2018. Prevalence of Guillain-Barre syndrome among ZIKV infected cases: a systematic review and meta-analysis. Braz J Infect Dis 22, 137-141.
Bardina, S.V., Bunduc, P., Tripathi, S., Duehr, J., Frere, J.J., Brown, J.A., Nachbagauer, R., Foster, G.A., Krysztof, D., Tortorella, D., Stramer, S.L., Garcia-Sastre, A., Krammer, F., Lim, J.K., 2017. Enhancement of ZIKV pathogenesis by preexisting antiflavivirus immunity. Science 356, 175-180.
Baronti, C., Piorkowski, G., Charrel, R.N., Boubis, L., Leparc-Goffart, I., de Lamballerie, X., 2014. Complete coding sequence of ZIKV from a French polynesia outbreak in 2013. Genome Announc 2.
Barouch, D.H., Thomas, S.J., Michael, N.L., 2017. Prospects for a ZIKV Vaccine. Immunity 46, 176-182.
Barreto-Vieira, D.F., Barth, O.M., Silva, M.A., Santos, C.C., Santos Ada, S., Filho, F.J., Filippis, A.M., 2016. Ultrastructure of ZIKV particles in cell cultures. Mem Inst Oswaldo Cruz 111, 532-534.
Barrows, N.J., Campos, R.K., Powell, S.T., Prasanth, K.R., Schott-Lerner, G., Soto-Acosta, R., Galarza-Munoz, G., McGrath, E.L., Urrabaz-Garza, R., Gao, J., Wu, P., Menon, R., Saade, G., Fernandez-Salas, I., Rossi, S.L., Vasilakis, N., Routh, A., Bradrick, S.S., Garcia-Blanco, M.A., 2016. A Screen of FDA-Approved Drugs for Inhibitors of ZIKV Infection. Cell Host Microbe 20, 259-270.
Bedrat, A., Lacroix, L., Mergny, J.L., 2016. Re-evaluation of G-quadruplex propensity with G4Hunter. Nucleic Acids Res 44, 1746-1759.
Beltramello, M., Williams, K.L., Simmons, C.P., Macagno, A., Simonelli, L., Quyen, N.T., Sukupolvi-Petty, S., Navarro-Sanchez, E., Young, P.R., de Silva, A.M., Rey, F.A., Varani, L., Whitehead, S.S., Diamond, M.S., Harris, E., Lanzavecchia, A., Sallusto, F., 2010. The human immune response to Dengue virus is dominated by highly cross-reactive antibodies endowed with neutralizing and enhancing activity. Cell Host Microbe 8, 271-283.

Bernatchez, J.A., Tran, L.T., Li, J., Luan, Y., Siqueira-Neto, J.L., Li, R., 2020. Drugs for the Treatment of ZIKV Infection. J Med Chem 63, 470-489.

Besnard, M., Lastere, S., Teissier, A., Cao-Lormeau, V., Musso, D., 2014. Evidence of perinatal transmission of ZIKV, French Polynesia, December 2013 and February 2014. Euro Surveill 19.

Best, S.M., 2017. The Many Faces of the Flavivirus NS5 Protein in Antagonism of Type I Interferon Signaling. J Virol 91.

Betancourt, D., de Queiroz, N.M., Xia, T., Ahn, J., Barber, G.N., 2017. Cutting Edge: Innate Immune Augmenting Vesicular Stomatitis Virus Expressing ZIKV Proteins Confers Protective Immunity. J Immunol 198, 3023-3028.

Biffi, G., Tannahill, D., McCafferty, J., Balasubramanian, S., 2013. Quantitative visualization of DNA G-quadruplex structures in human cells. Nat Chem 5, 182-186.

Boigard, H., Alimova, A., Martin, G.R., Katz, A., Gottlieb, P., Galarza, J.M., 2017. ZIKV-like particle (VLP) based vaccine. PLoS Negl Trop Dis 11, e0005608.

Boldescu, V., Behnam, M.A.M., Vasilakis, N., Klein, C.D., 2017. Broad-spectrum agents for flaviviral infections: dengue, Zika and beyond. Nat Rev Drug Discov 16, 565-586.

Bollati, M., Alvarez, K., Assenberg, R., Baronti, C., Canard, B., Cook, S., Coutard, B., Decroly, E., de Lamballerie, X., Gould, E.A., Grard, G., Grimes, J.M., Hilgenfeld, R., Jansson, A.M., Malet, H., Mancini, E.J., Mastrangelo, E., Mattevi, A., Milani, M., Moureau, G., Neyts, J., Owens, R.J., Ren, J., Selisko, B., Speroni, S., Steuber, H., Stuart, D.I., Unge, T., Bolognesi, M., 2010. Structure and functionality in flavivirus NS-proteins: perspectives for drug design. Antiviral Res 87, 125-148.

Boyer, S., Calvez, E., Chouin-Carneiro, T., Diallo, D., Failloux, A.B., 2018. An overview of mosquito vectors of ZIKV. Microbes Infect 20, 646-660.

Bradley, M.P., Nagamine, C.M., 2017. Animal Models of ZIKV. Comp Med 67, 242-252.

Brasil, P., Pereira, J.P., Jr., Moreira, M.E., Ribeiro Nogueira, R.M., Damasceno, L., Wakimoto, M., Rabello, R.S., Valderramos, S.G., Halai, U.A., Salles, T.S., Zin, A.A., Horovitz, D., Daltro, P., Boechat, M., Raja Gabaglia, C., Carvalho de Sequeira, P., Pilotto, J.H., Medialdea-Carrera, R., Cotrim da Cunha, D., Abreu de Carvalho, L.M., Pone, M., Machado Siqueira, A., Calvet, G.A., Rodrigues Baiao, A.E., Neves, E.S., Nassar de Carvalho, P.R., Hasue, R.H., Marschik, P.B., Einspieler, C., Janzen, C., Cherry, J.D., Bispo de Filippis, A.M., Nielsen-Saines, K., 2016. ZIKV Infection in Pregnant Women in Rio de Janeiro. N Engl J Med 375, 2321-2334.

Bullard, B.L., Corder, B.N., Gorman, M.J., Diamond, M.S., Weaver, E.A., 2018. Efficacy of a T Cell-Biased Adenovirus Vector as a ZIKV Vaccine. Sci Rep 8, 18017.

Burge, S., Parkinson, G.N., Hazel, P., Todd, A.K., Neidle, S., 2006. Quadruplex DNA: sequence, topology and structure. Nucleic Acids Res 34, 5402-5415.

Butcher, S.J., Grimes, J.M., Makeyev, E.V., Bamford, D.H., Stuart, D.I., 2001. A mechanism for initiating RNA-dependent RNA polymerization. Nature 410, 235-240.

Butovskaya, E., Solda, P., Scalabrin, M., Nadai, M., Richter, S.N., 2019. HIV-1 Nucleocapsid Protein Unfolds Stable RNA G-Quadruplexes in the Viral Genome and Is Inhibited by G-Quadruplex Ligands. ACS Infect Dis 5, 2127-2135.

Cabral-Miranda, G., Lim, S.M., Mohsen, M.O., Pobelov, I.V., Roesti, E.S., Heath, M.D., Skinner, M.A., Kramer, M.F., Martina, B.E.E., Bachmann, M.F., 2019. ZIKV-Derived E-DIII Protein Displayed on Immunologically Optimized VLPs Induces Neutralizing Antibodies without Causing Enhancement of Dengue Virus Infection. Vaccines (Basel) 7.

Caldas, L.A., Azevedo, R.C., da Silva, J.L., de Souza, W., 2020. Microscopy analysis of ZIKV morphogenesis in mammalian cells. Sci Rep 10, 8370.

Cao-Lormeau, V.M., Roche, C., Teissier, A., Robin, E., Berry, A.L., Mallet, H.P., Sall, A.A., Musso, D., 2014. ZIKV, French polynesia, South pacific, 2013. Emerg Infect Dis 20, 1085-1086.

Carneiro, B.M., Batista, M.N., Braga, A.C.S., Nogueira, M.L., Rahal, P., 2016. The green tea molecule EGCG inhibits ZIKV entry. Virology 496, 215-218.

Castanha, P.M.S., Nascimento, E.J.M., Braga, C., Cordeiro, M.T., de Carvalho, O.V., de Mendonca, L.R., Azevedo, E.A.N., Franca, R.F.O., Dhalia, R., Marques, E.T.A., 2017. Dengue Virus-Specific Antibodies Enhance Brazilian ZIKV Infection. J Infect Dis 215, 781-785.

Chambers, T.J., Nestorowicz, A., Amberg, S.M., Rice, C.M., 1993. Mutagenesis of the yellow fever virus NS2B protein: effects on proteolytic processing, NS2B-NS3 complex formation, and viral replication. J Virol 67, 6797-6807.

Chambers, V.S., Marsico, G., Boutell, J.M., Di Antonio, M., Smith, G.P., Balasubramanian, S., 2015. High-throughput sequencing of DNA G-quadruplex structures in the human genome. Nat Biotechnol 33, 877-881.

Chaumeil, J.C., 1998. Micronization: a method of improving the bioavailability of poorly soluble drugs. Methods Find Exp Clin Pharmacol 20, 211-215.

Chen, M.Y., Chai, K.M., Chiang, C.Y., Wu, C.C., Yu, G.Y., Liu, S.J., Chen, H.W., 2020. Recombinant lipidated ZIKV envelope protein domain III elicits durable neutralizing antibody responses against ZIKV in mice. J Biomed Sci 27, 51.

Chen, S., Yang, C., Zhang, W., Mahalingam, S., Wang, M., Cheng, A., 2018. Flaviviridae virus nonstructural proteins 5 and 5A mediate viral immune evasion and are promising targets in drug development. Pharmacol Ther 190, 1-14.

Chen, W., Foo, S.S., Hong, E., Wu, C., Lee, W.S., Lee, S.A., Evseenko, D., Moreira, M.E.L., Garcia-Sastre, A., Cheng, G., Nielsen-Saines, K., Brasil, P., Avvad-Portari, E., Jung, J.U., 2021. ZIKV NS3 protease induces bone morphogenetic protein-dependent brain calcification in human fetuses. Nat Microbiol 6, 455-466.

Chen, X., Yang, K., Wu, C., Chen, C., Hu, C., Buzovetsky, O., Wang, Z., Ji, X., Xiong, Y., Yang, H., 2016. Mechanisms of activation and inhibition of ZIKV NS2B-NS3 protease. Cell Res 26, 1260-1263.

Cheng, M., Cheng, Y., Hao, J., Jia, G., Zhou, J., Mergny, J.L., Li, C., 2018. Loop permutation affects the topology and stability of G-quadruplexes. Nucleic Acids Res 46, 9264-9275.

Cho, K.J., Shin, H.J., Lee, J.H., Kim, K.J., Park, S.S., Lee, Y., Lee, C., Park, S.S., Kim, K.H., 2009. The crystal structure of ferritin from Helicobacter pylori reveals unusual conformational changes for iron uptake. J Mol Biol 390, 83-98.

Choi, K.H., Rossmann, M.G., 2009. RNA-dependent RNA polymerases from Flaviviridae. Curr Opin Struct Biol 19, 746-751.

Choudhry, H., Alzahrani, F.A., Hassan, M.A., Alghamdi, A., Abdulaal, W.H., Bakhrebah, M.A., Zamzami, M.A., Helmi, N., Bokhari, F.F., Zeyadi, M., Baothman, O.A., Kamal, M.A., Warsi, M.K., Ali, A., Jarullah, B., Jamal, M.S., 2019. ZIKV Targeting by Screening Inhibitors against NS2B/NS3 Protease. Biomed Res Int 2019, 3947245.

Cibulski, S., Varela, A.P.M., Teixeira, T.F., Cancela, M.P., Sesterheim, P., Souza, D.O., Roehe, P.M., Silveira, F., 2021. ZIKV Envelope Domain III Recombinant Protein Delivered With Saponin-Based Nanoadjuvant From Quillaja brasiliensis Enhances Anti-Zika Immune Responses, Including Neutralizing Antibodies and Splenocyte Proliferation. Front Immunol 12, 632714.

Ciota, A.T., Bialosuknia, S.M., Ehrbar, D.J., Kramer, L.D., 2017. Vertical Transmission of ZIKV by Aedes aegypti and Ae. albopictus Mosquitoes. Emerg Infect Dis 23, 880-882.

Coluccia, A., Puxeddu, M., Nalli, M., Wei, C.K., Wu, Y.H., Mastrangelo, E., Elamin, T., Tarantino, D., Bugert, J.J., Schreiner, B., Nolte, J., Schwarze, F., La Regina, G., Lee, J.C., Silvestri, R., 2020. Discovery of ZIKV NS2B/NS3 Inhibitors That Prevent Mice from Life-Threatening Infection and Brain Damage. ACS Med Chem Lett 11, 1869-1874.

Cortese, M., Goellner, S., Acosta, E.G., Neufeldt, C.J., Oleksiuk, O., Lampe, M., Haselmann, U., Funaya, C., Schieber, N., Ronchi, P., Schorb, M., Pruunsild, P., Schwab, Y., Chatel-Chaix,

L., Ruggieri, A., Bartenschlager, R., 2017. Ultrastructural Characterization of ZIKV Replication Factories. Cell Rep 18, 2113-2123.
Coutard, B., Barral, K., Lichiere, J., Selisko, B., Martin, B., Aouadi, W., Lombardia, M.O., Debart, F., Vasseur, J.J., Guillemot, J.C., Canard, B., Decroly, E., 2017. ZIKV Methyltransferase: Structure and Functions for Drug Design Perspectives. J Virol 91.
Coyne, C.B., Lazear, H.M., 2016. ZIKV - reigniting the TORCH. Nat Rev Microbiol 14, 707-715.
Cugola, F.R., Fernandes, I.R., Russo, F.B., Freitas, B.C., Dias, J.L., Guimaraes, K.P., Benazzato, C., Almeida, N., Pignatari, G.C., Romero, S., Polonio, C.M., Cunha, I., Freitas, C.L., Brandao, W.N., Rossato, C., Andrade, D.G., Faria Dde, P., Garcez, A.T., Buchpigel, C.A., Braconi, C.T., Mendes, E., Sall, A.A., Zanotto, P.M., Peron, J.P., Muotri, A.R., Beltrao-Braga, P.C., 2016. The Brazilian ZIKV strain causes birth defects in experimental models. Nature 534, 267-271.
Cui, H., Zhang, L., 2020. G-Quadruplexes Are Present in Human Coronaviruses Including SARS-CoV-2. Front Microbiol 11, 567317.
D'Ortenzio, E., Matheron, S., Yazdanpanah, Y., de Lamballerie, X., Hubert, B., Piorkowski, G., Maquart, M., Descamps, D., Damond, F., Leparc-Goffart, I., 2016. Evidence of Sexual Transmission of ZIKV. N Engl J Med 374, 2195-2198.
Dai, L., Song, J., Lu, X., Deng, Y.Q., Musyoki, A.M., Cheng, H., Zhang, Y., Yuan, Y., Song, H., Haywood, J., Xiao, H., Yan, J., Shi, Y., Qin, C.F., Qi, J., Gao, G.F., 2016. Structures of the ZIKV Envelope Protein and Its Complex with a Flavivirus Broadly Protective Antibody. Cell Host Microbe 19, 696-704.
Dai, S., Zhang, T., Zhang, Y., Wang, H., Deng, F., 2018. ZIKV Baculovirus-Expressed Virus-Like Particles Induce Neutralizing Antibodies in Mice. Virol Sin 33, 213-226.
Dalton, A.C., Barton, W.A., 2014. Over-expression of secreted proteins from mammalian cell lines. Protein Sci 23, 517-525.
Davidson, A.D., 2009. Chapter 2. New insights into flavivirus nonstructural protein 5. Adv Virus Res 74, 41-101.
de Paula Freitas, B., de Oliveira Dias, J.R., Prazeres, J., Sacramento, G.A., Ko, A.I., Maia, M., Belfort, R., Jr., 2016. Ocular Findings in Infants With Microcephaly Associated With Presumed ZIKV Congenital Infection in Salvador, Brazil. JAMA Ophthalmol 134, 529-535.
de Paula Guimaraes, C., Macedo, M.S., Barbosa, M.A., Marques, S.M., Costa, P.S., de Oliveira, E.C., 2019. Clinical findings in congenital infection by ZIKV: a retrospective study in a reference hospital in Central-West Brazil. BMC Pediatr 19, 389.
De, S., Michor, F., 2011. DNA secondary structures and epigenetic determinants of cancer genome evolution. Nat Struct Mol Biol 18, 950-955.
Dejnirattisai, W., Jumnainsong, A., Onsirisakul, N., Fitton, P., Vasanawathana, S., Limpitikul, W., Puttikhunt, C., Edwards, C., Duangchinda, T., Supasa, S., Chawansuntati, K., Malasit, P., Mongkolsapaya, J., Screaton, G., 2010. Cross-reacting antibodies enhance dengue virus infection in humans. Science 328, 745-748.
Dejnirattisai, W., Supasa, P., Wongwiwat, W., Rouvinski, A., Barba-Spaeth, G., Duangchinda, T., Sakuntabhai, A., Cao-Lormeau, V.M., Malasit, P., Rey, F.A., Mongkolsapaya, J., Screaton, G.R., 2016. Dengue virus sero-cross-reactivity drives antibody-dependent enhancement of infection with ZIKV. Nat Immunol 17, 1102-1108.
Delvecchio, R., Higa, L.M., Pezzuto, P., Valadao, A.L., Garcez, P.P., Monteiro, F.L., Loiola, E.C., Dias, A.A., Silva, F.J., Aliota, M.T., Caine, E.A., Osorio, J.E., Bellio, M., O'Connor, D.H., Rehen, S., de Aguiar, R.S., Savarino, A., Campanati, L., Tanuri, A., 2016. Chloroquine, an Endocytosis Blocking Agent, Inhibits ZIKV Infection in Different Cell Models. Viruses 8.
Deng, Y.Q., Zhang, N.N., Li, C.F., Tian, M., Hao, J.N., Xie, X.P., Shi, P.Y., Qin, C.F., 2016. Adenosine Analog NITD008 Is a Potent Inhibitor of ZIKV. Open Forum Infect Dis 3, ofw175.

Diamond, M.S., Ledgerwood, J.E., Pierson, T.C., 2019. ZIKV Vaccine Development: Progress in the Face of New Challenges. Annu Rev Med 70, 121-135.
Diamond, M.S., Zachariah, M., Harris, E., 2002. Mycophenolic acid inhibits dengue virus infection by preventing replication of viral RNA. Virology 304, 211-221.
Dick, G.W., Kitchen, S.F., Haddow, A.J., 1952. ZIKV. I. Isolations and serological specificity. Trans R Soc Trop Med Hyg 46, 509-520.
Dowd, K.A., DeMaso, C.R., Pelc, R.S., Speer, S.D., Smith, A.R.Y., Goo, L., Platt, D.J., Mascola, J.R., Graham, B.S., Mulligan, M.J., Diamond, M.S., Ledgerwood, J.E., Pierson, T.C., 2016. Broadly Neutralizing Activity of ZIKV-Immune Sera Identifies a Single Viral Serotype. Cell Rep 16, 1485-1491.
Du, Z., Zhao, Y., Li, N., 2008. Genome-wide analysis reveals regulatory role of G4 DNA in gene transcription. Genome Res 18, 233-241.
Duan, W., Song, H., Wang, H., Chai, Y., Su, C., Qi, J., Shi, Y., Gao, G.F., 2017. The crystal structure of ZIKV NS5 reveals conserved drug targets. EMBO J 36, 919-933.
Duan, Y., Zeng, M., Jiang, B., Zhang, W., Wang, M., Jia, R., Zhu, D., Liu, M., Zhao, X., Yang, Q., Wu, Y., Zhang, S., Liu, Y., Zhang, L., Yu, Y., Pan, L., Chen, S., Cheng, A., 2019. Flavivirus RNA-Dependent RNA Polymerase Interacts with Genome UTRs and Viral Proteins to Facilitate Flavivirus RNA Replication. Viruses 11.
Dudley, D.M., Aliota, M.T., Mohr, E.L., Weiler, A.M., Lehrer-Brey, G., Weisgrau, K.L., Mohns, M.S., Breitbach, M.E., Rasheed, M.N., Newman, C.M., Gellerup, D.D., Moncla, L.H., Post, J., Schultz-Darken, N., Schotzko, M.L., Hayes, J.M., Eudailey, J.A., Moody, M.A., Permar, S.R., O'Connor, S.L., Rakasz, E.G., Simmons, H.A., Capuano, S., Golos, T.G., Osorio, J.E., Friedrich, T.C., O'Connor, D.H., 2016. A rhesus macaque model of Asian-lineage ZIKV infection. Nat Commun 7, 12204.
Duffy, M.R., Chen, T.H., Hancock, W.T., Powers, A.M., Kool, J.L., Lanciotti, R.S., Pretrick, M., Marfel, M., Holzbauer, S., Dubray, C., Guillaumot, L., Griggs, A., Bel, M., Lambert, A.J., Laven, J., Kosoy, O., Panella, A., Biggerstaff, B.J., Fischer, M., Hayes, E.B., 2009. ZIKV outbreak on Yap Island, Federated States of Micronesia. N Engl J Med 360, 2536-2543.
Duffy, S., 2018. Why are RNA virus mutation rates so damn high? PLoS Biol 16, e3000003.
Eddy, J., Maizels, N., 2006. Gene function correlates with potential for G4 DNA formation in the human genome. Nucleic Acids Res 34, 3887-3896.
Eddy, J., Vallur, A.C., Varma, S., Liu, H., Reinhold, W.C., Pommier, Y., Maizels, N., 2011. G4 motifs correlate with promoter-proximal transcriptional pausing in human genes. Nucleic Acids Res 39, 4975-4983.
Elshahawi, H., Syed Hassan, S., Balasubramaniam, V., 2019. Importance of ZIKV NS5 Protein for Viral Replication. Pathogens 8.
Espinosa, D., Mendy, J., Manayani, D., Vang, L., Wang, C., Richard, T., Guenther, B., Aruri, J., Avanzini, J., Garduno, F., Farness, P., Gurwith, M., Smith, J., Harris, E., Alexander, J., 2018. Passive Transfer of Immune Sera Induced by a ZIKV-Like Particle Vaccine Protects AG129 Mice Against Lethal ZIKV Challenge. EBioMedicine 27, 61-70.
Falgout, B., Pethel, M., Zhang, Y.M., Lai, C.J., 1991. Both nonstructural proteins NS2B and NS3 are required for the proteolytic processing of dengue virus nonstructural proteins. J Virol 65, 2467-2475.
Faria, N.R., Quick, J., Claro, I.M., Theze, J., de Jesus, J.G., Giovanetti, M., Kraemer, M.U.G., Hill, S.C., Black, A., da Costa, A.C., Franco, L.C., Silva, S.P., Wu, C.H., Raghwani, J., Cauchemez, S., du Plessis, L., Verotti, M.P., de Oliveira, W.K., Carmo, E.H., Coelho, G.E., Santelli, A., Vinhal, L.C., Henriques, C.M., Simpson, J.T., Loose, M., Andersen, K.G., Grubaugh, N.D., Somasekar, S., Chiu, C.Y., Munoz-Medina, J.E., Gonzalez-Bonilla, C.R., Arias, C.F., Lewis-Ximenez, L.L., Baylis, S.A., Chieppe, A.O., Aguiar, S.F., Fernandes, C.A., Lemos, P.S., Nascimento, B.L.S., Monteiro, H.A.O., Siqueira, I.C., de Queiroz, M.G., de Souza, T.R., Bezerra, J.F., Lemos, M.R., Pereira, G.F., Loudal, D., Moura, L.C., Dhalia,

R., Franca, R.F., Magalhaes, T., Marques, E.T., Jr., Jaenisch, T., Wallau, G.L., de Lima, M.C., Nascimento, V., de Cerqueira, E.M., de Lima, M.M., Mascarenhas, D.L., Neto, J.P.M., Levin, A.S., Tozetto-Mendoza, T.R., Fonseca, S.N., Mendes-Correa, M.C., Milagres, F.P., Segurado, A., Holmes, E.C., Rambaut, A., Bedford, T., Nunes, M.R.T., Sabino, E.C., Alcantara, L.C.J., Loman, N.J., Pybus, O.G., 2017. Establishment and cryptic transmission of ZIKV in Brazil and the Americas. Nature 546, 406-410.

Fernando, S., Fernando, T., Stefanik, M., Eyer, L., Ruzek, D., 2016. An Approach for ZIKV Inhibition Using Homology Structure of the Envelope Protein. Mol Biotechnol 58, 801-806.

Ferreira, A.C., Zaverucha-do-Valle, C., Reis, P.A., Barbosa-Lima, G., Vieira, Y.R., Mattos, M., Silva, P.P., Sacramento, C., de Castro Faria Neto, H.C., Campanati, L., Tanuri, A., Bruning, K., Bozza, F.A., Bozza, P.T., Souza, T.M.L., 2017. Sofosbuvir protects ZIKV-infected mice from mortality, preventing short- and long-term sequelae. Sci Rep 7, 9409.

Fiorentino, D.G., Montero, F.J., 2016. The ZIKV and Pregnancy. Current Obstetrics and Gynecology Reports 5, 234-238.

Fleming, A.M., Ding, Y., Alenko, A., Burrows, C.J., 2016. ZIKV Genomic RNA Possesses Conserved G-Quadruplexes Characteristic of the Flaviviridae Family. ACS Infect Dis 2, 674-681.

Foged, C., Nielsen, H.M., 2008. Cell-penetrating peptides for drug delivery across membrane barriers. Expert Opin Drug Deliv 5, 105-117.

Foy, B.D., Kobylinski, K.C., Chilson Foy, J.L., Blitvich, B.J., Travassos da Rosa, A., Haddow, A.D., Lanciotti, R.S., Tesh, R.B., 2011. Probable non-vector-borne transmission of ZIKV, Colorado, USA. Emerg Infect Dis 17, 880-882.

Freire, J.M., Santos, N.C., Veiga, A.S., Da Poian, A.T., Castanho, M.A., 2015. Rethinking the capsid proteins of enveloped viruses: multifunctionality from genome packaging to genome transfection. FEBS J 282, 2267-2278.

Fujiwara, N., Mazzola, M., Cai, E., Wang, M., Cave, J.W., 2015. TMPyP4, a Stabilizer of Nucleic Acid Secondary Structure, Is a Novel Acetylcholinesterase Inhibitor. PLoS One 10, e0139167.

Gallichotte, E.N., Young, E.F., Baric, T.J., Yount, B.L., Metz, S.W., Begley, M.C., de Silva, A.M., Baric, R.S., 2019. Role of ZIKV Envelope Protein Domain III as a Target of Human Neutralizing Antibodies. mBio 10.

Garg, H., Mehmetoglu-Gurbuz, T., Joshi, A., 2020. Virus Like Particles (VLP) as multivalent vaccine candidate against Chikungunya, Japanese Encephalitis, Yellow Fever and ZIKV. Sci Rep 10, 4017.

Gause, K.T., Wheatley, A.K., Cui, J., Yan, Y., Kent, S.J., Caruso, F., 2017. Immunological Principles Guiding the Rational Design of Particles for Vaccine Delivery. ACS Nano 11, 54-68.

Gellert, M., Lipsett, M.N., Davies, D.R., 1962. Helix formation by guanylic acid. Proc Natl Acad Sci U S A 48, 2013-2018.

Gerold, G., Bruening, J., Weigel, B., Pietschmann, T., 2017. Protein Interactions during the Flavivirus and Hepacivirus Life Cycle. Mol Cell Proteomics 16, S75-S91.

Giri, R., Kumar, D., Sharma, N., Uversky, V.N., 2016. Intrinsically Disordered Side of the ZIKV Proteome. Front Cell Infect Microbiol 6, 144.

Godoy, A.S., Lima, G.M., Oliveira, K.I., Torres, N.U., Maluf, F.V., Guido, R.V., Oliva, G., 2017. Crystal structure of ZIKV NS5 RNA-dependent RNA polymerase. Nat Commun 8, 14764.

Grant, A., Ponia, S.S., Tripathi, S., Balasubramaniam, V., Miorin, L., Sourisseau, M., Schwarz, M.C., Sanchez-Seco, M.P., Evans, M.J., Best, S.M., Garcia-Sastre, A., 2016. ZIKV Targets Human STAT2 to Inhibit Type I Interferon Signaling. Cell Host Microbe 19, 882-890.

Gratton, R., Agrelli, A., Tricarico, P.M., Brandao, L., Crovella, S., 2019. Autophagy in ZIKV Infection: A Possible Therapeutic Target to Counteract Viral Replication. Int J Mol Sci 20.

Grubaugh, N.D., Faria, N.R., Andersen, K.G., Pybus, O.G., 2018. Genomic Insights into ZIKV Emergence and Spread. Cell 172, 1160-1162.

Guedin, A., De Cian, A., Gros, J., Lacroix, L., Mergny, J.L., 2008. Sequence effects in single-base loops for quadruplexes. Biochimie 90, 686-696.

Guirakhoo, F., Heinz, F.X., Mandl, C.W., Holzmann, H., Kunz, C., 1991. Fusion activity of flaviviruses: comparison of mature and immature (prM-containing) tick-borne encephalitis virions. J Gen Virol 72 (Pt 6), 1323-1329.

Guler-Gane, G., Kidd, S., Sridharan, S., Vaughan, T.J., Wilkinson, T.C., Tigue, N.J., 2016. Overcoming the Refractory Expression of Secreted Recombinant Proteins in Mammalian Cells through Modification of the Signal Peptide and Adjacent Amino Acids. PLoS One 11, e0155340.

Guo, Q., Chan, J.F., Poon, V.K., Wu, S., Chan, C.C., Hou, L., Yip, C.C., Ren, C., Cai, J.P., Zhao, M., Zhang, A.J., Song, X., Chan, K.H., Wang, B., Kok, K.H., Wen, Y., Yuen, K.Y., Chen, W., 2018. Immunization With a Novel Human Type 5 Adenovirus-Vectored Vaccine Expressing the Premembrane and Envelope Proteins of ZIKV Provides Consistent and Sterilizing Protection in Multiple Immunocompetent and Immunocompromised Animal Models. J Infect Dis 218, 365-377.

Halstead, S.B., 2003. Neutralization and antibody-dependent enhancement of dengue viruses. Adv Virus Res 60, 421-467.

Hamburger, A.E., West, A.P., Jr., Hamburger, Z.A., Hamburger, P., Bjorkman, P.J., 2005. Crystal structure of a secreted insect ferritin reveals a symmetrical arrangement of heavy and light chains. J Mol Biol 349, 558-569.

Hamel, R., Dejarnac, O., Wichit, S., Ekchariyawat, P., Neyret, A., Luplertlop, N., Perera-Lecoin, M., Surasombatpattana, P., Talignani, L., Thomas, F., Cao-Lormeau, V.M., Choumet, V., Briant, L., Despres, P., Amara, A., Yssel, H., Misse, D., 2015. Biology of ZIKV Infection in Human Skin Cells. J Virol 89, 8880-8896.

Hansel-Hertsch, R., Beraldi, D., Lensing, S.V., Marsico, G., Zyner, K., Parry, A., Di Antonio, M., Pike, J., Kimura, H., Narita, M., Tannahill, D., Balasubramanian, S., 2016. G-quadruplex structures mark human regulatory chromatin. Nat Genet 48, 1267-1272.

Hassan, A.O., Dmitriev, I.P., Kashentseva, E.A., Zhao, H., Brough, D.E., Fremont, D.H., Curiel, D.T., Diamond, M.S., 2019. A Gorilla Adenovirus-Based Vaccine against ZIKV Induces Durable Immunity and Confers Protection in Pregnancy. Cell Rep 28, 2634-2646 e2634.

He, D., Marles-Wright, J., 2015. Ferritin family proteins and their use in bionanotechnology. N Biotechnol 32, 651-657.

Heinz, F.X., Stiasny, K., 2017. The Antigenic Structure of ZIKV and Its Relation to Other Flaviviruses: Implications for Infection and Immunoprophylaxis. Microbiol Mol Biol Rev 81.

Heinz, F.X., Stiasny, K., Puschner-Auer, G., Holzmann, H., Allison, S.L., Mandl, C.W., Kunz, C., 1994. Structural changes and functional control of the tick-borne encephalitis virus glycoprotein E by the heterodimeric association with protein prM. Virology 198, 109-117.

Hershman, S.G., Chen, Q., Lee, J.Y., Kozak, M.L., Yue, P., Wang, L.S., Johnson, F.B., 2008. Genomic distribution and functional analyses of potential G-quadruplex-forming sequences in Saccharomyces cerevisiae. Nucleic Acids Res 36, 144-156.

Heymann, D.L., Hodgson, A., Sall, A.A., Freedman, D.O., Staples, J.E., Althabe, F., Baruah, K., Mahmud, G., Kandun, N., Vasconcelos, P.F., Bino, S., Menon, K.U., 2016. ZIKV and microcephaly: why is this situation a PHEIC? Lancet 387, 719-721.

Hilgenfeld, R., 2016. ZIKV NS1, a pathogenicity factor with many faces. EMBO J 35, 2631-2633.

Hill, M.E., Kumar, A., Wells, J.A., Hobman, T.C., Julien, O., Hardy, J.A., 2018. The Unique Cofactor Region of ZIKV NS2B-NS3 Protease Facilitates Cleavage of Key Host Proteins. ACS Chem Biol 13, 2398-2405.

Hoen, B., Schaub, B., Funk, A.L., Ardillon, V., Boullard, M., Cabie, A., Callier, C., Carles, G., Cassadou, S., Cesaire, R., Douine, M., Herrmann-Storck, C., Kadhel, P., Laouenan, C., Madec, Y., Monthieux, A., Nacher, M., Najioullah, F., Rousset, D., Ryan, C., Schepers, K., Stegmann-Planchard, S., Tressieres, B., Volumenie, J.L., Yassinguezo, S., Janky, E., Fontanet, A., 2018. Pregnancy Outcomes after ZIKV Infection in French Territories in the Americas. N Engl J Med 378, 985-994.

Huppert, J.L., Balasubramanian, S., 2005. Prevalence of quadruplexes in the human genome. Nucleic Acids Res 33, 2908-2916.

In, H.J., Lee, Y.H., Jang, S., Lim, H.J., Kim, M.Y., Kim, J.A., Yoo, J.S., Chung, G.T., Kim, Y.J., 2020. Enhanced effect of modified ZIKV E antigen on the immunogenicity of DNA vaccine. Virology 549, 25-31.

Jagger, B.W., Dowd, K.A., Chen, R.E., Desai, P., Foreman, B., Burgomaster, K.E., Himansu, S., Kong, W.P., Graham, B.S., Pierson, T.C., Diamond, M.S., 2019. Protective Efficacy of Nucleic Acid Vaccines Against Transmission of ZIKV During Pregnancy in Mice. J Infect Dis 220, 1577-1588.

Jemielity, S., Wang, J.J., Chan, Y.K., Ahmed, A.A., Li, W., Monahan, S., Bu, X., Farzan, M., Freeman, G.J., Umetsu, D.T., Dekruyff, R.H., Choe, H., 2013. TIM-family proteins promote infection of multiple enveloped viruses through virion-associated phosphatidylserine. PLoS Pathog 9, e1003232.

Julander, J.G., Siddharthan, V., Evans, J., Taylor, R., Tolbert, K., Apuli, C., Stewart, J., Collins, P., Gebre, M., Neilson, S., Van Wettere, A., Lee, Y.M., Sheridan, W.P., Morrey, J.D., Babu, Y.S., 2017. Efficacy of the broad-spectrum antiviral compound BCX4430 against ZIKV in cell culture and in a mouse model. Antiviral Res 137, 14-22.

Kalathiya, U., Padariya, M., Fahraeus, R., Chakraborti, S., Hupp, T.R., 2021. Multivalent Display of SARS-CoV-2 Spike (RBD Domain) of COVID-19 to Nanomaterial, Protein Ferritin Nanocages. Biomolecules 11.

Kam, Y.W., Leite, J.A., Amrun, S.N., Lum, F.M., Yee, W.X., Bakar, F.A., Eng, K.E., Lye, D.C., Leo, Y.S., Chong, C.Y., Freitas, A.R.R., Milanez, G.P., Proenca-Modena, J.L., Renia, L., Costa, F.T.M., Ng, L.F.P., Zika-Unicamp, N., 2019. ZIKV-Specific NS1 Epitopes as Serological Markers of Acute ZIKV Infection. J Infect Dis 220, 203-212.

Kamiyama, N., Soma, R., Hidano, S., Watanabe, K., Umekita, H., Fukuda, C., Noguchi, K., Gendo, Y., Ozaki, T., Sonoda, A., Sachi, N., Runtuwene, L.R., Miura, Y., Matsubara, E., Tajima, S., Takasaki, T., Eshita, Y., Kobayashi, T., 2017. Ribavirin inhibits Zika virus (ZIKV) replication in vitro and suppresses viremia in ZIKV-infected STAT1-deficient mice. Antiviral Res 146, 1-11.

Kanekiyo, M., Bu, W., Joyce, M.G., Meng, G., Whittle, J.R., Baxa, U., Yamamoto, T., Narpala, S., Todd, J.P., Rao, S.S., McDermott, A.B., Koup, R.A., Rossmann, M.G., Mascola, J.R., Graham, B.S., Cohen, J.I., Nabel, G.J., 2015. Rational Design of an Epstein-Barr Virus Vaccine Targeting the Receptor-Binding Site. Cell 162, 1090-1100.

Kanekiyo, M., Wei, C.J., Yassine, H.M., McTamney, P.M., Boyington, J.C., Whittle, J.R., Rao, S.S., Kong, W.P., Wang, L., Nabel, G.J., 2013. Self-assembling influenza nanoparticle vaccines elicit broadly neutralizing H1N1 antibodies. Nature 499, 102-106.

Kang, C., Keller, T.H., Luo, D., 2017. ZIKV Protease: An Antiviral Drug Target. Trends Microbiol 25, 797-808.

Kariko, K., Buckstein, M., Ni, H., Weissman, D., 2005. Suppression of RNA recognition by Toll-like receptors: the impact of nucleoside modification and the evolutionary origin of RNA. Immunity 23, 165-175.

Kariko, K., Muramatsu, H., Welsh, F.A., Ludwig, J., Kato, H., Akira, S., Weissman, D., 2008. Incorporation of pseudouridine into mRNA yields superior nonimmunogenic vector with increased translational capacity and biological stability. Mol Ther 16, 1833-1840.

Kawiecki, A.B., Christofferson, R.C., 2016. ZIKV-Induced Antibody Response Enhances Dengue Virus Serotype 2 Replication In Vitro. J Infect Dis 214, 1357-1360.
Khou, C., Pardigon, N., 2017. Identifying Attenuating Mutations: Tools for a New Vaccine Design against Flaviviruses. Intervirology 60, 8-18.
Kim, Y.I., Kim, D., Yu, K.M., Seo, H.D., Lee, S.A., Casel, M.A.B., Jang, S.G., Kim, S., Jung, W., Lai, C.J., Choi, Y.K., Jung, J.U., 2021. Development of spike receptor-binding domain nanoparticle as a vaccine candidate against SARS-CoV-2 infection in ferrets. bioRxiv.
Konishi, E., Mason, P.W., 1993. Proper maturation of the Japanese encephalitis virus envelope glycoprotein requires cosynthesis with the premembrane protein. J Virol 67, 1672-1675.
Kou, Y., Xu, Y., Zhao, Z., Liu, J., Wu, Y., You, Q., Wang, L., Gao, F., Cai, L., Jiang, C., 2017. Tissue plasminogen activator (tPA) signal sequence enhances immunogenicity of MVA-based vaccine against tuberculosis. Immunol Lett 190, 51-57.
Krauer, F., Riesen, M., Reveiz, L., Oladapo, O.T., Martinez-Vega, R., Porgo, T.V., Haefliger, A., Broutet, N.J., Low, N., Group, W.H.O.Z.C.W., 2017. ZIKV Infection as a Cause of Congenital Brain Abnormalities and Guillain-Barre Syndrome: Systematic Review. PLoS Med 14, e1002203.
Kuhn, R.J., Zhang, W., Rossmann, M.G., Pletnev, S.V., Corver, J., Lenches, E., Jones, C.T., Mukhopadhyay, S., Chipman, P.R., Strauss, E.G., Baker, T.S., Strauss, J.H., 2002. Structure of dengue virus: implications for flavivirus organization, maturation, and fusion. Cell 108, 717-725.
Kumar, A., Hou, S., Airo, A.M., Limonta, D., Mancinelli, V., Branton, W., Power, C., Hobman, T.C., 2016. ZIKV inhibits type-I interferon production and downstream signaling. EMBO Rep 17, 1766-1775.
Kumar, A., Liang, B., Aarthy, M., Singh, S.K., Garg, N., Mysorekar, I.U., Giri, R., 2018. Hydroxychloroquine Inhibits ZIKV NS2B-NS3 Protease. ACS Omega 3, 18132-18141.
Kuno, G., Chang, G.J., Tsuchiya, K.R., Karabatsos, N., Cropp, C.B., 1998. Phylogeny of the genus Flavivirus. J Virol 72, 73-83.
Lai, F., Schlich, M., Pireddu, R., Corrias, F., Fadda, A.M., Sinico, C., 2015. Production of nanosuspensions as a tool to improve drug bioavailability: focus on topical delivery. Curr Pharm Des 21, 6089-6103.
Laidlaw, B.J., Cyster, J.G., 2021. Transcriptional regulation of memory B cell differentiation. Nat Rev Immunol 21, 209-220.
Lanciotti, R.S., Kosoy, O.L., Laven, J.J., Velez, J.O., Lambert, A.J., Johnson, A.J., Stanfield, S.M., Duffy, M.R., 2008. Genetic and serologic properties of ZIKV associated with an epidemic, Yap State, Micronesia, 2007. Emerg Infect Dis 14, 1232-1239.
Lanciotti, R.S., Lambert, A.J., Holodniy, M., Saavedra, S., Signor Ldel, C., 2016. Phylogeny of ZIKV in Western Hemisphere, 2015. Emerg Infect Dis 22, 933-935.
Larocca, R.A., Abbink, P., Peron, J.P., Zanotto, P.M., Iampietro, M.J., Badamchi-Zadeh, A., Boyd, M., Ng'ang'a, D., Kirilova, M., Nityanandam, R., Mercado, N.B., Li, Z., Moseley, E.T., Bricault, C.A., Borducchi, E.N., Giglio, P.B., Jetton, D., Neubauer, G., Nkolola, J.P., Maxfield, L.F., De La Barrera, R.A., Jarman, R.G., Eckels, K.H., Michael, N.L., Thomas, S.J., Barouch, D.H., 2016. Vaccine protection against ZIKV from Brazil. Nature 536, 474-478.
Lavezzo, E., Berselli, M., Frasson, I., Perrone, R., Palu, G., Brazzale, A.R., Richter, S.N., Toppo, S., 2018. G-quadruplex forming sequences in the genome of all known human viruses: A comprehensive guide. PLoS Comput Biol 14, e1006675.
Lazear, H.M., Govero, J., Smith, A.M., Platt, D.J., Fernandez, E., Miner, J.J., Diamond, M.S., 2016. A Mouse Model of ZIKV Pathogenesis. Cell Host Microbe 19, 720-730.
Lee, L.A., Wang, Q., 2006. Adaptations of nanoscale viruses and other protein cages for medical applications. Nanomedicine 2, 137-149.

Lei, J., Hansen, G., Nitsche, C., Klein, C.D., Zhang, L., Hilgenfeld, R., 2016. Crystal structure of ZIKV NS2B-NS3 protease in complex with a boronate inhibitor. Science 353, 503-505.

Leung, J.Y., Pijlman, G.P., Kondratieva, N., Hyde, J., Mackenzie, J.M., Khromykh, A.A., 2008. Role of nonstructural protein NS2A in flavivirus assembly. J Virol 82, 4731-4741.

Li, C., Zhu, X., Ji, X., Quanquin, N., Deng, Y.Q., Tian, M., Aliyari, R., Zuo, X., Yuan, L., Afridi, S.K., Li, X.F., Jung, J.U., Nielsen-Saines, K., Qin, F.X., Qin, C.F., Xu, Z., Cheng, G., 2017. Chloroquine, a FDA-approved Drug, Prevents ZIKV Infection and its Associated Congenital Microcephaly in Mice. EBioMedicine 24, 189-194.

Li, H., Saucedo-Cuevas, L., Regla-Nava, J.A., Chai, G., Sheets, N., Tang, W., Terskikh, A.V., Shresta, S., Gleeson, J.G., 2016a. ZIKV Infects Neural Progenitors in the Adult Mouse Brain and Alters Proliferation. Cell Stem Cell 19, 593-598.

Li, L., Lok, S.M., Yu, I.M., Zhang, Y., Kuhn, R.J., Chen, J., Rossmann, M.G., 2008. The flavivirus precursor membrane-envelope protein complex: structure and maturation. Science 319, 1830-1834.

Li, M., Azad, M., Dave, R., Bilgili, E., 2016b. Nanomilling of Drugs for Bioavailability Enhancement: A Holistic Formulation-Process Perspective. Pharmaceutics 8.

Li, M., Zhang, D., Li, C., Zheng, Z., Fu, M., Ni, F., Liu, Y., Du, T., Wang, H., Griffin, G.E., Zhang, M., Hu, Q., 2020. Characterization of ZIKV Endocytic Pathways in Human Glioblastoma Cells. Front Microbiol 11, 242.

Li, P.C., Jang, J., Hsia, C.Y., Groomes, P., Lian, W., de Wispelaere, M., Pitts, J.D., Wang, J., Kwaitkowski, N., Gray, N.S., Yang, P.L., 2019. Small molecules targeting the flavivirus E protein with broad-spectrum activity and antiviral efficacy in vivo. ACS Infect Dis.

Li, X.F., Dong, H.L., Wang, H.J., Huang, X.Y., Qiu, Y.F., Ji, X., Ye, Q., Li, C., Liu, Y., Deng, Y.Q., Jiang, T., Cheng, G., Zhang, F.C., Davidson, A.D., Song, Y.J., Shi, P.Y., Qin, C.F., 2018a. Development of a chimeric Zika vaccine using a licensed live-attenuated flavivirus vaccine as backbone. Nat Commun 9, 673.

Li, Y., Zhang, Z., Phoo, W.W., Loh, Y.R., Li, R., Yang, H.Y., Jansson, A.E., Hill, J., Keller, T.H., Nacro, K., Luo, D., Kang, C., 2018b. Structural Insights into the Inhibition of ZIKV NS2B-NS3 Protease by a Small-Molecule Inhibitor. Structure 26, 555-564 e553.

Liang, Q., Luo, Z., Zeng, J., Chen, W., Foo, S.S., Lee, S.A., Ge, J., Wang, S., Goldman, S.A., Zlokovic, B.V., Zhao, Z., Jung, J.U., 2016. ZIKV NS4A and NS4B Proteins Deregulate Akt-mTOR Signaling in Human Fetal Neural Stem Cells to Inhibit Neurogenesis and Induce Autophagy. Cell Stem Cell 19, 663-671.

Lim, S.-Y., Osuna, C., Lakritz, J., Chen, E., Yoon, G., Taylor, R., MacLennan, S., Leonard, M., Giuliano, E., Mathis, A., Berger, E., Babu, Y., Sheridan, W., Whitney, J., 2017. Galidesivir, a Direct-Acting Antiviral Drug, Abrogates Viremia in Rhesus Macaques Challenged with ZIKV. Open Forum Infectious Diseases 4, S55-S55.

Lim, S.P., Noble, C.G., Shi, P.Y., 2015. The dengue virus NS5 protein as a target for drug discovery. Antiviral Res 119, 57-67.

Lin, S., Yang, S., He, J., Guest, J.D., Ma, Z., Yang, L., Pierce, B.G., Tang, Q., Zhang, Y.J., 2019. ZIKV NS5 protein antagonizes type I interferon production via blocking TBK1 activation. Virology 527, 180-187.

Lindenbach, B.D., Rice, C.M., 2003. Molecular biology of flaviviruses. Adv Virus Res 59, 23-61.

Lindenbach, B.D., Rice, C.M., 2013. The ins and outs of hepatitis C virus entry and assembly. Nat Rev Microbiol 11, 688-700.

Link, A., Zabel, F., Schnetzler, Y., Titz, A., Brombacher, F., Bachmann, M.F., 2012. Innate immunity mediates follicular transport of particulate but not soluble protein antigen. J Immunol 188, 3724-3733.

Liu, R., Wang, X., Ma, Y., Wu, J., Mao, C., Yuan, L., Lu, J., 2019. Prevalence of ZIKV in blood donations: a systematic review and meta-analysis. BMC Infect Dis 19, 590.

Lopez-Camacho, C., De Lorenzo, G., Slon-Campos, J.L., Dowall, S., Abbink, P., Larocca, R.A., Kim, Y.C., Poggianella, M., Graham, V., Findlay-Wilson, S., Rayner, E., Carmichael, J., Dejnirattisai, W., Boyd, M., Hewson, R., Mongkolsapaya, J., Screaton, G.R., Barouch, D.H., Burrone, O.R., Patel, A.H., Reyes-Sandoval, A., 2020. Immunogenicity and Efficacy of ZIKV Envelope Domain III in DNA, Protein, and ChAdOx1 Adenoviral-Vectored Vaccines. Vaccines (Basel) 8.

Lopez-Sagaseta, J., Malito, E., Rappuoli, R., Bottomley, M.J., 2016. Self-assembling protein nanoparticles in the design of vaccines. Comput Struct Biotechnol J 14, 58-68.

Lorenz, I.C., Allison, S.L., Heinz, F.X., Helenius, A., 2002. Folding and dimerization of tick-borne encephalitis virus envelope proteins prM and E in the endoplasmic reticulum. J Virol 76, 5480-5491.

Lu, G., Gong, P., 2013. Crystal Structure of the full-length Japanese encephalitis virus NS5 reveals a conserved methyltransferase-polymerase interface. PLoS Pathog 9, e1003549.

Ma, J., Ketkar, H., Geng, T., Lo, E., Wang, L., Xi, J., Sun, Q., Zhu, Z., Cui, Y., Yang, L., Wang, P., 2018. ZIKV Non-structural Protein 4A Blocks the RLR-MAVS Signaling. Front Microbiol 9, 1350.

Maizels, N., Gray, L.T., 2013. The G4 genome. PLoS Genet 9, e1003468.

Majee, P., Pattnaik, A., Sahoo, B.R., Shankar, U., Pattnaik, A.K., Kumar, A., Nayak, D., 2021. Inhibition of ZIKV replication by G-quadruplex-binding ligands. Mol Ther Nucleic Acids 23, 691-701.

Malet, H., Masse, N., Selisko, B., Romette, J.L., Alvarez, K., Guillemot, J.C., Tolou, H., Yap, T.L., Vasudevan, S., Lescar, J., Canard, B., 2008. The flavivirus polymerase as a target for drug discovery. Antiviral Res 80, 23-35.

Manangeeswaran, M., Kielczewski, J.L., Sen, H.N., Xu, B.C., Ireland, D.D.C., McWilliams, I.L., Chan, C.C., Caspi, R.R., Verthelyi, D., 2018. ZIKV infection causes persistent chorioretinal lesions. Emerg Microbes Infect 7, 96.

Marquez-Jurado, S., Nogales, A., Avila-Perez, G., Iborra, F.J., Martinez-Sobrido, L., Almazan, F., 2018. An Alanine-to-Valine Substitution in the Residue 175 of ZIKV NS2A Protein Affects Viral RNA Synthesis and Attenuates the Virus In Vivo. Viruses 10.

Marsico, G., Chambers, V.S., Sahakyan, A.B., McCauley, P., Boutell, J.M., Antonio, M.D., Balasubramanian, S., 2019. Whole genome experimental maps of DNA G-quadruplexes in multiple species. Nucleic Acids Res 47, 3862-3874.

Mastrangelo, E., Pezzullo, M., De Burghgraeve, T., Kaptein, S., Pastorino, B., Dallmeier, K., de Lamballerie, X., Neyts, J., Hanson, A.M., Frick, D.N., Bolognesi, M., Milani, M., 2012. Ivermectin is a potent inhibitor of flavivirus replication specifically targeting NS3 helicase activity: new prospects for an old drug. J Antimicrob Chemother 67, 1884-1894.

Medeiros, D.B.A., Nunes, M.R.T., Vasconcelos, P.F.C., Chang, G.J., Kuno, G., 2007. Complete genome characterization of Rocio virus (Flavivirus: Flaviviridae), a Brazilian flavivirus isolated from a fatal case of encephalitis during an epidemic in Sao Paulo state. J Gen Virol 88, 2237-2246.

Meertens, L., Labeau, A., Dejarnac, O., Cipriani, S., Sinigaglia, L., Bonnet-Madin, L., Le Charpentier, T., Hafirassou, M.L., Zamborlini, A., Cao-Lormeau, V.M., Coulpier, M., Misse, D., Jouvenet, N., Tabibiazar, R., Gressens, P., Schwartz, O., Amara, A., 2017. Axl Mediates ZIKV Entry in Human Glial Cells and Modulates Innate Immune Responses. Cell Rep 18, 324-333.

Mendez, N., Oviedo-Pastrana, M., Mattar, S., Caicedo-Castro, I., Arrieta, G., 2017. ZIKV disease, microcephaly and Guillain-Barre syndrome in Colombia: epidemiological situation during 21 months of the ZIKV outbreak, 2015-2017. Arch Public Health 75, 65.

Mesci, P., Macia, A., Moore, S.M., Shiryaev, S.A., Pinto, A., Huang, C.T., Tejwani, L., Fernandes, I.R., Suarez, N.A., Kolar, M.J., Montefusco, S., Rosenberg, S.C., Herai, R.H., Cugola, F.R., Russo, F.B., Sheets, N., Saghatelian, A., Shresta, S., Momper, J.D., Siqueira-

Neto, J.L., Corbett, K.D., Beltrao-Braga, P.C.B., Terskikh, A.V., Muotri, A.R., 2018. Blocking ZIKV vertical transmission. Sci Rep 8, 1218.
Miner, J.J., Diamond, M.S., 2017. ZIKV Pathogenesis and Tissue Tropism. Cell Host Microbe 21, 134-142.
Miner, J.J., Sene, A., Richner, J.M., Smith, A.M., Santeford, A., Ban, N., Weger-Lucarelli, J., Manzella, F., Ruckert, C., Govero, J., Noguchi, K.K., Ebel, G.D., Diamond, M.S., Apte, R.S., 2016. ZIKV Infection in Mice Causes Panuveitis with Shedding of Virus in Tears. Cell Rep 16, 3208-3218.
Miranda, H.A., 2nd, Costa, M.C., Frazao, M.A.M., Simao, N., Franchischini, S., Moshfeghi, D.M., 2016. Expanded Spectrum of Congenital Ocular Findings in Microcephaly with Presumed Zika Infection. Ophthalmology 123, 1788-1794.
Mishra, S.K., Tawani, A., Mishra, A., Kumar, A., 2016. G4IPDB: A database for G-quadruplex structure forming nucleic acid interacting proteins. Sci Rep 6, 38144.
Mlakar, J., Korva, M., Tul, N., Popovic, M., Poljsak-Prijatelj, M., Mraz, J., Kolenc, M., Resman Rus, K., Vesnaver Vipotnik, T., Fabjan Vodusek, V., Vizjak, A., Pizem, J., Petrovec, M., Avsic Zupanc, T., 2016. ZIKV Associated with Microcephaly. N Engl J Med 374, 951-958.
Modis, Y., Ogata, S., Clements, D., Harrison, S.C., 2004. Structure of the dengue virus envelope protein after membrane fusion. Nature 427, 313-319.
Mohd Ropidi, M.I., Khazali, A.S., Nor Rashid, N., Yusof, R., 2020. Endoplasmic reticulum: a focal point of ZIKV infection. J Biomed Sci 27, 27.
Morrison, T.E., Diamond, M.S., 2017. Animal Models of ZIKV Infection, Pathogenesis, and Immunity. J Virol 91.
Mounce, B.C., Cesaro, T., Carrau, L., Vallet, T., Vignuzzi, M., 2017. Curcumin inhibits Zika and chikungunya virus infection by inhibiting cell binding. Antiviral Res 142, 148-157.
Muller, D.A., Landsberg, M.J., Bletchly, C., Rothnagel, R., Waddington, L., Hankamer, B., Young, P.R., 2012. Structure of the dengue virus glycoprotein non-structural protein 1 by electron microscopy and single-particle analysis. J Gen Virol 93, 771-779.
Mumtaz, N., Jimmerson, L.C., Bushman, L.R., Kiser, J.J., Aron, G., Reusken, C., Koopmans, M.P.G., van Kampen, J.J.A., 2017. Cell-line dependent antiviral activity of sofosbuvir against ZIKV. Antiviral Res 146, 161-163.
Musso, D., Baud, D., Gubler, D.J., 2016a. ZIKV: what do we know? Clin Microbiol Infect 22, 494-496.
Musso, D., Nilles, E.J., Cao-Lormeau, V.M., 2014. Rapid spread of emerging ZIKV in the Pacific area. Clin Microbiol Infect 20, O595-596.
Musso, D., Stramer, S.L., Committee, A.T.-T.D., Busch, M.P., International Society of Blood Transfusion Working Party on Transfusion-Transmitted Infectious, D., 2016b. ZIKV: a new challenge for blood transfusion. Lancet 387, 1993-1994.
Muthumani, K., Griffin, B.D., Agarwal, S., Kudchodkar, S.B., Reuschel, E.L., Choi, H., Kraynyak, K.A., Duperret, E.K., Keaton, A.A., Chung, C., Kim, Y.K., Booth, S.A., Racine, T., Yan, J., Morrow, M.P., Jiang, J., Lee, B., Ramos, S., Broderick, K.E., Reed, C.C., Khan, A.S., Humeau, L., Ugen, K.E., Park, Y.K., Maslow, J.N., Sardesai, N.Y., Joseph Kim, J., Kobinger, G.P., Weiner, D.B., 2016. In vivo protection against ZIKV infection and pathogenesis through passive antibody transfer and active immunisation with a prMEnv DNA vaccine. NPJ Vaccines 1, 16021.
Nambala, P., Su, W.C., 2018. Role of ZIKV prM Protein in Viral Pathogenicity and Use in Vaccine Development. Front Microbiol 9, 1797.
Ng, K.K., Arnold, J.J., Cameron, C.E., 2008. Structure-function relationships among RNA-dependent RNA polymerases. Curr Top Microbiol Immunol 320, 137-156.
Ni, P., Cheng Kao, C., 2013. Non-encapsidation activities of the capsid proteins of positive-strand RNA viruses. Virology 446, 123-132.

Nurnberger, C., Bodmer, B.S., Fiedler, A.H., Gabriel, G., Muhlebach, M.D., 2019. A Measles Virus-Based Vaccine Candidate Mediates Protection against ZIKV in an Allogeneic Mouse Pregnancy Model. J Virol 93.

Oli, A.N., Obialor, W.O., Ifeanyichukwu, M.O., Odimegwu, D.C., Okoyeh, J.N., Emechebe, G.O., Adejumo, S.A., Ibeanu, G.C., 2020. Immunoinformatics and Vaccine Development: An Overview. Immunotargets Ther 9, 13-30.

Oliphant, T., Engle, M., Nybakken, G.E., Doane, C., Johnson, S., Huang, L., Gorlatov, S., Mehlhop, E., Marri, A., Chung, K.M., Ebel, G.D., Kramer, L.D., Fremont, D.H., Diamond, M.S., 2005. Development of a humanized monoclonal antibody with therapeutic potential against West Nile virus. Nat Med 11, 522-530.

Omura, S., Crump, A., 2017. Ivermectin and malaria control. Malar J 16, 172.

Osuna, C.E., Lim, S.Y., Deleage, C., Griffin, B.D., Stein, D., Schroeder, L.T., Omange, R.W., Best, K., Luo, M., Hraber, P.T., Andersen-Elyard, H., Ojeda, E.F., Huang, S., Vanlandingham, D.L., Higgs, S., Perelson, A.S., Estes, J.D., Safronetz, D., Lewis, M.G., Whitney, J.B., 2016. Zika viral dynamics and shedding in rhesus and cynomolgus macaques. Nat Med 22, 1448-1455.

Panchaud, A., Stojanov, M., Ammerdorffer, A., Vouga, M., Baud, D., 2016. Emerging Role of ZIKV in Adverse Fetal and Neonatal Outcomes. Clin Microbiol Rev 29, 659-694.

Pardi, N., Hogan, M.J., Pelc, R.S., Muramatsu, H., Andersen, H., DeMaso, C.R., Dowd, K.A., Sutherland, L.L., Scearce, R.M., Parks, R., Wagner, W., Granados, A., Greenhouse, J., Walker, M., Willis, E., Yu, J.S., McGee, C.E., Sempowski, G.D., Mui, B.L., Tam, Y.K., Huang, Y.J., Vanlandingham, D., Holmes, V.M., Balachandran, H., Sahu, S., Lifton, M., Higgs, S., Hensley, S.E., Madden, T.D., Hope, M.J., Kariko, K., Santra, S., Graham, B.S., Lewis, M.G., Pierson, T.C., Haynes, B.F., Weissman, D., 2017. ZIKV protection by a single low-dose nucleoside-modified mRNA vaccination. Nature 543, 248-251.

Pathak, N., Kuo, Y.P., Chang, T.Y., Huang, C.T., Hung, H.C., Hsu, J.T., Yu, G.Y., Yang, J.M., 2020. ZIKV NS3 Protease Pharmacophore Anchor Model and Drug Discovery. Sci Rep 10, 8929.

Pattnaik, A., Palermo, N., Sahoo, B.R., Yuan, Z., Hu, D., Annamalai, A.S., Vu, H.L.X., Correas, I., Prathipati, P.K., Destache, C.J., Li, Q., Osorio, F.A., Pattnaik, A.K., Xiang, S.H., 2018. Discovery of a non-nucleoside RNA polymerase inhibitor for blocking ZIKV replication through in silico screening. Antiviral Res 151, 78-86.

Pattnaik, A., Sahoo, B.R., Pattnaik, A.K., 2020. Current Status of ZIKV Vaccines: Successes and Challenges. Vaccines (Basel) 8.

Perera, R., Kuhn, R.J., 2008. Structural proteomics of dengue virus. Curr Opin Microbiol 11, 369-377.

Perrone, R., Butovskaya, E., Daelemans, D., Palu, G., Pannecouque, C., Richter, S.N., 2014. Anti-HIV-1 activity of the G-quadruplex ligand BRACO-19. J Antimicrob Chemother 69, 3248-3258.

Perrone, R., Doria, F., Butovskaya, E., Frasson, I., Botti, S., Scalabrin, M., Lago, S., Grande, V., Nadai, M., Freccero, M., Richter, S.N., 2015. Synthesis, Binding and Antiviral Properties of Potent Core-Extended Naphthalene Diimides Targeting the HIV-1 Long Terminal Repeat Promoter G-Quadruplexes. J Med Chem 58, 9639-9652.

Phoo, W.W., Zhang, Z., Wirawan, M., Chew, E.J.C., Chew, A.B.L., Kouretova, J., Steinmetzer, T., Luo, D., 2018. Structures of ZIKV NS2B-NS3 protease in complex with peptidomimetic inhibitors. Antiviral Res 160, 17-24.

Piekna-Przybylska, D., Sullivan, M.A., Sharma, G., Bambara, R.A., 2014. U3 region in the HIV-1 genome adopts a G-quadruplex structure in its RNA and DNA sequence. Biochemistry 53, 2581-2593.

Pierson, T.C., Diamond, M.S., 2015. A game of numbers: the stoichiometry of antibody-mediated neutralization of flavivirus infection. Prog Mol Biol Transl Sci 129, 141-166.

Plotkin, S., 2014. History of vaccination. Proc Natl Acad Sci U S A 111, 12283-12287.
Poland, G.A., Ovsyannikova, I.G., Kennedy, R.B., 2019. Zika Vaccine Development: Current Status. Mayo Clin Proc 94, 2572-2586.
Pomar, L., Vouga, M., Lambert, V., Pomar, C., Hcini, N., Jolivet, A., Benoist, G., Rousset, D., Matheus, S., Malinger, G., Panchaud, A., Carles, G., Baud, D., 2018. Maternal-fetal transmission and adverse perinatal outcomes in pregnant women infected with ZIKV: prospective cohort study in French Guiana. BMJ 363, k4431.
Prasad, V.M., Miller, A.S., Klose, T., Sirohi, D., Buda, G., Jiang, W., Kuhn, R.J., Rossmann, M.G., 2017. Structure of the immature ZIKV at 9 A resolution. Nat Struct Mol Biol 24, 184-186.
Prasasty, V.D., Grazzolie, K., Rosmalena, R., Yazid, F., Ivan, F.X., Sinaga, E., 2019. Peptide-Based Subunit Vaccine Design of T- and B-Cells Multi-Epitopes against ZIKV Using Immunoinformatics Approaches. Microorganisms 7.
Priyamvada, L., Quicke, K.M., Hudson, W.H., Onlamoon, N., Sewatanon, J., Edupuganti, S., Pattanapanyasat, K., Chokephaibulkit, K., Mulligan, M.J., Wilson, P.C., Ahmed, R., Suthar, M.S., Wrammert, J., 2016. Human antibody responses after dengue virus infection are highly cross-reactive to ZIKV. Proc Natl Acad Sci U S A 113, 7852-7857.
Prow, N.A., Liu, L., Nakayama, E., Cooper, T.H., Yan, K., Eldi, P., Hazlewood, J.E., Tang, B., Le, T.T., Setoh, Y.X., Khromykh, A.A., Hobson-Peters, J., Diener, K.R., Howley, P.M., Hayball, J.D., Suhrbier, A., 2018. A vaccinia-based single vector construct multi-pathogen vaccine protects against both Zika and chikungunya viruses. Nat Commun 9, 1230.
Qin, Y., Hurley, L.H., 2008. Structures, folding patterns, and functions of intramolecular DNA G-quadruplexes found in eukaryotic promoter regions. Biochimie 90, 1149-1171.
Ra, J.S., Shin, H.H., Kang, S., Do, Y., 2014. Lumazine synthase protein cage nanoparticles as antigen delivery nanoplatforms for dendritic cell-based vaccine development. Clin Exp Vaccine Res 3, 227-234.
Ramharack, P., Soliman, M.E.S., 2018. ZIKV NS5 protein potential inhibitors: an enhanced in silico approach in drug discovery. J Biomol Struct Dyn 36, 1118-1133.
Rastogi, M., Sharma, N., Singh, S.K., 2016. Flavivirus NS1: a multifaceted enigmatic viral protein. Virol J 13, 131.
Rausch, K., Hackett, B.A., Weinbren, N.L., Reeder, S.M., Sadovsky, Y., Hunter, C.A., Schultz, D.C., Coyne, C.B., Cherry, S., 2017. Screening Bioactives Reveals Nanchangmycin as a Broad Spectrum Antiviral Active against ZIKV. Cell Rep 18, 804-815.
Rhodes, D., Lipps, H.J., 2015. G-quadruplexes and their regulatory roles in biology. Nucleic Acids Res 43, 8627-8637.
Richard, A.S., Shim, B.S., Kwon, Y.C., Zhang, R., Otsuka, Y., Schmitt, K., Berri, F., Diamond, M.S., Choe, H., 2017. AXL-dependent infection of human fetal endothelial cells distinguishes ZIKV from other pathogenic flaviviruses. Proc Natl Acad Sci U S A 114, 2024-2029.
Richner, J.M., Himansu, S., Dowd, K.A., Butler, S.L., Salazar, V., Fox, J.M., Julander, J.G., Tang, W.W., Shresta, S., Pierson, T.C., Ciaramella, G., Diamond, M.S., 2017a. Modified mRNA Vaccines Protect against ZIKV Infection. Cell 169, 176.
Richner, J.M., Jagger, B.W., Shan, C., Fontes, C.R., Dowd, K.A., Cao, B., Himansu, S., Caine, E.A., Nunes, B.T.D., Medeiros, D.B.A., Muruato, A.E., Foreman, B.M., Luo, H., Wang, T., Barrett, A.D., Weaver, S.C., Vasconcelos, P.F.C., Rossi, S.L., Ciaramella, G., Mysorekar, I.U., Pierson, T.C., Shi, P.Y., Diamond, M.S., 2017b. Vaccine Mediated Protection Against ZIKV-Induced Congenital Disease. Cell 170, 273-283 e212.
Rodriguez, A.K., Munoz, A.L., Segura, N.A., Rangel, H.R., Bello, F., 2019. Molecular characteristics and replication mechanism of dengue, zika and chikungunya arboviruses, and their treatments with natural extracts from plants: An updated review. EXCLI J 18, 988-1006.

Rossi, S.L., Tesh, R.B., Azar, S.R., Muruato, A.E., Hanley, K.A., Auguste, A.J., Langsjoen, R.M., Paessler, S., Vasilakis, N., Weaver, S.C., 2016a. Characterization of a Novel Murine Model to Study ZIKV. Am J Trop Med Hyg 94, 1362-1369.

Rossi, S.L., Tesh, R.B., Azar, S.R., Muruato, A.E., Hanley, K.A., Auguste, A.J., Langsjoen, R.M., Paessler, S., Vasilakis, N., Weaver, S.C., 2016b. Characterization of a Novel Murine Model to Study ZIKV. The American journal of tropical medicine and hygiene 94, 1362-1369.

Ruggiero, E., Richter, S.N., 2018. G-quadruplexes and G-quadruplex ligands: targets and tools in antiviral therapy. Nucleic Acids Res 46, 3270-3283.

Russell, K., Hills, S.L., Oster, A.M., Porse, C.C., Danyluk, G., Cone, M., Brooks, R., Scotland, S., Schiffman, E., Fredette, C., White, J.L., Ellingson, K., Hubbard, A., Cohn, A., Fischer, M., Mead, P., Powers, A.M., Brooks, J.T., 2017. Male-to-Female Sexual Transmission of ZIKV-United States, January-April 2016. Clin Infect Dis 64, 211-213.

Russell, L.J., Weaver, D.D., Bull, M.J., Weinbaum, M., 1984. In utero brain destruction resulting in collapse of the fetal skull, microcephaly, scalp rugae, and neurologic impairment: the fetal brain disruption sequence. Am J Med Genet 17, 509-521.

Sahakyan, A.B., Chambers, V.S., Marsico, G., Santner, T., Di Antonio, M., Balasubramanian, S., 2017. Machine learning model for sequence-driven DNA G-quadruplex formation. Sci Rep 7, 14535.

Sahoo, B.R., Pattnaik, A., Annamalai, A.S., Franco, R., Pattnaik, A.K., 2020. Mechanistic Target of Rapamycin Signaling Activation Antagonizes Autophagy To Facilitate ZIKV Replication. J Virol 94.

Samsa, M.M., Mondotte, J.A., Iglesias, N.G., Assuncao-Miranda, I., Barbosa-Lima, G., Da Poian, A.T., Bozza, P.T., Gamarnik, A.V., 2009. Dengue virus capsid protein usurps lipid droplets for viral particle formation. PLoS Pathog 5, e1000632.

Sapparapu, G., Fernandez, E., Kose, N., Bin, C., Fox, J.M., Bombardi, R.G., Zhao, H., Nelson, C.A., Bryan, A.L., Barnes, T., Davidson, E., Mysorekar, I.U., Fremont, D.H., Doranz, B.J., Diamond, M.S., Crowe, J.E., 2016. Neutralizing human antibodies prevent ZIKV replication and fetal disease in mice. Nature 540, 443-447.

Sariyer, I.K., Gordon, J., Burdo, T.H., Wollebo, H.S., Gianti, E., Donadoni, M., Bellizzi, A., Cicalese, S., Loomis, R., Robinson, J.A., Carnevale, V., Steiner, J., Ozdener, M.H., Miller, A.D., Amini, S., Klein, M.L., Khalili, K., 2019. Suppression of ZIKV Infection in the Brain by the Antiretroviral Drug Rilpivirine. Mol Ther 27, 2067-2079.

Sasisekharan, V., Zimmerman, S., Davies, D.R., 1975. The structure of helical 5′-guanosine monophosphate. Journal of Molecular Biology 92, 171-179.

Sattin, G., Artese, A., Nadai, M., Costa, G., Parrotta, L., Alcaro, S., Palumbo, M., Richter, S.N., 2013. Conformation and stability of intramolecular telomeric G-quadruplexes: sequence effects in the loops. PLoS One 8, e84113.

Scaturro, P., Cortese, M., Chatel-Chaix, L., Fischl, W., Bartenschlager, R., 2015. Dengue Virus Non-structural Protein 1 Modulates Infectious Particle Production via Interaction with the Structural Proteins. PLoS Pathog 11, e1005277.

Sen, D., Gilbert, W., 1988. Formation of parallel four-stranded complexes by guanine-rich motifs in DNA and its implications for meiosis. Nature 334, 364-366.

Sen, D., Gilbert, W., 1990. A sodium-potassium switch in the formation of four-stranded G4-DNA. Nature 344, 410-414.

Shan, C., Muruato, A.E., Jagger, B.W., Richner, J., Nunes, B.T.D., Medeiros, D.B.A., Xie, X., Nunes, J.G.C., Morabito, K.M., Kong, W.P., Pierson, T.C., Barrett, A.D., Weaver, S.C., Rossi, S.L., Vasconcelos, P.F.C., Graham, B.S., Diamond, M.S., Shi, P.Y., 2017a. A single-dose live-attenuated vaccine prevents ZIKV pregnancy transmission and testis damage. Nat Commun 8, 676.

Shan, C., Muruato, A.E., Nunes, B.T.D., Luo, H., Xie, X., Medeiros, D.B.A., Wakamiya, M., Tesh, R.B., Barrett, A.D., Wang, T., Weaver, S.C., Vasconcelos, P.F.C., Rossi, S.L., Shi, P.Y., 2017b. A live-attenuated ZIKV vaccine candidate induces sterilizing immunity in mouse models. Nat Med 23, 763-767.

Shan, C., Xie, X., Shi, P.Y., 2018. ZIKV Vaccine: Progress and Challenges. Cell Host Microbe 24, 12-17.

Shang, Z., Song, H., Shi, Y., Qi, J., Gao, G.F., 2018. Crystal Structure of the Capsid Protein from ZIKV. J Mol Biol 430, 948-962.

Shi, Y., Gao, G.F., 2017. Structural Biology of the ZIKV. Trends Biochem Sci 42, 443-456.

Shiryaev, S.A., Farhy, C., Pinto, A., Huang, C.T., Simonetti, N., Elong Ngono, A., Dewing, A., Shresta, S., Pinkerton, A.B., Cieplak, P., Strongin, A.Y., Terskikh, A.V., 2017. Characterization of the ZIKV two-component NS2B-NS3 protease and structure-assisted identification of allosteric small-molecule antagonists. Antiviral Res 143, 218-229.

Shrestha, P., Jonchhe, S., Emura, T., Hidaka, K., Endo, M., Sugiyama, H., Mao, H., 2017. Confined space facilitates G-quadruplex formation. Nat Nanotechnol 12, 582-588.

Shukla, R., Beesetti, H., Brown, J.A., Ahuja, R., Ramasamy, V., Shanmugam, R.K., Poddar, A., Batra, G., Krammer, F., Lim, J.K., Kale, S., Lal, A.A., Swaminathan, S., Khanna, N., 2020a. Dengue and ZIKV infections are enhanced by live attenuated dengue vaccine but not by recombinant DSV4 vaccine candidate in mouse models. EBioMedicine 60, 102991.

Shukla, R., Ramasamy, V., Shanmugam, R.K., Ahuja, R., Khanna, N., 2020b. Antibody-Dependent Enhancement: A Challenge for Developing a Safe Dengue Vaccine. Front Cell Infect Microbiol 10, 572681.

Shukla, R., Shanmugam, R.K., Ramasamy, V., Arora, U., Batra, G., Acklin, J.A., Krammer, F., Lim, J.K., Swaminathan, S., Khanna, N., 2020c. ZIKV envelope nanoparticle antibodies protect mice without risk of disease enhancement. EBioMedicine 54, 102738.

Siddharthan, V., Van Wettere, A.J., Li, R., Miao, J., Wang, Z., Morrey, J.D., Julander, J.G., 2017. ZIKV infection of adult and fetal STAT2 knock-out hamsters. Virology 507, 89-95.

Simmonds, P., Becher, P., Bukh, J., Gould, E.A., Meyers, G., Monath, T., Muerhoff, S., Pletnev, A., Rico-Hesse, R., Smith, D.B., Stapleton, J.T., Ictv Report, C., 2017. ICTV Virus Taxonomy Profile: Flaviviridae. J Gen Virol 98, 2-3.

Sirohi, D., Chen, Z., Sun, L., Klose, T., Pierson, T.C., Rossmann, M.G., Kuhn, R.J., 2016. The 3.8 A resolution cryo-EM structure of ZIKV. Science 352, 467-470.

Sirohi, D., Kuhn, R.J., 2017. ZIKV Structure, Maturation, and Receptors. J Infect Dis 216, S935-S944.

Sliepen, K., Ozorowski, G., Burger, J.A., van Montfort, T., Stunnenberg, M., LaBranche, C., Montefiori, D.C., Moore, J.P., Ward, A.B., Sanders, R.W., 2015. Presenting native-like HIV-1 envelope trimers on ferritin nanoparticles improves their immunogenicity. Retrovirology 12, 82.

Smith, D.R., Hollidge, B., Daye, S., Zeng, X., Blancett, C., Kuszpit, K., Bocan, T., Koehler, J.W., Coyne, S., Minogue, T., Kenny, T., Chi, X., Yim, S., Miller, L., Schmaljohn, C., Bavari, S., Golden, J.W., 2017. Neuropathogenesis of ZIKV in a Highly Susceptible Immunocompetent Mouse Model after Antibody Blockade of Type I Interferon. PLoS Negl Trop Dis 11, e0005296.

Somnuke, P., Hauhart, R.E., Atkinson, J.P., Diamond, M.S., Avirutnan, P., 2011. N-linked glycosylation of dengue virus NS1 protein modulates secretion, cell-surface expression, hexamer stability, and interactions with human complement. Virology 413, 253-264.

Stettler, K., Beltramello, M., Espinosa, D.A., Graham, V., Cassotta, A., Bianchi, S., Vanzetta, F., Minola, A., Jaconi, S., Mele, F., Foglierini, M., Pedotti, M., Simonelli, L., Dowall, S., Atkinson, B., Percivalle, E., Simmons, C.P., Varani, L., Blum, J., Baldanti, F., Cameroni, E., Hewson, R., Harris, E., Lanzavecchia, A., Sallusto, F., Corti, D., 2016. Specificity, cross-reactivity, and function of antibodies elicited by ZIKV infection. Science 353, 823-826.

Styczynski, A.R., Malta, J., Krow-Lucal, E.R., Percio, J., Nobrega, M.E., Vargas, A., Lanzieri, T.M., Leite, P.L., Staples, J.E., Fischer, M.X., Powers, A.M., Chang, G.J., Burns, P.L., Borland, E.M., Ledermann, J.P., Mossel, E.C., Schonberger, L.B., Belay, E.B., Salinas, J.L., Badaro, R.D., Sejvar, J.J., Coelho, G.E., 2017. Increased rates of Guillain-Barre syndrome associated with ZIKV outbreak in the Salvador metropolitan area, Brazil. PLoS Negl Trop Dis 11, e0005869.

Tai, W., Chen, J., Zhao, G., Geng, Q., He, L., Chen, Y., Zhou, Y., Li, F., Du, L., 2019. Rational Design of ZIKV Subunit Vaccine with Enhanced Efficacy. J Virol 93.

Tan, T.Y., Fibriansah, G., Kostyuchenko, V.A., Ng, T.S., Lim, X.X., Zhang, S., Lim, X.N., Wang, J., Shi, J., Morais, M.C., Corti, D., Lok, S.M., 2020. Capsid protein structure in ZIKV reveals the flavivirus assembly process. Nat Commun 11, 895.

Tian, H., Ji, X., Yang, X., Xie, W., Yang, K., Chen, C., Wu, C., Chi, H., Mu, Z., Wang, Z., Yang, H., 2016a. The crystal structure of ZIKV helicase: basis for antiviral drug design. Protein Cell 7, 450-454.

Tian, H., Ji, X., Yang, X., Zhang, Z., Lu, Z., Yang, K., Chen, C., Zhao, Q., Chi, H., Mu, Z., Xie, W., Wang, Z., Lou, H., Yang, H., Rao, Z., 2016b. Structural basis of ZIKV helicase in recognizing its substrates. Protein Cell 7, 562-570.

Tluckova, K., Marusic, M., Tothova, P., Bauer, L., Sket, P., Plavec, J., Viglasky, V., 2013. Human papillomavirus G-quadruplexes. Biochemistry 52, 7207-7216.

Todd, A.K., Johnston, M., Neidle, S., 2005. Highly prevalent putative quadruplex sequence motifs in human DNA. Nucleic Acids Res 33, 2901-2907.

Tomar, S., Mudgal, R., Fatma, B., 2017. Chapter 6 - Flavivirus Protease: An Antiviral Target, in: Gupta, S.P. (Ed.), Viral Proteases and Their Inhibitors. Academic Press, pp. 137-161.

Turmel, J.M., Abgueguen, P., Hubert, B., Vandamme, Y.M., Maquart, M., Le Guillou-Guillemette, H., Leparc-Goffart, I., 2016. Late sexual transmission of ZIKV related to persistence in the semen. Lancet 387, 2501.

Upadhyay, A.K., Cyr, M., Longenecker, K., Tripathi, R., Sun, C., Kempf, D.J., 2017. Crystal structure of full-length ZIKV NS5 protein reveals a conformation similar to Japanese encephalitis virus NS5. Acta Crystallogr F Struct Biol Commun 73, 116-122.

Valentine, M.J., Murdock, C.C., Kelly, P.J., 2019. Sylvatic cycles of arboviruses in non-human primates. Parasit Vectors 12, 463.

van Hemert, F., Berkhout, B., 2016. Nucleotide composition of the ZIKV RNA genome and its codon usage. Virol J 13, 95.

Verma, A., Halder, K., Halder, R., Yadav, V.K., Rawal, P., Thakur, R.K., Mohd, F., Sharma, A., Chowdhury, S., 2008. Genome-wide computational and expression analyses reveal G-quadruplex DNA motifs as conserved cis-regulatory elements in human and related species. J Med Chem 51, 5641-5649.

Viranaicken, W., Ndebo, A., Bos, S., Souque, P., Gadea, G., El-Kalamouni, C., Krejbich-Trotot, P., Charneau, P., Despres, P., Roche, M., 2017. Recombinant Zika NS1 Protein Secreted from Vero Cells Is Efficient for Inducing Production of Immune Serum Directed against NS1 Dimer. Int J Mol Sci 19.

Vy Thi Le, T., Han, S., Chae, J., Park, H.J., 2012. G-quadruplex binding ligands: from naturally occurring to rationally designed molecules. Curr Pharm Des 18, 1948-1972.

Wang, B., Tan, X.F., Thurmond, S., Zhang, Z.M., Lin, A., Hai, R., Song, J., 2017. The structure of ZIKV NS5 reveals a conserved domain conformation. Nat Commun 8, 14763.

Wang, S.R., Min, Y.Q., Wang, J.Q., Liu, C.X., Fu, B.S., Wu, F., Wu, L.Y., Qiao, Z.X., Song, Y.Y., Xu, G.H., Wu, Z.G., Huang, G., Peng, N.F., Huang, R., Mao, W.X., Peng, S., Chen, Y.Q., Zhu, Y., Tian, T., Zhang, X.L., Zhou, X., 2016a. A highly conserved G-rich consensus sequence in hepatitis C virus core gene represents a new anti-hepatitis C target. Sci Adv 2, e1501535.

Wang, S.R., Zhang, Q.Y., Wang, J.Q., Ge, X.Y., Song, Y.Y., Wang, Y.F., Li, X.D., Fu, B.S., Xu, G.H., Shu, B., Gong, P., Zhang, B., Tian, T., Zhou, X., 2016b. Chemical Targeting of a G-Quadruplex RNA in the Ebola Virus L Gene. Cell Chem Biol 23, 1113-1122.

Weaver, S.C., Costa, F., Garcia-Blanco, M.A., Ko, A.I., Ribeiro, G.S., Saade, G., Shi, P.Y., Vasilakis, N., 2016. ZIKV: History, emergence, biology, and prospects for control. Antiviral Res 130, 69-80.

Weger-Lucarelli, J., Duggal, N.K., Bullard-Feibelman, K., Veselinovic, M., Romo, H., Nguyen, C., Ruckert, C., Brault, A.C., Bowen, R.A., Stenglein, M., Geiss, B.J., Ebel, G.D., 2017. Development and Characterization of Recombinant Virus Generated from a New World ZIKV Infectious Clone. Journal of virology 91.

Wells, M.F., Salick, M.R., Wiskow, O., Ho, D.J., Worringer, K.A., Ihry, R.J., Kommineni, S., Bilican, B., Klim, J.R., Hill, E.J., Kane, L.T., Ye, C., Kaykas, A., Eggan, K., 2016. Genetic Ablation of AXL Does Not Protect Human Neural Progenitor Cells and Cerebral Organoids from ZIKV Infection. Cell Stem Cell 19, 703-708.

Xie, X., Gayen, S., Kang, C., Yuan, Z., Shi, P.Y., 2013. Membrane topology and function of dengue virus NS2A protein. J Virol 87, 4609-4622.

Xie, X., Yang, Y., Muruato, A.E., Zou, J., Shan, C., Nunes, B.T., Medeiros, D.B., Vasconcelos, P.F., Weaver, S.C., Rossi, S.L., Shi, P.Y., 2017. Understanding ZIKV Stability and Developing a Chimeric Vaccine through Functional Analysis. mBio 8.

Xu, K., Song, Y., Dai, L., Zhang, Y., Lu, X., Xie, Y., Zhang, H., Cheng, T., Wang, Q., Huang, Q., Bi, Y., Liu, W.J., Liu, W., Li, X., Qin, C., Shi, Y., Yan, J., Zhou, D., Gao, G.F., 2018. Recombinant Chimpanzee Adenovirus Vaccine AdC7-M/E Protects against ZIKV Infection and Testis Damage. J Virol 92.

Xu, M., Lee, E.M., Wen, Z., Cheng, Y., Huang, W.K., Qian, X., Tcw, J., Kouznetsova, J., Ogden, S.C., Hammack, C., Jacob, F., Nguyen, H.N., Itkin, M., Hanna, C., Shinn, P., Allen, C., Michael, S.G., Simeonov, A., Huang, W., Christian, K.M., Goate, A., Brennand, K.J., Huang, R., Xia, M., Ming, G.L., Zheng, W., Song, H., Tang, H., 2016. Identification of small-molecule inhibitors of ZIKV infection and induced neural cell death via a drug repurposing screen. Nat Med 22, 1101-1107.

Xu, S., Ci, Y., Wang, L., Yang, Y., Zhang, L., Xu, C., Qin, C., Shi, L., 2019. ZIKV NS3 is a canonical RNA helicase stimulated by NS5 RNA polymerase. Nucleic Acids Res 47, 8693-8707.

Yang, M., Dent, M., Lai, H., Sun, H., Chen, Q., 2017a. Immunization of ZIKV envelope protein domain III induces specific and neutralizing immune responses against ZIKV. Vaccine 35, 4287-4294.

Yang, M., Lai, H., Sun, H., Chen, Q., 2017b. Virus-like particles that display ZIKV envelope protein domain III induce potent neutralizing immune responses in mice. Sci Rep 7, 7679.

Yap, T.L., Xu, T., Chen, Y.L., Malet, H., Egloff, M.P., Canard, B., Vasudevan, S.G., Lescar, J., 2007. Crystal structure of the dengue virus RNA-dependent RNA polymerase catalytic domain at 1.85-angstrom resolution. J Virol 81, 4753-4765.

Yassine, H.M., Boyington, J.C., McTamney, P.M., Wei, C.J., Kanekiyo, M., Kong, W.P., Gallagher, J.R., Wang, L., Zhang, Y., Joyce, M.G., Lingwood, D., Moin, S.M., Andersen, H., Okuno, Y., Rao, S.S., Harris, A.K., Kwong, P.D., Mascola, J.R., Nabel, G.J., Graham, B.S., 2015. Hemagglutinin-stem nanoparticles generate heterosubtypic influenza protection. Nat Med 21, 1065-1070.

Yoshii, K., Igarashi, M., Ichii, O., Yokozawa, K., Ito, K., Kariwa, H., Takashima, I., 2012. A conserved region in the prM protein is a critical determinant in the assembly of flavivirus particles. J Gen Virol 93, 27-38.

Yu, J., Liu, X., Ke, C., Wu, Q., Lu, W., Qin, Z., He, X., Liu, Y., Deng, J., Xu, S., Li, Y., Zhu, L., Wan, C., Zhang, Q., Xiao, W., Xie, Q., Zhang, B., Zhao, W., 2017. Effective Suckling

C57BL/6, Kunming, and BALB/c Mouse Models with Remarkable Neurological Manifestation for ZIKV Infection. Viruses 9.
Yuan, J., Yu, J., Huang, Y., He, Z., Luo, J., Wu, Y., Zheng, Y., Wu, J., Zhu, X., Wang, H., Li, M., 2020. Antibiotic fidaxomicin is an RdRp inhibitor as a potential new therapeutic agent against ZIKV. BMC Med 18, 204.
Yuan, L., Huang, X.Y., Liu, Z.Y., Zhang, F., Zhu, X.L., Yu, J.Y., Ji, X., Xu, Y.P., Li, G., Li, C., Wang, H.J., Deng, Y.Q., Wu, M., Cheng, M.L., Ye, Q., Xie, D.Y., Li, X.F., Wang, X., Shi, W., Hu, B., Shi, P.Y., Xu, Z., Qin, C.F., 2017. A single mutation in the prM protein of ZIKV contributes to fetal microcephaly. Science 358, 933-936.
Zacharias, N., Whitty, J., Noblin, S., Tsakiri, S., Garcia, J., Covinsky, M., Bhattacharjee, M., Saulino, D., Tatevian, N., Blackwell, S., 2017. First Neonatal Demise with Travel-Associated ZIKV Infection in the United States of America. AJP Rep 7, e68-e73.
Zanluca, C., de Noronha, L., Duarte Dos Santos, C.N., 2018. Maternal-fetal transmission of the ZIKV: An intriguing interplay. Tissue Barriers 6, e1402143.
Zanluca, C., Melo, V.C., Mosimann, A.L., Santos, G.I., Santos, C.N., Luz, K., 2015. First report of autochthonous transmission of ZIKV in Brazil. Mem Inst Oswaldo Cruz 110, 569-572.
Zhang, J., Lan, Y., Li, M.Y., Lamers, M.M., Fusade-Boyer, M., Klemm, E., Thiele, C., Ashour, J., Sanyal, S., 2018. Flaviviruses Exploit the Lipid Droplet Protein AUP1 to Trigger Lipophagy and Drive Virus Production. Cell Host Microbe 23, 819-831 e815.
Zhang, X., Jia, R., Shen, H., Wang, M., Yin, Z., Cheng, A., 2017. Structures and Functions of the Envelope Glycoprotein in Flavivirus Infections. Viruses 9.
Zhao, B., Yi, G., Du, F., Chuang, Y.C., Vaughan, R.C., Sankaran, B., Kao, C.C., Li, P., 2017. Structure and function of the ZIKV full-length NS5 protein. Nat Commun 8, 14762.
Zhao, H., Fernandez, E., Dowd, K.A., Speer, S.D., Platt, D.J., Gorman, M.J., Govero, J., Nelson, C.A., Pierson, T.C., Diamond, M.S., Fremont, D.H., 2016. Structural Basis of ZIKV-Specific Antibody Protection. Cell 166, 1016-1027.
Zhou, T., Zhu, J., Yang, Y., Gorman, J., Ofek, G., Srivatsan, S., Druz, A., Lees, C.R., Lu, G., Soto, C., Stuckey, J., Burton, D.R., Koff, W.C., Connors, M., Kwong, P.D., 2014. Transplanting supersites of HIV-1 vulnerability. PLoS One 9, e99881.
Zhou, Y., Ray, D., Zhao, Y., Dong, H., Ren, S., Li, Z., Guo, Y., Bernard, K.A., Shi, P.Y., Li, H., 2007. Structure and function of flavivirus NS5 methyltransferase. Journal of virology 81, 3891-3903.
Zimmerman, M.G., Quicke, K.M., O'Neal, J.T., Arora, N., Machiah, D., Priyamvada, L., Kauffman, R.C., Register, E., Adekunle, O., Swieboda, D., Johnson, E.L., Cordes, S., Haddad, L., Chakraborty, R., Coyne, C.B., Wrammert, J., Suthar, M.S., 2018. Cross-Reactive Dengue Virus Antibodies Augment ZIKV Infection of Human Placental Macrophages. Cell Host Microbe 24, 731-742 e736.
Zimmerman, S.B., Cohen, G.H., Davies, D.R., 1975. X-ray fiber diffraction and model-building study of polyguanylic acid and polyinosinic acid. J Mol Biol 92, 181-192.
Zmurko, J., Marques, R.E., Schols, D., Verbeken, E., Kaptein, S.J., Neyts, J., 2016. The Viral Polymerase Inhibitor 7-Deaza-2'-C-Methyladenosine Is a Potent Inhibitor of In Vitro ZIKV Replication and Delays Disease Progression in a Robust Mouse Infection Model. PLoS Negl Trop Dis 10, e0004695.
Zou, J., Shi, P.Y., 2019. Strategies for Zika drug discovery. Curr Opin Virol 35, 19-26.